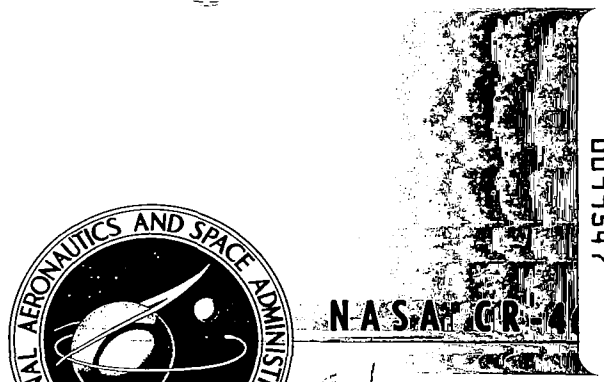

NASA CONTRACTOR REPORT

NASA CR-464

TRANSFER FUNCTION APPROXIMATIONS FOR LARGE HIGHLY COUPLED ELASTIC BOOSTERS WITH FUEL SLOSH

by R. L. Stapleford, L. G. Hofmann, J. J. Best, C. D. Wezeman, and W. A. Johnson

Prepared under Contract No. NAS 8-11419 *by*
SYSTEMS TECHNOLOGY, INC.
Hawthorne, Calif.
for George C. Marshall Space Flight Center

NATIONAL AERONAUTICS AND SPACE ADMINISTRATION • WASHINGTON, D. C. • APRIL 1966

NASA CR-464

TRANSFER FUNCTION APPROXIMATIONS FOR LARGE HIGHLY COUPLED ELASTIC BOOSTERS WITH FUEL SLOSH

By R. L. Stapleford, L. G. Hofmann, J. J. Best,
C. D. Wezeman, and W. A. Johnson

Prepared under Contract No. NAS 8-11419 by
SYSTEMS TECHNOLOGY, INC.
Hawthorne, Calif.

for George C. Marshall Space Flight Center

NATIONAL AERONAUTICS AND SPACE ADMINISTRATION

For sale by the Clearinghouse for Federal Scientific and Technical Information
Springfield, Virginia 22151 – Price $5.00

ABSTRACT

Approximations are derived for the transfer function factors (poles, zeros, gain) of a large highly flexible liquid-fueled boost vehicle. Various levels of approximations are evaluated and compared with exact factors for a hypothetical eleven-degree-of-freedom vehicle (the MSFC Model Vehicle No. 2). Agreement within 1 to 5 percent is achieved, depending on the amount of coupling taken into account.

The approximations are developed to provide physical insights to the basic dynamic characteristics of the vehicle, to allow simplified but meaningful preliminary synthesis studies, and to rapidly identify and evaluate the effects of variation in vehicle characteristics. The results explain or increase the understanding of previously observed coupling phenomena and provide ready means of assessing, by inspection or relatively simple computation, the consequences of change in vehicle characteristics. They also may be employed at the preliminary analysis and synthesis level to provide appropriate vehicle models without requiring large scale digital or analog computer facilities.

FOREWORD

This report was prepared under Contract NAS8-11419 between Systems Technology, Inc., Hawthorne, California, and the National Aeronautics and Space Administration, Marshall Space Flight Center. The NASA project monitor was Mr. J. R. Redus. The STI project engineer was Donald E. Johnston. Technical direction was provided by Irving L. Ashkenas, Dunstan Graham, and Duane T. McRuer of STI.

The authors gratefully acknowledge the fine work of the STI production department in the preparation of this report. Special acknowledgment is due Mr. Donald E. Johnston for his many constructive suggestions on organization and content.

CONTENTS

FIGURES

TABLES

SYMBOLS

a_{ij}	Slosh cross-coupling term, $a_{ij} = \frac{1}{M} + \frac{l_{s_i} l_{s_j}}{I}$
A	Effective actuator area
A_Δ	Lead coefficient of denominator
A_λ	Lead coefficient of λ/β_c numerator
$[A]$	Equations of motion matrix, see Eq. C-1
c_{ij}	Bending cross-coupling term, see Eq. 2
c_{s_j}	Effective damping coefficient of fundamental sloshing mass in jth tank
C	Number of gimbaled engines
C_{Z_α}	Aerodynamic normal force coefficient
D	Dissipation function
f	Load on an actuator
F	Total number of booster engines
F_X	Total force in X direction
F_Z	Total force in Z direction
$\bar{g}$	Artificial gravitational acceleration, $\bar{g} = \frac{T - X_a}{M}$
g_i	η_i input to φ equation, see Eq. 41
I	Total booster moment of inertia
I'	Running total section moment of inertia
I_A'	Running section moment of inertia of the empty airframe less engines
I_E	Moment of inertia of each engine about gimbal point
$I_{E_{CG}}$	Moment of inertia of each engine about its own CG
I_{o_j}	Moment of inertia of the fixed mass in the jth tank

k_{s_j}	Effective spring constant of fundamental sloshing mass in the jth tank
K_L	Effective spring constant of actuator–nozzle compliance
K_0	Effective hydraulic spring constant
K_1	Actuator open-loop gain
K_3	Valve pressure feedback gain
l_β	Distance from booster CG to engine gimbal point, positive forward
l_{CP}	Distance from booster CG to aerodynamic center of pressure, positive forward
l_E	Distance from engine CG to gimbal point, positive forward
l_{o_j}	Distance from booster CG to CG of fixed mass in the jth tank, positive forward
l_{s_j}	Distance from vehicle CG to the CG of the fundamental sloshing mass in the jth tank, positive forward
L	Total length of booster
M	Total booster mass
M'	Running total mass
M'_A	Running mass of the empty airframe less engines
M_E	Mass of each booster engine
M_i	Generalized mass of ith bending mode
M_{s_j}	Fundamental sloshing mass in the jth tank
M_y	Pitching moment about Y axis
M_α	Aerodynamic pitching moment derivative, see Eq. B-24
$\bar{M}_\alpha$	Aerodynamic pitching moment derivative with static correction for the first bending mode, see Eq. 9
$M_{\dot{\phi}}$	Aerodynamic pitching moment derivative, see Eq. B-29
M_{η_i}	Aerodynamic pitching moment derivative, see Eq. B-30
$M_{\dot{\eta}_i}$	Aerodynamic pitching moment derivative, see Eq. B-31

N_α	Aerodynamic normal force derivative, see Eq. B-23
$\bar{N}_\alpha$	Aerodynamic normal force derivative with static correction for the first bending mode, see Eq. 8
N_{η_i}	Aerodynamic normal force derivative, see Eq. B-25
$N_{\dot{\eta}_i}$	Aerodynamic normal force derivative, see Eq. B-26
$N_{\eta_{ik}}$	Aerodynamic normal force derivative, see Eq. B-33
$N_{\dot{\eta}_{ik}}$	Aerodynamic normal force derivative, see Eq. B-34
$N_\lambda(s)$	Numerator of λ/β_c transfer function
$N_{\dot{\varphi}}$	Aerodynamic normal force derivative, see Eq. B-28
$\bar{1}_x$, $\bar{1}_y$, $\bar{1}_z$	Unit vectors along X, Y, Z axes
p	Negative of transfer function pole
q	Dynamic pressure
q_i	Generalized coordinate
Q	Flow rate into an actuator
Q	Aeroelastic correction matrix, see Eq. C-7
Q_i	Generalized force
R_{IC}	Radial distance from origin of earth-centered inertial coordinates to booster CG
R_{ID}	Radial distance from origin of earth-centered inertial coordinates to origin of X, Y, Z coordinates
s	Laplace variable
S	Reference area for aerodynamic derivative C_{Z_α}
S_3	3-by-3 matrix of Eq. D-3
S_4	4-by-4 matrix of Eq. 18
T	Total kinetic energy
T	Total thrust of booster engines
V	Booster velocity

V	Total potential energy
V_{air}	Booster velocity relative to air mass
V_N	Nominal booster velocity
w	Component of wind velocity parallel to Z axis
W	Wind velocity
x_{CG}	Station of booster CG
x_{o_j}	Station of the fixed mass in the jth tank
x_{s_j}	Station of the CG of the fundamental sloshing mass in the jth tank
x_β	Station of engine gimbals
$\{x\}$	Column matrix of dependent variables
X, Y, Z	Right hand coordinate system with origin at vehicle CG and X axis along the nominal boost trajectory velocity vector
X_a	Aerodynamic axial force, positive aft
$Y_i(x)$	Normalized amplitude of ith bending mode at station x
$Y_i'(x)$	Slope of ith bending mode at station x, $Y_i'(x) = \frac{\partial}{\partial x} Y_i(x)$
z	Negative of transfer function zero
z_{s_j}	Displacement of the fundamental sloshing mass in the jth tank, perpendicular to the elastic axis
Z	Translation of weighted average vehicle centerline, perpendicular to nominal trajectory
α	Angle of attack of weighted average centerline
$\alpha(x)$	Local angle of attack at station x
β	Rotation of gimbaled engine centerline from elastic centerline
β_a	Rotation of actuator output from elastic axis
β_c	Commanded rotation of gimbaled engines
δq_i	Virtual displacement of q_i

δW_e	Virtual work done by external forces
$\{\delta\}$	Column matrix of inputs
$\Delta(s)$	Transfer function denominator
ζ	Damping ratio
$\overline{\zeta_i \omega_i}$	Damping of ith bending mode with self-coupling correction, see Eq. D-1
η_i	Generalized displacement of ith bending mode
θ	Angle between local vertical and X axis, positive for negative rotation about Y axis
λ	General dependent variable
φ	Vehicle pitch angle, angle between weighted average vehicle centerline and X axis, positive for negative rotation about Y axis
ψ	Angle between gimbaled engine centerline and X axis, see Fig. B-3
ω	Undamped natural frequency
ω_E	Uncoupled natural frequency of actuator–nozzle compliance
ω_i	Uncoupled natural frequency of ith bending mode
$\overline{\omega_i^2}$	Square of the natural frequency of the ith bending mode with self-coupling corrections, see Eq. 10
ω_{s_j}	Uncoupled natural frequency of the fundamental sloshing mass in the jth tank
Ω	Angular velocity of XYZ coordinates

SECTION I

INTRODUCTION

This report presents the results of a research study accomplished under Marshall Space Flight Center Contract NAS8-11419, "Control Study for Reduced Bending Frequencies and Increased Coupling for Rigid and Elastic Modes." The contract covers analytical studies of the control of large space boosters for which the elastic and fuel slosh modes have frequencies very near to the desired control frequencies, and for which there is a great deal of intermodal coupling. The basic objectives of this study are:

- The development of a model of the vehicle dynamics which can provide the control engineer with the physical insights into the modal coupling and vehicle characteristics which are necessary for a solution of this complex control problem.
- The determination of the limits of conventional control systems for this general class of vehicle, and to provide guidelines for determining what degree of vehicle dynamic complexity requires more advanced control techniques.
- The evaluation of advanced control concepts for solution of the stability and control problems for the extreme cases in which conventional techniques are inadequate.

The material contained in this report deals only with the first objective. As such, its purpose is to provide the simplest of vehicle dynamic models, consistent with maintaining physical relationships, to maximize physical insights into modal coupling and vehicle characteristics. The result should increase the control engineer's understanding of boost vehicle dynamics. In addition, the approximate models developed can also be used to perform meaningful preliminary synthesis operations on a much simplified basis, and to assist the designer in determining effects of deliberate variations in vehicle characteristics or possible uncertainties in estimated dynamic parameters.

The transfer function for the response of a dependent variable, λ, to an engine deflection command, β_c, may be expressed in the form

$$\frac{\lambda(s)}{\beta_c(s)} = \frac{N_\lambda(s)}{\Delta(s)} = \frac{A_\lambda \prod(s + z_i) \prod(s^2 + 2\zeta_i\omega_i s + \omega_i^2)}{A_\Delta \prod(s + p_i) \prod(s^2 + 2\zeta_i'\omega_i' s + \omega_i'^2)} \qquad (1)$$

The basic objective of this report is to find suitable approximations for the denominator and numerator roots and lead coefficients of a highly coupled vehicle.

The numerical values used throughout this report are for a hypothetical large space booster — the Marshall Space Flight Center Model Vehicle No. 2, Fig. 1 — at three flight conditions, lift-off (LO), maximum dynamic pressure (Max Q), and burnout (BO).* This vehicle was deliberately contrived to have a great deal of intermodal coupling and to have bending mode and fuel slosh frequencies very near desired control frequencies. For example, at lift-off the first bending mode has a frequency of 2.6 rad/sec, and there are three fuel slosh modes in the frequency band from 2.0 to 2.2 rad/sec.** In all, two rigid-body, four bending, and three slosh degrees of freedom plus the control actuation and compliance degrees of freedom are considered (because of the symmetry of the vehicle only motion in the pitch plane is considered, but the results apply equally well to the yaw plane).

A basic problem encountered in this work was that of determining the degree of accuracy required in the approximations. For conventional aircraft studies an approximation is generally considered adequate if it predicts transfer function pole and zero locations to within 10 percent. While this same criterion should be valid for most boost vehicle poles and zeros, the slosh modes pose a special problem. These modes are represented by pairs of very closely spaced, lightly damped poles and zeros. Small percentage errors in either pole or zero locations can mean the difference between predicted closed-loop stability and instability. Consequently it was decided to try to approximate the slosh modes to

*The burnout condition is taken as just prior to thrust decay.

**A detailed list of the pertinent dynamic characteristics of Model Vehicle No. 2 is given in Appendix I.

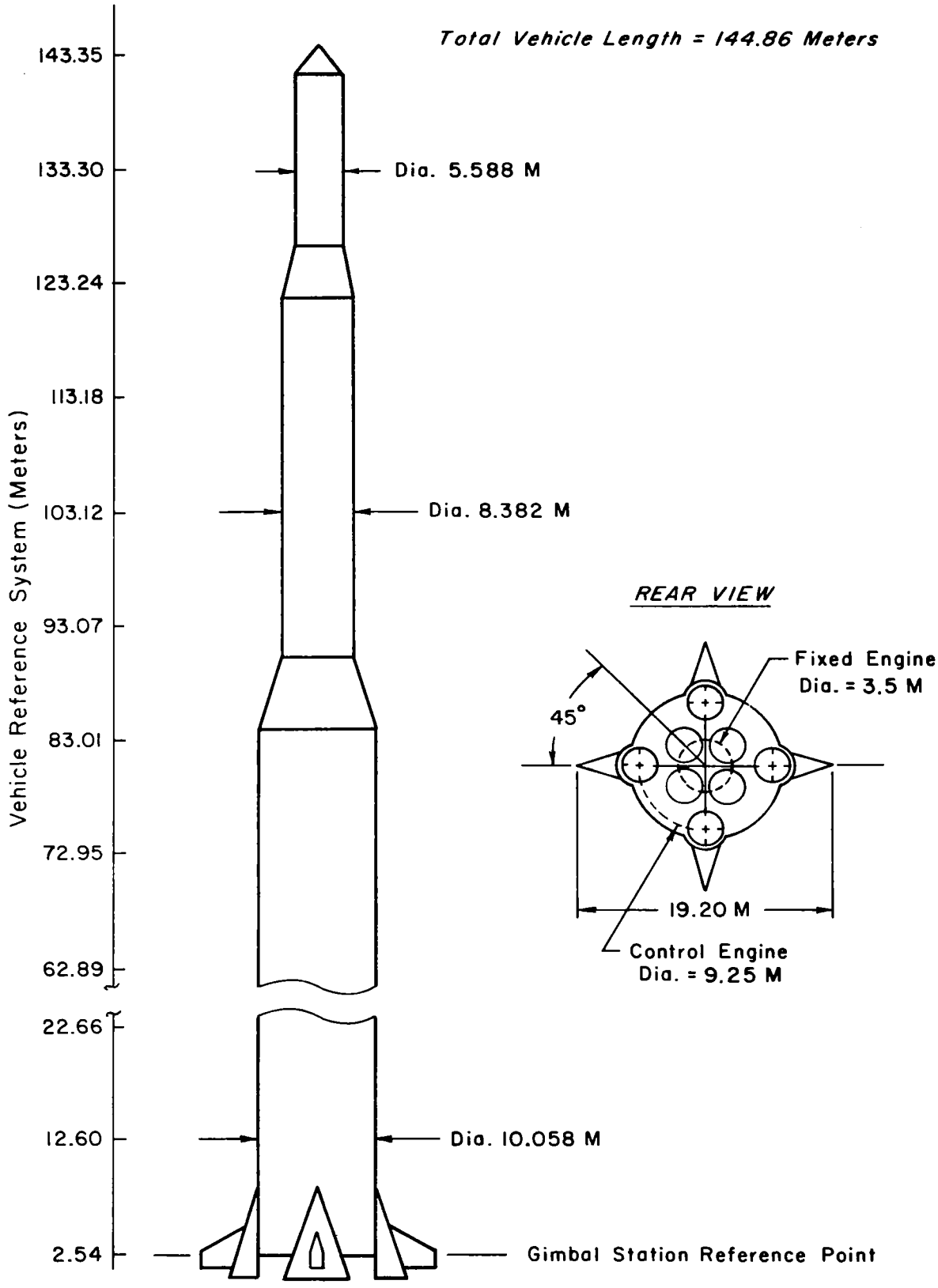

Figure 1. Model Vehicle No. 2

within 1 percent. Subsequent comparisons of approximate and exact pole–zero separations, as detailed in Part 4 of Appendix G, indicate that the errors for the slosh modes should be restricted to this order of magnitude.

ORGANIZATION OF THE REPORT

The body of the report contains the final forms of the approximations with brief discussions of their accuracy and how they were obtained. The derivations and detailed comparison of exact and approximate values are relegated to the numerous appendices. Our objective here was to allow the casual reader to obtain an overview of the results from the body of the report without becoming bogged down with innumerable matrices and tables of numbers.

For those who are interested in applying the approximations to a booster configuration considerably different from the Model Vehicle No. 2, the details of the derivations must be understood. In this instance the reader must become aware of the validity conditions associated with the approximations, and should know how and when the approximations should be modified. We recommend that this individual first read the body of the report and then the pertinent appendices.

The coordinate system and equations of motion used herein are discussed in Section II. Section III describes the general technique used to derive the approximations as well as the approximations for the transfer function denominator (open-loop poles and denominator lead coefficient). Approximations for the pitch angle and bending numerators are covered in Section IV. These numerators were selected because they constitute the elements of the sensor numerators for the most common types of sensors—attitude and rate gyros. Section V summarizes and reviews highlights of the approximations and coupling effects.

As noted above, the appendices contain the derivations and detailed comparisons of exact and approximate solutions. Pertinent information on Model Vehicle No. 2 is also presented.

SECTION II

COORDINATE SYSTEM AND EQUATIONS OF MOTION

The basic coordinate system used in this report follows a nominal booster trajectory. The origin of the XYZ coordinates is located at the center of gravity of the vehicle as it moves along this nominal trajectory. The X axis is aligned with the nominal velocity vector, $\bar{V}_N$ (see Fig. 2). Displacements of an actual booster from the nominal trajectory, but within the XZ plane, are given by X and Z.

It is shown in Appendix A that the equations of motion can be separated into trim and perturbation components. The trim equations define the relationships among certain variables, such as velocity and flight path angle, for a nominal trajectory. In this report a no-wind, gravity turn nominal trajectory is used, but the method could also be applied to any other type of nominal trajectory.

The perturbation equations describe vehicle deviations about the nominal trajectory. These equations are commonly used in vehicle stability and control analyses and are of primary concern in this study. As shown in Appendix A, the perturbation equations can be obtained by simply

- Assuming the XYZ coordinates to be inertial
- Suppressing the X degree of freedom
- Omitting the gravity force
- Adding an artificial gravity force which acts along the negative X axis with a magnitude $M\bar{g} = T - X_a$ (T = total vehicle thrust, X_a = axial drag)

The approach indicated by these four steps is used in Appendix B to derive generalized perturbation equations of motion of a flexible booster including body bending modes, fuel sloshing modes, actuator to gimbaled engine compliance, and actuator dynamics. The example vehicle for this study (Ref. 11) has three slosh and four bending modes. These, plus actuator to gimbaled engine compliance, a first-order actuator lag, and

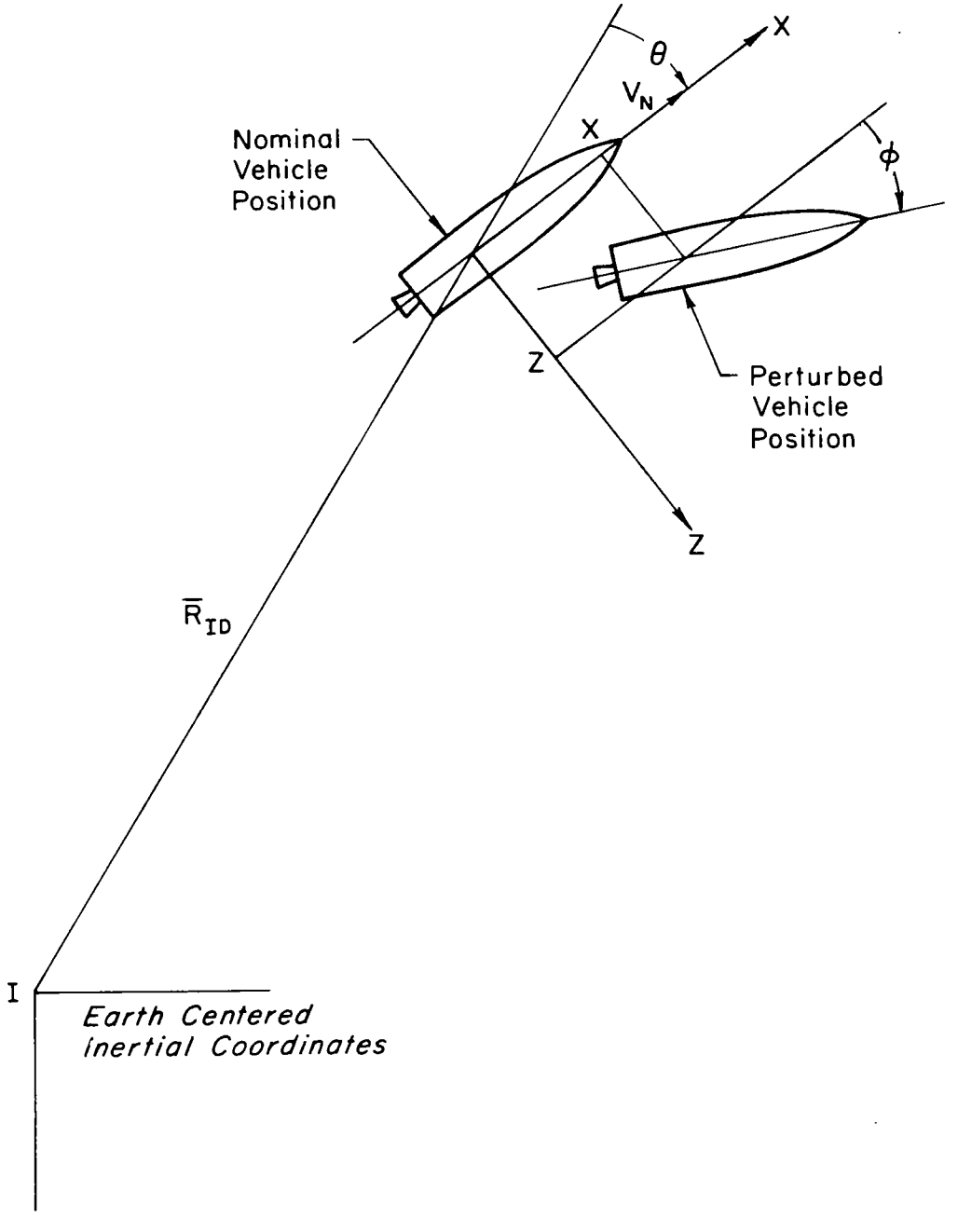

Figure 2. Coordinate System

the rigid-body modes, provide the eleven degrees of freedom in the complete perturbation equations (see Fig. 3*).

The authors realize that several other derivations of booster equations have been published. Each of these earlier works appears to contain simplifying assumptions regarding modal cross-coupling which were justified for their particular situations. In this study we are especially concerned about model coupling. Consequently, the derivation presented here retains all possible terms consistent with a linear analysis.

One term shown in Fig. 3 deserves particular attention because of a controversy over its inclusion. The element c_{ij}, which cross-couples the bending modes, is given by

$$c_{ij} = \frac{1}{M_i}\left[-N\eta_{i_j} + \bar{g}FM_E l_E Y_i'(x_\beta)Y_j'(x_\beta) - \underline{(T - X_a)Y_i(x_\beta)Y_j'(x_\beta)}\right] \qquad (2)$$

The underlined term is due to the lateral translation and rotation of the aft end of the booster and the resultant axial force $(T - X_a)$ caused by the bending modes.

The bending displacements, $Y_i(x)\eta_i$, have been defined (Appendix B) to be perpendicular to the booster undeflected centerline, or x axis, in keeping with the traditional approach to vibrating beam analysis. Under these conditions only forces perpendicular to the x axis can contribute to the generalized forces for the bending modes.

Now, in actual fact, the bending of the vehicle does produce some motion of an element in the x direction. This longitudinal translation of the axial forces should produce an additional generalized force for the bending modes. This longitudinal force was omitted here because there appears to be no tractable method of evaluating it (except for uniform rods).

---

*Note that the variable for the first column of Fig. 3 is the velocity, $\dot{Z}$, because the displacement, Z, does not appear in the equations of motion. Numerical values of the matrix elements, as well as transfer function poles, zeros, and lead coefficients, for Model Vehicle No. 2 are given in Appendix J.

$\dot{z}$		ϕ			z_{s_1}			z_{s_2}			z_{s_3}			η_1		
s^1	s^0	s^2	s^1	s^0	s^2	s^1	s^0	s^2	s^1	s^0	s^2	s^1	s^0	s^2	s^1	s^0
1	$\frac{N_\alpha}{MV_N}$	0	$\frac{N_\phi}{MV_N}$	$-g-\frac{M_\alpha}{M}$	$\frac{M_{S_1}}{M}$	0	0	$\frac{M_{S_2}}{M}$	0	0	$\frac{M_{S_3}}{M}$	0	0	0	$\frac{N\dot{\eta}_1}{MV_N}$	$-\bar{g}Y_1'(x_\beta)-\frac{N_{\eta_1}}{M}$
0	$\frac{M_\alpha}{IV_N}$	1	$\frac{M_\phi}{IV_N}$	$-\frac{M_\alpha}{I}$	$\frac{M_{S_1}l_{S_1}}{I}$	0	$-\frac{\bar{g}M_{S_1}}{I}$	$\frac{M_{S_2}l_{S_2}}{I}$	0	$-\frac{\bar{g}M_{S_2}}{I}$	$\frac{M_{S_3}l_{S_3}}{I}$	0	$-\frac{\bar{g}M_{S_3}}{I}$	0	$\frac{M\dot{\eta}_1}{IV_N}$	$-\frac{q_1}{I}$
1	0	l_{s_1}	0	$-\bar{g}$	1	$2\zeta_{s_1}\omega_{s_1}$	$\omega_{s_1}^2$	0	0	0	0	0	0	$Y_1(x_{s_1})$	0	$-\bar{g}Y_1'(x_{s_1})$
1	0	l_{s_2}	0	$-\bar{g}$	0	0	0	1	$2\zeta_{s_2}\omega_{s_2}$	$\omega_{s_2}^2$	0	0	0	$Y_1(x_{s_2})$	0	$-\bar{g}Y_1'(x_{s_2})$
1	0	l_{s_3}	0	$-\bar{g}$	0	0	0	0	0	0	1	$2\zeta_{s_3}\omega_{s_3}$	$\omega_{s_3}^2$	$Y_1(x_{s_3})$	0	$-\bar{g}Y_1'(x_{s_3})$
0	$\frac{N\dot{\eta}_1}{M_1V_N}$	0	$\frac{M\dot{\eta}_1}{M_1V_N}$	$-\frac{N_{\eta_1}}{M_1}$	$\frac{M_{S_1}Y_1(x_{S_1})}{M_1}$	0	$-\frac{\bar{g}M_{S_1}Y_1'(x_{S_1})}{M_1}$	$\frac{M_{S_2}Y_1(x_{S_2})}{M_1}$	0	$-\frac{\bar{g}M_{S_2}Y_1'(x_{S_2})}{M_1}$	$\frac{M_{S_3}Y_1(x_{S_3})}{M_1}$	0	$-\frac{\bar{g}M_{S_3}Y_1'(x_{S_3})}{M_1}$	1	$2\overline{\zeta_1\omega_1}$	$\overline{\omega}_1^2$
0	$\frac{N\dot{\eta}_2}{M_2V_N}$	0	$\frac{M\dot{\eta}_2}{M_2V_N}$	$-\frac{N_{\eta_2}}{M_2}$	$\frac{M_{S_1}Y_2(x_{S_1})}{M_2}$	0	$-\frac{\bar{g}M_{S_1}Y_2'(x_{S_1})}{M_2}$	$\frac{M_{S_2}Y_2(x_{S_2})}{M_2}$	0	$-\frac{\bar{g}M_{S_2}Y_2'(x_{S_2})}{M_2}$	$\frac{M_{S_3}Y_2(x_{S_3})}{M_2}$	0	$-\frac{\bar{g}M_{S_3}Y_2'(x_{S_3})}{M_2}$	0	$\frac{N\dot{\eta}_{21}}{M_2V_N}$	c_{21}
0	$\frac{N\dot{\eta}_3}{M_3V_N}$	0	$\frac{M\dot{\eta}_3}{M_3V_N}$	$-\frac{N_{\eta_3}}{M_3}$	$\frac{M_{S_1}Y_3(x_{S_1})}{M_3}$	0	$-\frac{\bar{g}M_{S_1}Y_3'(x_{S_1})}{M_3}$	$\frac{M_{S_2}Y_3(x_{S_2})}{M_3}$	0	$-\frac{\bar{g}M_{S_2}Y_3'(x_{S_2})}{M_3}$	$\frac{M_{S_3}Y_3(x_{S_3})}{M_3}$	0	$-\frac{\bar{g}M_{S_3}Y_3'(x_{S_3})}{M_3}$	0	$\frac{N\dot{\eta}_{31}}{M_3V_N}$	c_{31}
0	$\frac{N\dot{\eta}_4}{M_4V_N}$	0	$\frac{M\dot{\eta}_4}{M_4V_N}$	$-\frac{N_{\eta_4}}{M_4}$	$\frac{M_{S_1}Y_4(x_{S_1})}{M_4}$	0	$-\frac{\bar{g}M_{S_1}Y_4'(x_{S_1})}{M_4}$	$\frac{M_{S_2}Y_4(x_{S_2})}{M_4}$	0	$-\frac{\bar{g}M_{S_2}Y_4'(x_{S_2})}{M_4}$	$\frac{M_{S_3}Y_4(x_{S_3})}{M_4}$	0	$-\frac{\bar{g}M_{S_3}Y_4'(x_{S_3})}{M_4}$	0	$\frac{N\dot{\eta}_{41}}{M_4V_N}$	c_{41}
$-\frac{M_\xi l_\xi}{I_\xi}$	0	$1-\frac{M_\xi l_\xi l_\beta}{I_\xi}$	0	$\frac{\bar{g}M_\xi l_\xi}{I_\xi}$	0	0	0	0	0	0	0	0	0	$Y_1(x_\beta)-\frac{M_\xi l_\xi Y_1(x_\beta)}{I_\xi}$	0	$\frac{\bar{g}M_\xi l_\xi Y_1'(x_\beta)}{I_\xi}$
0	0	0	0	0	0	0	0	0	0	0	0	0	0	0	0	0

$$q_i = M\eta_i + \bar{g}M\left[l_\beta Y_i'(x_\beta) - Y_i(x_\beta)\right]$$

$$c_{ik} = \frac{1}{M_i}\left[-N_{\eta_{ik}} + \bar{g}FM_\xi l_\xi Y_i'(x_\beta)Y_k'(x_\beta) - \underline{\bar{g}MY_i(x_\beta)Y_k'(x_\beta)}\right]$$; *Underlined term may be omitted as discussed on page 10*

$$2\overline{\zeta_i\omega_i} = 2\zeta_i\omega_i + \frac{N\dot{\eta}_{ii}}{M_iV_N}$$

$$\overline{\omega}_i^2 = \omega_i^2 + c_{ii}$$

Figure 3. Exact Equations of Motion

η_2			η_3			η_4			β			β_α		β_c	w
s^2	s^1	s^0	s^2	s^1	s^0	s^2	s^1	s^0	s^2	s^1	s^0	s^1	s^0	s^0	s^0
0	$\frac{N\dot{n}_2}{MV_N}$	$-\bar{g}Y_2'(x_\beta)-\frac{N_{n_2}}{M}$	0	$\frac{N\dot{n}_3}{MV_N}$	$-\bar{g}Y_3'(x_\beta)-\frac{N_{n_3}}{M}$	0	$\frac{N\dot{n}_4}{MV_N}$	$-\bar{g}Y_4'(x_\beta)-\frac{N_{n_4}}{M}$	$-\frac{CM_E l_E}{M}$	0	$-\frac{CT}{FM}$	0	0	0	$\frac{N_\alpha}{MV_N}$
0	$\frac{M\dot{n}_2}{IV_N}$	$-\frac{q_2}{I}$	0	$\frac{M\dot{n}_3}{IV_N}$	$-\frac{q_3}{I}$	0	$\frac{M\dot{n}_4}{IV_N}$	$-\frac{q_4}{I}$	$\frac{C\left[I_E-M_E l_E l_\beta\right]}{I}$	0	$\frac{C}{I}\left[\bar{g}M_E l_E-\frac{T}{F}l_\beta\right]$	0	0	0	$\frac{M_\alpha}{IV_N}$
$Y_2(x_{s_1})$	0	$-\bar{g}Y_2'(x_{s_1})$	$Y_3(x_{s_1})$	0	$-\bar{g}Y_3'(x_{s_1})$	$Y_4(x_{s_1})$	0	$-\bar{g}Y_4'(x_{s_1})$	0	0	0	0	0	0	0
$Y_2(x_{s_2})$	0	$-\bar{g}Y_2'(x_{s_2})$	$Y_3(x_{s_2})$	0	$-\bar{g}Y_3'(x_{s_2})$	$Y_4(x_{s_2})$	0	$-\bar{g}Y_4'(x_{s_2})$	0	0	0	0	0	0	0
$Y_2(x_{s_3})$	0	$-\bar{g}Y_2'(x_{s_3})$	$Y_3(x_{s_3})$	0	$-\bar{g}Y_3'(x_{s_3})$	$Y_4(x_{s_3})$	0	$-\bar{g}Y_4'(x_{s_3})$	0	0	0	0	0	0	0
0	$\frac{N\dot{n}_{12}}{M_1V_N}$	c_{12}	0	$\frac{N\dot{n}_{13}}{M_1V_N}$	c_{13}	0	$\frac{N\dot{n}_{14}}{M_1V_N}$	c_{14}	$\frac{C\left[I_E Y_1'(x_\beta)\ M_E l_E Y_1(x_\beta)\right]}{M_1}$	0	$\frac{C}{M_1}\left[\bar{g}M_E l_E Y_1'(x_\beta)-\frac{T}{F}Y_1(x_\beta)\right]$	0	0	0	$\frac{N\dot{n}_1}{M_1V_N}$
1	$2\zeta_2\omega_2$	$\bar{\omega}_2^2$	0	$\frac{N\dot{n}_{23}}{M_2V_N}$	c_{23}	0	$\frac{N\dot{n}_{24}}{M_2V_N}$	c_{24}	$\frac{C\left[I_E Y_2'(x_\beta)-M_E l_E Y_2(x_\beta)\right]}{M_2}$	0	$\frac{C}{M_2}\left[\bar{g}M_E l_E Y_2'(x_\beta)-\frac{T}{F}Y_2(x_\beta)\right]$	0	0	0	$\frac{N\dot{n}_2}{M_2V_N}$
0	$\frac{N\dot{n}_{32}}{M_3V_N}$	c_{32}	1	$2\zeta_3\omega_3$	$\bar{\omega}_3^2$	0	$\frac{N\dot{n}_{34}}{M_3V_N}$	c_{34}	$\frac{C\left[I_E Y_3'(x_\beta)-M_E l_E Y_3(x_\beta)\right]}{M_3}$	0	$\frac{C}{M_3}\left[\bar{g}M_E l_E Y_3'(x_\beta)-\frac{T}{F}Y_3(x_\beta)\right]$	0	0	0	$\frac{N\dot{n}_3}{M_3V_N}$
0	$\frac{N\dot{n}_{42}}{M_4V_N}$	c_{42}	0	$\frac{N\dot{n}_{43}}{M_4V_N}$	c_{43}	1	$2\zeta_4\omega_4$	$\bar{\omega}_4^2$	$\frac{C\left[I_E Y_4'(x_\beta)-M_E l_E Y_4(x_\beta)\right]}{M_4}$	0	$\frac{C}{M_4}\left[\bar{g}M_E l_E Y_4'(x_\beta)-\frac{T}{F}Y_4(x_\beta)\right]$	0	0	0	$\frac{N\dot{n}_4}{M_4V_N}$
$Y_2(x_\beta)-\frac{M_E l_E Y_2(x_\beta)}{I_E}$	0	$\frac{\bar{g}M_E l_E Y_2'(x_\beta)}{I_E}$	$Y_3(x_\beta)-\frac{M_E l_E Y_3(x_\beta)}{I_E}$	0	$\frac{\bar{g}M_E l_E Y_3'(x_\beta)}{I_E}$	$Y_4(x_\beta)-\frac{M_E l_E Y_4(x_\beta)}{I_E}$	0	$\frac{\bar{g}M_E l_E Y_4'(x_\beta)}{I_E}$	1	$2\zeta_E\omega_E$	$\omega_E^2+\frac{\bar{g}M_E l_E}{I_E}$	0	$-\omega_E^2$	0	0
0	0	0	0	0	0	0	0	0	0	$-\frac{AK_L}{K_0}$	$-\frac{K_3K_L}{A}$	$\frac{A(K_0+K_L)}{K_0}$	$K_1+\frac{K_3K_L}{A}$	K_1	0

Figure 3 (Concluded)

The controversy then arises as to whether the lateral term, which is readily evaluated, also should be excluded. Of six authoritative documents, three (Refs. 1 – 3) omit it in the development of the bending equations and three (Refs. 4 – 6) include it. Reference 1 indicates that the longitudinal work is generally equal to or greater than the lateral work — and of opposite sign — for a slender uniform rod. The strongest argument for omitting the lateral term is that it increases the bending mode frequencies, whereas the actual thrust effects are to decrease the frequencies (Refs. 7, 8).

Since one of the major objectives of this study is to develop transfer function approximate expressions for a flexible vehicle exhibiting strong modal cross-coupling; and since the lateral term in question generally increases the bending mode cross-coupling, inclusion of the lateral term throughout this study was deemed both useful and conservative. However, the presence of this term did make the above task more difficult by forcing retention of terms which otherwise would be negligible. The omission of the term would simplify certain of the approximations presented herein and, if anything, should increase their accuracy. For the reader who prefers to exclude the lateral term, it is identified in Fig. 3 and elsewhere throughout the report by underlining, as in Eq. 2.

SECTION III

DENOMINATOR APPROXIMATIONS

Having established the complete 11-by-11 matrix for the perturbation equations of motion, the task is now to develop approximations for transfer function poles, zeros, and gains. The approximations will be evaluated by comparison of the numerical results with the exact values obtained from solutions of the complete matrix.

Approximations for the denominator roots of the 11-by-11 determinant (Fig. 3) are presented in this section. Approximations for the numerator roots will be discussed in the next section.

The denominator has 20 roots. These roots are considered in three groups — the three rigid-body roots, the 14 roots from the three slosh and four bending modes, and the three roots from the first-order actuator lag and the actuator–nozzle compliance. But before discussing these approximations, the general approach used in obtaining them will be outlined.

A. GENERAL TECHNIQUE

The general technique used in deriving both numerator and denominator approximations can best be described by a simple example. Consider a two-degree-of-freedom system which has equations of motion of the form

$$\begin{bmatrix} s^2 + \omega_1^2 & a_1 s^2 + b_1 \\ a_2 s^2 + b_2 & s^2 + \omega_2^2 \end{bmatrix} \begin{Bmatrix} x_1 \\ x_2 \end{Bmatrix} = 0 \qquad (3)$$

where $\omega_1 \ll \omega_2$

If the two natural modes of this system are lightly coupled, then coupled natural frequencies may be approximated by ω_1 and ω_2. A better approximation for the lower frequency mode may be obtained by including a "static correction" for the contribution of the higher frequency mode, i.e., the

characteristic equation is written

$$\begin{vmatrix} s^2 + \omega_1^2 & b_1 \\ b_2 & \omega_2^2 \end{vmatrix} = 0 \qquad (4)$$

Since $s \doteq j\omega_1$ in the mode, Eq. 4 amounts to assuming

$$\omega_1^2 \ll \omega_2^2$$

$$|a_1\omega_1^2| \ll |b_1|$$

$$|a_2\omega_1^2| \ll |b_2|$$

The first inequality is true by definition. The other two inequalities do not necessarily follow from the first, but generally have been found to hold for the problem at hand. The few exceptions that do occur will be noted later.

Likewise, the higher frequency mode may be better approximated by including a "dynamic correction" for the contribution of the lower frequency mode. This gives a characteristic equation of

$$\begin{vmatrix} s^2 & a_1 s^2 \\ a_2 s^2 & s^2 + \omega_2^2 \end{vmatrix} = 0 \qquad (5)$$

or

$$\begin{vmatrix} 1 & a_1 s^2 \\ a_2 & s^2 + \omega_2^2 \end{vmatrix} = 0 \qquad (6)$$

This is equivalent to assuming

$$\omega_2^2 \gg \omega_1^2$$

$$|a_1\omega_2^2| \gg |b_1|$$

$$|a_2\omega_2^2| \gg |b_2|$$

Once again the last two inequalities do not necessarily follow from the first one, but have been found to be valid in general.

The key to application of the above approach is "sufficient" separation of the uncoupled frequencies (ω_1 and ω_2). Unfortunately, "sufficient" cannot be defined in general because the required separation strongly depends on the degree of coupling and the accuracy desired. For the booster problem considered here the method has given satisfactory results for frequency separations as small as a factor of two. This is due, in part, to the fact that the coupling actually causes relatively small frequency shifts. Thus if coupling only changes a frequency by 5 percent, a 20 percent error in approximating coupling effects still gives a final result accurate to 0.5 x 0.2 = 1 percent.

If the uncoupled frequencies do not exhibit adequate separation, all the terms in the diagonal elements must be retained; but it may be possible to eliminate some of the less important off-diagonal terms if the previously noted inequalities regarding $a_i s^2$ and b_i are valid.

B. RIGID-BODY MODES

For low dynamic pressure flight conditions the rigid-body modes are adequately approximated by the 2-by-2 matrix of the rigid-body degrees of freedom, $\dot{Z}$ and φ:

$$\begin{bmatrix} s + \dfrac{N_\alpha}{MV_N} & \dfrac{N_{\dot{\varphi}}}{MV_N} s - \bar{g} - \dfrac{N_\alpha}{M} \\ \dfrac{M_\alpha}{IV_N} & s^2 + \dfrac{M_{\dot{\varphi}}}{IV_N} s - \dfrac{M_\alpha}{I} \end{bmatrix} \begin{Bmatrix} \dot{Z} \\ \varphi \end{Bmatrix} = 0 \qquad (7)$$

For high dynamic pressure flight conditions it is necessary to add a static correction for the bending modes. This is equivalent to correcting the aerodynamic terms N_α and M_α for vehicle flexing under aerodynamic loads. Inclusion of the first bending contribution was considered sufficient for Model Vehicle No. 2 in spite of the high degree of flexibility involved. This provided an approximation within 3 percent of the exact

rigid-body modes — an order of magnitude improvement over the uncorrected approximations.

The corrected derivatives are given by

$$\bar{N}_\alpha = N_\alpha + \frac{N_{\dot{\eta}_1}\left[\bar{g}MY_1'(x_\beta) + N_{\eta_1}\right]}{M_1\bar{\omega}_1^2} \tag{8}$$

$$\bar{M}_\alpha = M_\alpha + \frac{N_{\dot{\eta}_1}\left\{\bar{g}M\left[l_\beta Y_1'(x_\beta) - Y_1(x_\beta)\right] + M_{\eta_1}\right\}}{M_1\bar{\omega}_1^2} \tag{9}$$

where*

$$\bar{\omega}_1^2 = \omega_1^2 + \frac{1}{M_1}\left\{-N_{\eta_{11}} + \bar{g}FM_E l_E\left[Y_1'(x_\beta)\right]^2 - \underline{\bar{g}MY_1(x_\beta)Y_1'(x_\beta)}\right\} \tag{10}$$

Thus the approximate characteristic equation for the rigid-body modes is

$$\begin{vmatrix} s + \frac{\bar{N}_\alpha}{MV_N} & \frac{N_{\dot{\varphi}}}{MV_N}s - \bar{g} - \frac{\bar{N}_\alpha}{M} \\ \frac{\bar{M}_\alpha}{IV_N} & s^2 + \frac{M_{\dot{\varphi}}}{IV_N}s - \frac{\bar{M}_\alpha}{I} \end{vmatrix} = 0 \tag{11}$$

or

$$s^3 + s^2\left(\frac{\bar{N}_\alpha}{MV_N} + \frac{M_{\dot{\varphi}}}{IV_N}\right) + s\left(\frac{-\bar{M}_\alpha}{I} + \frac{\bar{N}_\alpha M_{\dot{\varphi}}}{MIV_N^2} - \frac{N_{\dot{\varphi}}\bar{M}_\alpha}{MIV_N^2}\right) + \frac{g\bar{M}_\alpha}{IV_N} = 0 \tag{12}$$

Unless the vehicle has a small (positive or negative) static margin, the following condition is satisfied:

$$|\bar{M}_\alpha| \gg \left|\frac{\bar{N}_\alpha M_{\dot{\varphi}} - N_{\dot{\varphi}}\bar{M}_\alpha}{MV_N^2}\right|$$

*The underlined term may be omitted, as discussed on page 10.

and the three roots of Eq. 11 can be rapidly approximated by

$$p_z \doteq \frac{-\bar{g}}{V_N} \tag{13}$$

$$(p_{\varphi_1} + p_{\varphi_2}) \text{ or } (2\zeta_\varphi \omega_\varphi) \doteq \frac{\bar{N}_\alpha}{MV_N} + \frac{M_{\dot{\varphi}}}{IV_N} + \frac{\bar{g}}{V_N} \tag{14}$$

$$(p_{\varphi_1} p_{\varphi_2}) \text{ or } (\omega_\varphi^2) \doteq \frac{-\bar{M}_\alpha}{I} \tag{15}$$

An additional validity condition for the above approximations is that they should satisfy the inequality

$$\left|p_{\varphi_1} p_{\varphi_2}\right| \gg \left|p_z (p_{\varphi_1} + p_{\varphi_2})\right| \quad \text{or} \quad \omega_\varphi \gg \left|2\zeta_\varphi p_z\right|$$

Furthermore, if $\bar{M}_\alpha$ is positive (statically unstable vehicle) and satisfies

$$\left|\frac{\bar{M}_\alpha}{I}\right| \gg \left[\frac{\bar{N}_\alpha}{MV_N} + \frac{M_{\dot{\varphi}}}{IV_N} + \frac{\bar{g}}{V_N}\right]^2$$

the two real φ roots are approximated by

$$p_{\varphi_1} = -\sqrt{\frac{\bar{M}_\alpha}{I}} + \frac{1}{2}\left(\frac{\bar{N}_\alpha}{MV_N} + \frac{M_{\dot{\varphi}}}{IV_N} + \frac{\bar{g}}{V_N}\right) \tag{16}$$

$$p_{\varphi_2} = \sqrt{\frac{\bar{M}_\alpha}{I}} + \frac{1}{2}\left(\frac{\bar{N}_\alpha}{MV_N} + \frac{M_{\dot{\varphi}}}{IV_N} + \frac{\bar{g}}{V_N}\right) \tag{17}$$

C. SLOSH AND BENDING MODES

The derivation of coupled approximations for the three slosh and first bending modes of Model Vehicle No. 2 is a complex task because of

the very small frequency separations among these four modes. As a first step in studying the coupling, some of the modal response ratios will be examined.

If a single second-order characteristic mode of the vehicle could be excited by itself, then all the dependent variables would be damped sinusoidal functions of time. The modal response ratios for this mode are a set of complex numbers (magnitudes and phase angles). The magnitudes are the ratios of the envelopes of the sinusoidal oscillations for any two variables; the angle indicates the relative phasing between the two variables. Thus, the modal response ratios (MRR) indicate the relative amount of each variable which is present in each mode; this, in turn, indicates which coupling terms are the most significant.*

Some of the MRR for the Max Q and BO conditions are listed in Table I. Examination of the table provides clues as to which modes are not so strongly coupled. The results also show that the labels "ith bending mode" or "jth slosh mode" are somewhat misleading** as each mode has significant contributions from several variables. In fact, for the Max Q condition the "first" slosh mode has more motion of the second slosh mass than the first slosh mass; the "second" slosh mode has more motion of the first slosh mass than the second.

The most significant conclusions to be drawn from the MRR of Table I are that there is extreme coupling among the slosh masses, strong coupling between the slosh masses and the bending degrees of freedom, but weak coupling among the bending degrees of freedom. The mechanisms which produce these couplings are discussed next.

---

*The reader is cautioned to distinguish between the terms "slosh mode," "slosh mass," and "slosh frequency." Each slosh mode is comprised of contributions from all the degrees of freedom and, hence, is a coupled phenomenon. The motions of the slosh masses are dominant in the slosh modes, however the rigid-body and bending contributions may be important.

**The slosh modes were numbered in the order of increasing frequency before the MRR were computed.

TABLE I

MODAL RESPONSE RATIOS

(a) Max Q

MODE	MODAL FREQ. (rad/sec)	$\left\lvert \frac{Z}{\eta_1} \right\rvert$	$\left\lvert \frac{\varphi}{\eta_1} \right\rvert$ (rad/m)	$\left\lvert \frac{z_{s_1}}{\eta_1} \right\rvert$	$\left\lvert \frac{z_{s_2}}{\eta_1} \right\rvert$	$\left\lvert \frac{z_{s_3}}{\eta_1} \right\rvert$	$\left\lvert \frac{\eta_2}{\eta_1} \right\rvert$	$\left\lvert \frac{\eta_3}{\eta_1} \right\rvert$	$\left\lvert \frac{\eta_4}{\eta_1} \right\rvert$
First slosh	2.750	0.308^{+}	0.00066^{*}	34.9^{-}	38.3^{+}	23.2^{-}	0.984^{-}	0.498^{-}	0.0275^{-}
Second slosh	3.047	2.34^{+}	0.0785^{-}	21.8^{-}	13.4^{-}	5.33^{-}	$0.0126^{\dagger}$	0.0276^{+}	0.00753^{+}
Third slosh	3.131	0.138^{+}	0.00743^{-}	4.87^{-}	0.955^{-}	5.19^{+}	0.231^{-}	0.0240^{+}	0.00193^{+}
First bending	2.234	0.129^{+}	0.00258^{-}	1.26^{+}	0.0408^{-}	1.31^{-}	0.071^{-}	0.0202^{-}	0.00434^{-}
Second bending	6.022	0.0908^{+}	0.00976^{-}	4.36^{-}	2.14^{+}	3.49^{+}	5.24^{+}	0.545^{-}	0.00551^{-}
Third bending	9.944	1.16^{+}	0.0405^{-}	36.8^{-}	39.7^{+}	31.9^{-}	9.99^{+}	66.5^{+}	4.41^{-}
Fourth bending	12.89	6.07^{-}	0.127^{-}	73.6^{+}	108^{-}	187^{+}	8.60^{-}	69.1^{-}	110^{-}
(b) Burnout									
First slosh	3.680			15.7^{-}	10.1^{+}	0.156^{-}	0.118^{-}		
Second slosh	4.027			5.21^{-}	5.72^{-}	0.045^{-}	0.146^{-}		
Third slosh	4.951			2.52^{+}	2.10^{+}	8.26^{+}	0.998^{-}		
First bending	3.409			7.54^{+}	1.99^{+}	0.148^{-}	0.0659^{-}		
Second bending	7.419			4.26^{-}	1.74^{-}	1.57^{+}	2.73^{+}		

$^{+}$Phase is approximately zero

$^{-}$Phase is approximately 180°

*Phase not determined

†Phase equals 106°

The spring mass analogy for fuel slosh will be used to visualize the nature of the coupled sloshing and first bending modes. Figure 4 represents the four types of motion involved. The MRR, $|z_{si}/\eta_1|$, of the first slosh mode for Max Q indicate an oscillation of type "A" shown in Fig. 4a.* The forces introduced by the upper and lower slosh masses tend to balance those of the middle slosh mass so there is relatively little motion of the main mass, M_m; the coupled frequency should be very near the uncoupled frequency of the first or second slosh mass (the actual difference is less than 1 percent).

In the second slosh mode the three slosh masses vibrate together and are opposed by the motion of the main mass (see Fig. 4b). The motion of the main mass increases the frequency above that of the uncoupled value.

The third slosh mode is primarily the first and third slosh masses vibrating in opposition, the coupling arising through the first bending mode (see Fig. 4c). For the upper and lower masses, the bending and slosh motions oppose each other, i.e., the bending tends to reduce the motion of the slosh masses relative to inertial space. This should increase the frequency of this slosh mode and it actually does.

The first bending mode is similar to the third slosh mode, except that the phasing of the slosh and bending motions is reversed (Fig. 4d). This should decrease the frequency of the first bending mode and it does.

Note that the slosh–bending cross-coupling illustrated by modes "C" and "D" increases the frequency separation between those two modes.

The situation at burnout is somewhat different because there is a moderate separation of the uncoupled frequency of the third slosh mass from that for the first or second slosh mass. The third slosh mass is also an order of magnitude larger than the other two. From Table Ib we see that, in the first slosh mode, the first and second masses are vibrating in opposition (mode "A"). In the second they are vibrating in unison,

*In Figure 4 the main mass, M_m, represents the entire booster less slosh masses.

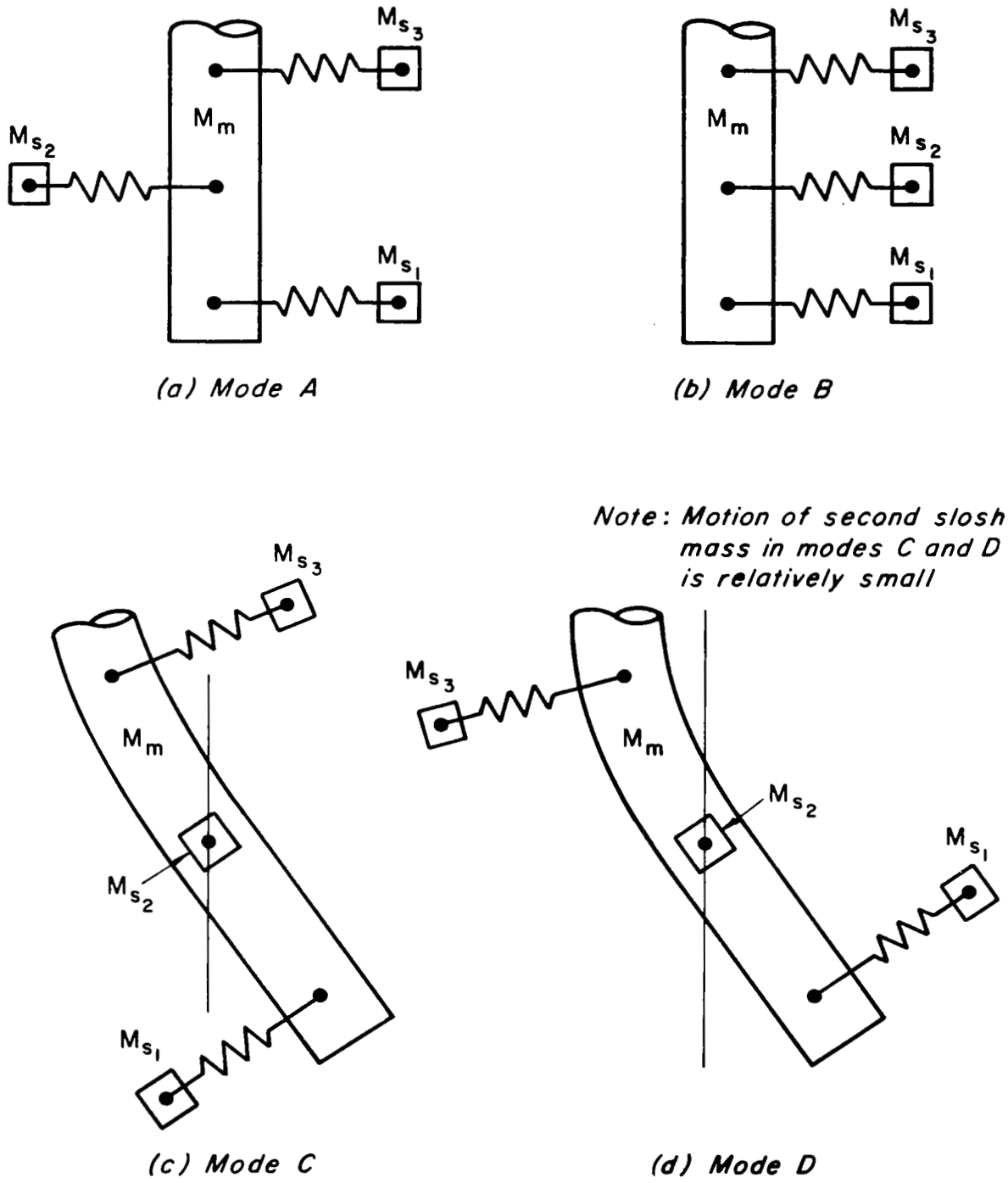

Figure 4. Spring Mass Model for Three Slosh and First Bending Modes

presumably against the main mass of the vehicle (mode "B"). The third mode is primarily an oscillation of the third slosh mass.

Although numerical values of the MRR were not calculated of lift-off, certain characteristics of the slosh modes can be estimated. Because the uncoupled slosh frequencies are all identical, one would expect to have a coupled mode at that frequency (the second slosh mode frequency is within 0.2 percent of the uncoupled value). In this mode the upper and lower masses oppose the middle mass (mode "A") and there should be little motion of the vehicle.

We would also predict a higher frequency mode in which the three slosh masses vibrate together against the main mass (mode "B"). This should correspond to the third slosh mode since it is the only slosh mode that increases in frequency. The remaining slosh modes are probably the upper two opposing the lower slosh mass with coupling through the first bending mode.* Since the uncoupled slosh frequency is less than the uncoupled first bending mode frequency, we would expect the coupling to reduce the slosh frequency (mode "D") and increase the bending frequency (mode "C"). This result is shown in Appendix D.

Having learned something of the characteristics of the slosh modes, we will now develop an approximate model to accurately predict the coupled frequencies. The slosh modes couple indirectly through the finite inertia of the vehicle and directly through the first bending mode; therefore as a first approximation we use the three slosh and the first bending modes with a dynamic correction for the rigid-body modes. As shown in Appendix D the resultant characteristic equation can be written:

*The lower node of the first bending mode is approximately midway between the first and second slosh masses for this flight condition.

$$\begin{vmatrix} s^2\left(1 - M_{s_1}a_{11}\right) + 2\zeta_{s_1}\omega_{s_1}s + \omega_{s_1}^2 & -M_{s_2}a_{12}s^2 & -M_{s_3}a_{13}s^2 & Y_1\left(x_{s_1}\right)s^2 \\ -M_{s_1}a_{12}s^2 & s^2\left(1 - M_{s_2}a_{22}\right) + 2\zeta_{s_2}\omega_{s_2}s + \omega_{s_2}^2 & -M_{s_3}a_{23}s^2 & Y_1\left(x_{s_2}\right)s^2 \\ -M_{s_1}a_{13}s^2 & -M_{s_2}a_{23}s^2 & s^2\left(1 - M_{s_3}a_{33}\right) + 2\zeta_{s_3}\omega_{s_3}s + \omega_{s_3}^2 & Y_1\left(x_{s_3}\right)s^2 \\ \frac{M_{s_1}}{M_1}Y_1\left(x_{s_1}\right)s^2 & \frac{M_{s_2}}{M_1}Y_1\left(x_{s_2}\right)s^2 & \frac{M_{s_3}}{M_1}Y_1\left(x_{s_3}\right)s^2 & s^2 + 2\overline{\zeta_1\omega_1}s + \overline{\omega}_1^2 \end{vmatrix} = 0 \quad (18)$$

where

$$a_{ij} = \frac{1}{M} + \frac{l_{s_i}l_{s_j}}{I} \quad (19)$$

The a_{ij}'s are coupling parameters, which result from the rigid-body dynamic correction, and are in some aspects similar to structural influence coefficients. If a unit force is applied to a rigid body at a point l_{s_i} from the c.g., the linear acceleration at a point l_{s_j} from the c.g. is given by a_{ij}. The a_{ij}'s, like influence coefficients, are symmetrical, i.e., $a_{ij} = a_{ji}$.

The center-of-percussion concept plays a key role here. If one slosh mass is located at the center of percussion with respect to the location of a second slosh mass ($l_{s_i}l_{s_j} = -I/M$), then the cross-coupling between these two masses is zero ($a_{ij} = 0$). The greater the separation between the slosh mass and the center of percussion, the greater the coupling.

The errors obtained with the approximation of Eq. 18 are tabulated in Table D-I. The worst error is only 3.6 percent (the first bending mode frequency at LO), but in several instances the slosh errors are greater than 1 percent. As noted in the "Introduction," these errors may be unacceptable if pole–zero sequence is of prime importance. In this event, the following refinements must be included.

It can be determined from the modal response coefficients and the magnitudes of the terms in the equations of motion that a correction for static effects of the higher bending modes should be added to Eq. 18. Consequently a static correction for the second bending mode was included. This gave satisfactory results with two expections — first bending mode at LO and third slosh mode at BO. Adding a static correction for the third bending mode gave good results for the LO case. The problem with the third slosh mode at BO will be treated in the last portion of this section.

With a static correction for the second and third bending modes, the characteristic equation can be written as:

$$\left|\begin{array}{cccc|cc} & & & & 0 & 0 \\ & S_4 & & & 0 & 0 \\ & & & & 0 & 0 \\ & & & & c_{12} & c_{13} \\ \hline \dfrac{M_{s_1}Y_2(x_{s_1})s^2}{M_2\bar{\omega}_2^2} & \dfrac{M_{s_2}Y_2(x_{s_2})s^2}{M_2\bar{\omega}_2^2} & \dfrac{M_{s_3}Y_2(x_{s_3})s^2}{M_2\bar{\omega}_2^2} & \dfrac{c_{21}}{\bar{\omega}_2^2} & 1 & \dfrac{c_{23}}{\bar{\omega}_2^2} \\ \dfrac{M_{s_1}Y_3(x_{s_1})s^2}{M_3\bar{\omega}_3^2} & \dfrac{M_{s_2}Y_3(x_{s_2})s^2}{M_3\bar{\omega}_3^2} & \dfrac{M_{s_3}Y_3(x_{s_3})s^2}{M_3\bar{\omega}_3^2} & \dfrac{c_{31}}{\bar{\omega}_3^2} & \dfrac{c_{32}}{\bar{\omega}_3^2} & 1 \end{array}\right| = 0 \qquad (20)$$

where*

S_4 is the 4-by-4 matrix of Eq. 18

$$c_{ij} = \frac{1}{M_i}\left[-N\eta_{ij} + \bar{g}M_E l_E Y_i'(x_\beta)Y_j'(x_\beta) - \underline{\bar{g}MY_i(x_\beta)Y_j'(x_\beta)}\right] \qquad (21)$$

*The underlined term may be omitted, as discussed on page 10.

Equation 20 is easily reduced* to a 4-by-4 determinant which is identical to Eq. 18 except for the last row (the first bending mode equation). The reduced 4-by-4 determinant then contains static corrections to the first bending mode equation for the second and third bending modes.

Let us now consider the higher (second, third, and fourth) bending modes. Appendix D shows that the diagonal terms in the equations of motion always underestimate the higher bending mode frequencies with errors as large as 6.5 percent. From the MRR and the equations of motion we find that this is primarily due to an inertial coupling with the slosh masses. Therefore a dynamic correction should be applied to each higher bending mode for the slosh masses. This gives the approximation:

$$\begin{vmatrix} s^2 & 0 & 0 & s^2 Y_i(x_{s_1}) \\ 0 & s^2 & 0 & s^2 Y_i(x_{s_2}) \\ 0 & 0 & s^2 & s^2 Y_i(x_{s_3}) \\ \dfrac{M_{s_1} Y_i(x_{s_1}) s^2}{M_i} & \dfrac{M_{s_2} Y_i(x_{s_2}) s^2}{M_i} & \dfrac{M_{s_3} Y_i(x_{s_3}) s^2}{M_i} & s^2 + 2\overline{\zeta_i \omega_i} s + \overline{\omega}_i^2 \end{vmatrix} = 0 \qquad (22)$$

which reduces to the following characteristic equation for the ith bending mode:

$$\frac{1}{M_i}\left[M_i - M_{s_1} Y_i^2(x_{s_1}) - M_{s_2} Y_i^2(x_{s_2}) - M_{s_3} Y_i^2(x_{s_3})\right] s^2 + 2\overline{\zeta_i \omega_i} s + \overline{\omega}_i^2 = 0 \qquad (23)$$

Physically, Eq. 23 amounts to removing the slosh masses from the ith mode generalized mass. That is, the uncoupled solution treats the bending mode

*Equation 20 is first reduced to a 5-by-5 by multiplying the last row by c_{13} and subtracting it from the fourth row, then multiplying the last row by $c_{23}/\overline{\omega_2}$ and subtracting it from the fifth row. A similar operation on the fifth row of the reduced matrix will lower it to a 4-by-4. To correct only for the second bending mode, one simply starts with the first five rows and columns of Eq. 20.

frequency as if the slosh masses were rigidly attached to the vehicle so that they followed the bending motions exactly ($z_{s_j} = 0$). But in the actual case, the higher bending mode frequencies are greater than the slosh frequencies so the slosh masses tend to remain fixed in inertial space $\left[z_{s_j} \doteq -Y_i(x_{s_j})\eta_i\right]$. Equation 23 is equivalent to completely disconnecting the slosh masses from the vehicle and should therefore give good results as long as the slosh frequencies are substantially less than the bending frequencies.

The actual errors obtained from using Eq. 23 are listed in Appendix D. Except for the second bending mode at BO, the frequency errors are all less than 2 percent. The relatively poor accuracy for the second bending mode at BO is not really surprising since its frequency is only 50 percent greater than that of the third slosh mode, which also has a significant error as noted earlier. The coupling of these two modes is discussed next.

From the MRR of Table Ib we see that at BO both the first and second bending modes have considerable coupling with the third slosh mode. To approximate this effect the characteristic equation need only contain rigid-body, third slosh mass, plus first and second bending. The first and second slosh masses are a factor of ten less than the third and are neglected. The resultant characteristic equation can be written:

$$\begin{vmatrix} 1 & 0 & \frac{M_{s_3}}{M}s^2 & 0 & 0 \\ 0 & 1 & \frac{M_{s_3}l_{s_3}}{I}s^2 & 0 & 0 \\ 1 & l_{s_3} & s^2 + 2\zeta_{s_3}\omega_{s_3}s + \omega^2 & Y_1(x_{s_3})s^2 & Y_2(x_{s_3})s^2 \\ 0 & 0 & \frac{M_{s_3}Y_1(x_{s_3})}{M_1}s^2 & s^2 + 2\overline{\zeta_1\omega_1}s + \overline{\omega_1^2} & c_{12} \\ 0 & 0 & \frac{M_{s_3}Y_2(x_{s_3})}{M_2}s^2 & c_{21} & s^2 + 2\overline{\zeta_2\omega_2}s + \overline{\omega_2^2} \end{vmatrix} = 0 \quad (24)$$

This can be reduced to

$$\begin{vmatrix} \left(1 - \frac{M_{s_3}}{M} - \frac{M_{s_3} l_{s_3}^2}{I}\right)s^2 + 2\zeta_{s_3}\omega_{s_3}s + \omega_{s_3}^2 & Y_1(x_{s_3})s^2 & Y_2(x_{s_3})s^2 \\ \frac{M_{s_3} Y_1(x_{s_3})}{M_1} s^2 & s^2 + 2\overline{\zeta_1}\omega_1 s + \overline{\omega}_1^2 & c_{12} \\ \frac{M_{s_3} Y_2(x_{s_3})}{M_2} s^2 & c_{21} & s^2 + 2\overline{\zeta_2}\omega_2 s + \overline{\omega}_2^2 \end{vmatrix} = 0 \quad (25)$$

The characteristic roots obtained from Eq. 25 are listed in Appendix D.

The above equations considerably improve approximation of the third slosh and second bending modes, with errors reduced to 0.7 and 1.4 percent, respectively. The frequency approximation for the first bending mode has a large, 5.8 percent, error but a good approximation for it was found previously. This error is apparently due to neglecting the first and second slosh masses. The addition of these two should give an accurate, albeit complex, approximation for all five modes simultaneously.

Let us now briefly review the results of the slosh and bending mode approximations derived above. For slosh and first bending modes the 4-by-4 determinant (Eq. 18) provides gross corrections (error less than 3.6 percent) for direct slosh–bending inertial coupling and indirect slosh–slosh inertial coupling through the rigid-body modes. The accurate (error less than or equal to 1 percent) determination of coupled slosh and first bending mode frequencies at LO and Max Q requires the addition of static corrections for the second bending mode (at LO a static correction for the third bending mode must also be included). The BO condition is somewhat more complicated because of the proximity of the third slosh and second bending mode frequencies. The error for the third slosh can be reduced to 0.7 percent by considering the third slosh mass plus the

first and second bending modes (Eq. 25); this also gives the second bending mode frequency within 1.4 percent error.

The second, third, and fourth (or third and fourth at BO) bending mode frequencies can be accurately approximated by simply including the complete diagonal term (self-couplings) and applying a dynamic correction for the slosh masses.

D. ACTUATOR MODES

The first-order lag due to the actuator and the second-order mode due to the actuator–nozzle compliance are considered next. Two of the three approximations for these modes derived in Appendix E are presented here. The simplest one gives literal expressions for the three modes, i.e.,

$$p_a \doteq \frac{K_1}{A} \tag{26}$$

$$2\zeta_a\omega_a \doteq 2\zeta_E\omega_E + \frac{K_L}{A}\left(\frac{\frac{K_0K_3}{A} - K_1}{K_0 + K_L}\right) \tag{27}$$

$$\omega_a^2 \doteq \omega_E^2 \frac{K_0}{K_0 + K_L} \tag{28}$$

where A is effective actuator area

K_0 is effective hydraulic spring constant

K_1 is actuator open-loop gain

K_3 is valve pressure feedback gain

K_L is effective spring constant of actuator–nozzle compliance

ζ_E is uncoupled damping ratio of actuator–nozzle compliance

ω_E is uncoupled natural frequency of actuator–nozzle compliance

The maximum error in the first-order lag is 3.6 percent and is 10.3 percent for the second-order frequency. This level of accuracy is adequate for most design purposes if there is wide frequency separation between the compliance and bending modes.

A more more accurate approximation was derived primarily to reduce the adverse effect the above errors have on the approximation for the denominator lead coefficient, A_Δ. This approximation consists of the lower right 2-by-2 submatric of Fig. 3 with dynamic corrections for the rigid-body and bending modes, i.e.,

$$\begin{vmatrix} \left\{1 - \frac{C}{I_E}\left[\frac{(M_E l_E)^2}{M} + \frac{(I_E - M_E l_E l_\beta)^2}{I} + \sum_i \frac{1}{M_i}\left(I_E Y_i'(x_\beta) - M_E l_E Y_i(x_\beta)\right)^2\right]\right\} s^2 & -\omega_E^2 \\ + 2\zeta_E \omega_E s + \omega_E^2 + \frac{\bar{g} M_E l_E}{I_E} & \\ \frac{-AK_L}{K_0} s - \frac{K_3 K_L}{A} & \frac{A(K_0 + K_L)}{K_0} s + K_1 + \frac{K_3 K_L}{A} \end{vmatrix} = 0 \quad (29)$$

The application of Eq. 29 reduces the maximum actuator and compliance approximation errors to 2.7 percent for p_a and 1.7 percent for ω_a.

E. LEAD COEFFICIENT, A_Δ

The lead coefficient for the denominator, coefficient of s^{20}, can be approximated by simply multiplying the lead coefficients from the approximations for the various roots,* i.e.,

$$A_\Delta \doteq \left[\text{Lead coefficient of 3 slosh} + \eta_1 \text{ characteristic equation (Eq. 20)}\right]$$

$$\times \left[\prod_{i=2}^{4}\left(1 - \frac{M_{s_1} Y_i^2(x_{s_1})}{M_i} - \frac{M_{s_2} Y_i^2(x_{s_2})}{M_i} - \frac{M_{s_3} Y_i^2(x_{s_3})}{M_i}\right)\right]\left[\frac{A(K_0 + K_L)}{K_0}\right]$$

$$\times \left[1 - \frac{C}{I_E}\left(\frac{(M_E l_E)^2}{M} + \frac{(I_E - M_E l_E l_\beta)^2}{I} + \sum_{i=1}^{4} \frac{\left(I_E Y_i'(x_\beta) - M_E l_E Y_i(x_\beta)\right)^2}{M_i}\right)\right] \quad (30)$$

*Lead coefficient from rigid-body modes is unity.

The comparison of exact and approximate values is given below.* The maximum error of 2.8 percent is certainly acceptable.

	Lift-Off	Max Q	Burnout
A_Δ (exact).....	46.51	35.51	38.75
A_Δ (approximation).....	46.57	36.49	39.71
Percent error.....	+0.1	+2.8	+2.5

*The units of A_Δ are $(\text{meters})^2$.

SECTION IV

NUMERATOR APPROXIMATIONS

The previous section dealt with the approximations for the transfer function denominator. This section presents the approximations for the numerators for some of the motion variables. Complete approximations are presented for the φ and η_i numerators as these variables are the only ones which affect the motion sensed by a position or rate gyro. An accelerometer or angle of attack vane is also sensitive to $\dot{Z}$. Since these sensors are normally used in low bandwidth load relief loops, only the approximations for the low frequency (rigid-body) zeros of the $\dot{Z}$ numerator are presented. Approximations for the higher frequency zeros could be developed by applying the same techniques used for the φ numerator.

The discussion of numerator approximations will proceed in a manner similar to that used for the denominator. The tail-wags-dog zeros are considered first, then the rigid-body zeros, the slosh and bending zeros, and finally the numerator lead coefficients. This discussion sequence is shown in the following flow chart.

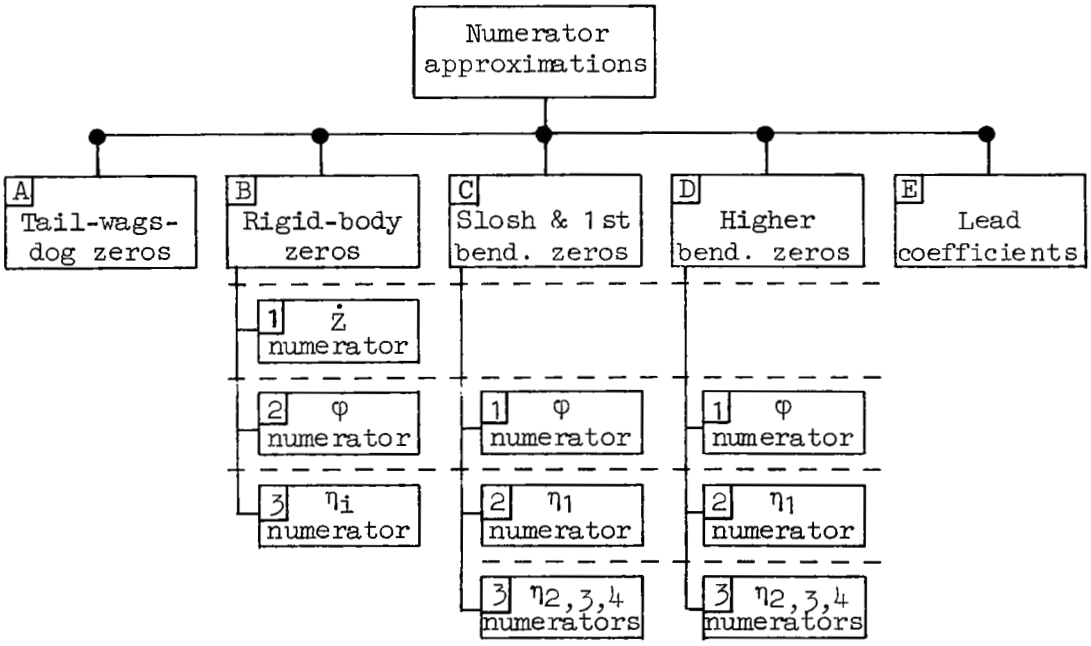

Before delving into the numerator approximations, let us briefly review the forms the numerators will take. For the example vehicle all numerators (except $\dot{Z}$) will be of seventeenth-order. Identifying the zeros with the poles they must closely resemble and adding the tail-wags-dog effect, the 17 zeros are:

Tail-wags-dog.....	2
Rigid-body.....	3
Three second-order slosh.....	6
Four second-order bending.....	8
	19
Less second-order for particular numerator variable.....	−2
	17

Two zeros are subtracted because the φ numerator does not contain φ zeros, the η_1 numerator does not contain η_1 zeros, etc. In each numerator the missing zeros are replaced by the tail-wags-dog pair. Thus the transfer function for φ, z_{s_j}, or η_i is composed of tail-wags-dog zeros divided by the second-order mode (poles) in which the variable is dominant; one first-order and seven second-order nearly canceling pole–zero combinations; plus the three poles from the actuator lag and actuator–nozzle compliance. For example, the φ/β_c transfer function at Max Q is:

$$\frac{\varphi}{\beta_c} = \underbrace{\frac{-1054}{35.51}}_{\text{Gain}} \times \underbrace{\frac{s^2 + 2(-0.00005)(24.64)s + (24.64)^2}{(s - 0.2786)(s + 0.3644)}}_{\text{Tail-wags-dog zeros and } \varphi \text{ mode poles}} \times \underbrace{\frac{s + 0.01369}{s - 0.04202}}_{\text{Z mode}}$$

$$\times \underbrace{\frac{s^2 + 2(0.00402)(2.750)s + (2.750)^2}{s^2 + 2(0.00498)(2.750)s + (2.750)^2}}_{\text{First slosh mode}} \times \underbrace{\frac{s^2 + 2(0.00528)(2.764)s + (2.764)^2}{s^2 + 2(0.00571)(3.047)s + (3.047)^2}}_{\text{Second slosh mode}} \times \underbrace{\frac{s^2 + 2(0.00646)(3.081)s + (3.081)^2}{s^2 + 2(0.00870)(3.131)s + (3.131)^2}}_{\text{Third slosh mode}}$$

$$\times \underbrace{\frac{s^2 + 2(0.0220)(2.142)s + (2.142)^2}{s^2 + 2(0.0141)(2.234)s + (2.234)^2}}_{\text{First bending mode}} \times \underbrace{\frac{s^2 + 2(0.00696)(5.783)s + (5.783)^2}{s^2 + 2(0.00838)(6.022)s + (6.022)^2}}_{\text{Second bending mode}}$$

$$\times \underbrace{\frac{s^2 + 2(0.00829)(9.795)s + (9.795)^2}{s^2 + 2(0.00712)(9.944)s + (9.944)^2}}_{\text{Third bending mode}} \times \underbrace{\frac{s^2 + 2(0.00624)(12.98)s + (12.98)^2}{s^2 + 2(0.00639)(12.89)s + (12.89)^2}}_{\text{Fourth bending mode}}$$

$$\times \underbrace{\frac{1}{s + 14.52}}_{\text{Actuator lag}} \times \underbrace{\frac{1}{s^2 + 2(0.0986)(47.53)s + (47.53)^2}}_{\text{Actuator–nozzle compliance}} \qquad (31)$$

The $\dot{Z}$ numerator is eighteenth-order because the first-order Z mode (gravity turn) term is replaced by the second-order tail-wags-dog zeros.

It is to be noted that the 11-by-11 matrix of Fig. 3 can be reduced to a 9-by-9 matrix in obtaining the rigid-body, slosh, or bending mode numerators. That is, the β_c column is zero except for the last row, while the β_a column is zero except for the last two rows; thus the numerator determinant for $\dot{Z}$, φ, z_{s_j}, and η_i reduces to a 9-by-9 determinant multiplied by $K_1\omega_E^2$. The same 9-by-9 would be obtained if the last two rows plus the β_a and β_c columns were eliminated and β considered to be the input. Looking at it in another way, the 9-by-9 is the first nine rows and columns of the complete matrix with the negative of the β column substituted for the variable of interest. Throughout the remainder of this section we will deal only with the 9-by-9 determinants.

A. TAIL-WAGS-DOG ZEROS

It is well known that the tail-wags-dog effect results from the inertial reaction forces due to swiveling the control engines. These inertial reaction terms appear in the s^2 coefficients of the β column. We therefore approximate the TWD zeros by taking the appropriate term from the β column, i.e., for the φ numerator,

$$\omega_{TWD} \doteq \sqrt{\frac{\frac{T}{F}\, l_\beta - \bar{g}M_E l_E}{M_E l_E l_\beta - I_E}} \tag{32}$$

for the η_i numerator,

$$\omega_{TWD} \doteq \sqrt{\frac{\frac{T}{F}\, Y_i(x_\beta) - \bar{g}M_E l_E Y_i'(x_\beta)}{M_E l_E Y_i(x_\beta) - I_E Y_i'(x_\beta)}} \tag{33}$$

and

$$\zeta_{TWD} \doteq 0 \tag{34}$$

These approximations are exceptionally accurate in the φ and η_i numerators at all three flight conditions. The frequency errors are less than 0.3 percent except for a 1 percent error in the η_4 numerator at BO. In all cases the exact damping ratio is within the narrow range $-0.87 \times 10^{-4} \leq \zeta_{TWD} \leq 0.74 \times 10^{-4}$.

B. RIGID-BODY ZEROS

1. $\dot{Z}$ Numerator

For the $\dot{Z}$ numerator, the rigid-body mode is represented by a pair of zeros, z_{φ_1} and z_{φ_2}. As shown in Appendix F, it is only necessary to include the $\dot{Z}$ and φ equations with static correction terms for the first bending mode coupling. This gives a characteristic equation of

$$\begin{vmatrix} 1 & \frac{N_{\dot{\varphi}}}{MV_N}s - \bar{g} - \frac{N_\alpha}{M} & -\bar{g}Y_1'(x_\beta) - \frac{N_{\eta_1}}{M} \\ \frac{Ml_\beta}{I} & s^2 + \frac{M_{\dot{\varphi}}}{IV_N}s - \frac{M_\alpha}{I} & \frac{-M_{\eta_1} + \bar{g}M\left[Y_1(x_\beta) - l_\beta Y_1'(x_\beta)\right]}{I} \\ \frac{MY_1(x_\beta)}{M_1\bar{\omega}_1^2} & \frac{-N_{\dot{\eta}_1}}{M_1\bar{\omega}_1^2} & 1 \end{vmatrix} = 0 \quad (35)$$

Note that in Eq. 35 only the thrust portions of the static terms in the β column have been retained, and that the β column and η_1 row have been normalized to provide unity values in the main diagonal. Similar normalization will be employed throughout the remainder of this section to avoid confusion in the expressions for the numerator lead coefficients.

Equation 35 results in rigid-body approximations within 5 percent of exact values. Since these zeros are relatively well separated from any vehicle poles, this approximation is considered adequate.

2. φ Numerator

The φ numerator has a first-order rigid-body zero at very low frequency; the maximum value for Model Vehicle No. 2 is 0.014 sec^{-1}. This zero is approximated within 2.5 percent by

$$z_z \doteq \frac{1}{MV_N}\left(N_\alpha - \frac{M_\alpha}{l_\beta}\right) \quad (36)$$

3. η_1 Numerators

At LO the three rigid-body zeros of all the η_i numerators are at the origin because:

- The constant terms in the $\dot{Z}$ column are zero
- The constant terms in the φ column are equal to $-\bar{g}$ times the s terms in the $\dot{Z}$ column
- The s terms in the φ column are zero

For the η_1 numerator at other flight conditions it is only necessary to include the rigid-body equations and the static effects of η_1, i.e.,

$$\begin{vmatrix} s + \frac{N_\alpha}{MV_N} & \frac{N_{\dot{\varphi}}}{MV_N} s - \bar{g} - \frac{N_\alpha}{M} & \frac{M_1}{MY_1(x_\beta)} \\ \frac{M_\alpha}{IV_N} & s^2 + \frac{M_{\dot{\varphi}}}{IV_N} s - \frac{M_\alpha}{I} & \frac{M_1 l_\beta}{IY_1(x_\beta)} \\ \frac{N\dot{\eta}_1}{M_1 V_N} & \frac{-N\dot{\eta}_1}{M_1} & 1 \end{vmatrix} = 0 \qquad (37)$$

For the η_2, η_3, and η_4 numerators at Max Q it is necessary to add a static correction of the first bending mode. This gives the characteristic equation for the rigid-body zeros:

$$\begin{vmatrix} s + \frac{N_\alpha}{MV_N} & \frac{N_{\dot{\varphi}}}{MV_N} s - \bar{g} - \frac{N_\alpha}{M} & -\bar{g}Y_1'(x_\beta) - \frac{N_{\eta_1}}{M} & \frac{M_i}{MY_i(x_\beta)} \\ \frac{M_\alpha}{IV_N} & s^2 + \frac{M_{\dot{\varphi}}}{IV_N} s - \frac{M_\alpha}{I} & -M_{\eta_1} + \bar{g}M\left[Y_1(x_\beta) - l_\beta Y_1'(x_\beta)\right] & \frac{M_i l_\beta}{IY_i(x_\beta)} \\ \frac{N\dot{\eta}_1}{M_1 V_N \bar{\omega}_1^2} & \frac{-N\dot{\eta}_1}{M_1 \bar{\omega}_1^2} & 1 & \frac{M_i Y_1(x_\beta)}{M_1 Y_i(x_\beta)\bar{\omega}_1^2} \\ \frac{N\dot{\eta}_i}{M_i V_N} & \frac{-N\dot{\eta}_i}{M_i} & c_{i1} & 1 \end{vmatrix} = 0 \qquad (38)$$

where $i = 2, 3, 4$

At BO the static correction for the first bending mode is small because the M_{η_i}, N_{η_i}, and $N_{\dot{\eta}_i}$ were assumed zero in the exact solution. The main source of coupling is the third slosh mass (the other two are very small). Addition of the third slosh mass static correction gives the characteristic equation (note in this case that it was found to be important to retain the s and $l_{s_3}s^2$ terms in the slosh equation):

$$\begin{vmatrix} s + \frac{N_\alpha}{MV_N} & \frac{N_{\dot{\varphi}}}{MV_N}s - \bar{g} - \frac{N_\alpha}{M} & 0 & \frac{M_i}{MY_i(x_\beta)} \\ \frac{M_\alpha}{IV_N} & s^2 + \frac{M_{\dot{\varphi}}}{IV_N}s - \frac{M_\alpha}{I} & \frac{-\bar{g}M_{s_3}}{I} & \frac{M_i l_\beta}{IY_i(x_\beta)} \\ \frac{s}{\omega_{s_3}^2} & \frac{1}{\omega_{s_3}^2}\left(l_{s_3}s^2 - \bar{g}\right) & 1 & 0 \\ \frac{N_{\dot{\eta}_i}}{M_i V_N} & \frac{-N_{\dot{\eta}_i}}{M_i} & \frac{-gM_{s_3}Y_i'(x_{s_3})}{M_i} & 1 \end{vmatrix} = 0 \quad (39)$$

where $i = 2, 3, 4$

Using Eqs. 37 – 39 as applicable, the maximum error in the rigid-body zeros of the η_i numerators is an acceptable 8 percent. A complete tabulation of errors is given in Appendix F.

C. SLOSH AND FIRST BENDING ZEROS

1. φ Numerator

The situation for the slosh and first bending zeros of the φ numerator is similar to that for the slosh and first bending mode poles. As shown in Appendix G, it is generally necessary to construct the characteristic equation from the slosh and first bending equations with a dynamic correction for $\dot{Z}$ and a static correction for the second bending mode. The characteristic equation can then be written as Eq. 40.

$$
\begin{vmatrix}
\left[1 + \frac{M_{s_1}}{M}\left(\frac{l_{s_1}}{l_\beta} - 1\right)\right]s^2 + 2\zeta_{s_1}\omega_{s_1}s + \omega_{s_1}^2 & \frac{M_{s_2}}{M}\left(\frac{l_{s_2}}{l_\beta} - 1\right)s^2 & \frac{M_{s_3}}{M}\left(\frac{l_{s_3}}{l_\beta} - 1\right)s^2 & Y_1(x_{s_1})s^2 & 0 \\
\frac{M_{s_1}}{M}\left(\frac{l_{s_1}}{l_\beta} - 1\right)s^2 & \left[1 + \frac{M_{s_2}}{M}\left(\frac{l_{s_2}}{l_\beta} - 1\right)\right]s^2 + 2\zeta_{s_2}\omega_{s_2}s + \omega_{s_2}^2 & \frac{M_{s_3}}{M}\left(\frac{l_{s_3}}{l_\beta} - 1\right)s^2 & Y_1(x_{s_2})s^2 & 0 \\
\frac{M_{s_1}}{M}\left(\frac{l_{s_1}}{l_\beta} - 1\right)s^2 & \frac{M_{s_2}}{M}\left(\frac{l_{s_2}}{l_\beta} - 1\right)s^2 & \left[1 + \frac{M_{s_3}}{M}\left(\frac{l_{s_3}}{l_\beta} - 1\right)\right]s^2 + 2\zeta_{s_3}\omega_{s_3}s + \omega_{s_3}^2 & Y_1(x_{s_3})s^2 & 0 \\
\frac{M_{s_1}}{M_1}\left[Y_1(x_{s_1}) - \frac{l_{s_1}Y_1(x_\beta)}{l_\beta}\right]s^2 & \frac{M_{s_2}}{M_1}\left[Y_1(x_{s_2}) - \frac{l_{s_2}Y_1(x_\beta)}{l_\beta}\right]s^2 & \frac{M_{s_3}}{M_1}\left[Y_1(x_{s_3}) - \frac{l_{s_3}Y_1(x_\beta)}{l_\beta}\right]s^2 & s^2 + \left[2\overline{\zeta_1\omega_1} - \frac{Y_1(x_\beta)M\dot{\eta}_1}{M_1 l_\beta V_N}\right]s + \bar{\omega}_1^2 + \frac{Y_1(x_\beta)}{M_1 l_\beta}g_1 & c_{12} + \frac{Y_1(x_\beta)}{M_1 l_\beta}g_2 \\
\frac{\frac{M_{s_1}}{M_2}\left[Y_2(x_{s_1}) - \frac{l_{s_1}Y_2(x_\beta)}{l_\beta}\right]s^2}{\bar{\omega}_2^2 + \frac{Y_2(x_\beta)}{M_2 l_\beta}g_2} & \frac{\frac{M_{s_2}}{M_2}\left[Y_2(x_{s_2}) - \frac{l_{s_2}Y_2(x_\beta)}{l_\beta}\right]s^2}{\bar{\omega}_2^2 + \frac{Y_2(x_\beta)}{M_2 l_\beta}g_2} & \frac{\frac{M_{s_3}}{M_2}\left[Y_2(x_{s_3}) - \frac{l_{s_3}Y_2(x_\beta)}{l_\beta}\right]s^2}{\bar{\omega}_2^2 + \frac{Y_2(x_\beta)}{M_2 l_\beta}g_2} & \frac{\frac{-Y_2(x_\beta)M\dot{\eta}_1 s}{M_2 l_\beta V_N} + c_{21} + \frac{Y_2(x_\beta)}{M_2 l_\beta}g_1}{\bar{\omega}_2^2 + \frac{Y_2(x_\beta)}{M_2 l_\beta}g_2} & 1
\end{vmatrix} = 0 \quad (40)
$$

where

$$
g_i = M_{\eta_i} + \bar{g}M\left[l_\beta Y_i'(x_\beta) - Y_i(x_\beta)\right] \quad (41)
$$

The most important difference between Eq. 40 and the denominator approximation is the inclusion of the g_i and $M_{\dot{\eta}_1}$ terms. These terms result from the bending inputs to the φ equation. They were not included in the denominator approximation because the diagonally opposite terms (the φ contributions to the bending equations) were only small aerodynamic terms. In the φ numerator the small aerodynamic terms are replaced by sizable ones from the β column. In other words, there is little open-loop coupling between φ and the bending modes; but with a high gain φ loop closed, there is considerable coupling because of the appreciable β inputs to the bending modes.

The frequency errors from the approximate zeros of Eq. 40 are less than 1 percent, except for the third slosh zero at BO which is 2.6 percent. The problem here is the same as for the denominator — the frequency of the third slosh zero is too close to that of the second bending zero. The remedy is also the same — use an approximation which includes the third slosh, first and second bending modes, and the dynamic effects of the rigid body. The resultant characteristic equation is:

$$\begin{vmatrix} \left[1 + \frac{M_{s_3}}{M}\left(\frac{l_{s_3}}{l_\beta} - 1\right)\right]s^2 + 2\zeta_{s_3}\omega_{s_3}s + \omega_{s_3}^2 & Y_1\left(x_{s_3}\right)s^2 & Y_2\left(x_{s_3}\right)s^2 \\ \frac{M_{s_3}}{M_1}\left[Y_1\left(x_{s_3}\right) - \frac{l_{s_3}Y_1(x_\beta)}{l_\beta}\right]s^2 & s^2 + 2\overline{\zeta_1}\omega_1 s + \overline{\omega_1^2} + \frac{Y_1(x_\beta)}{M_1 l_\beta}g_1 & 0 \\ \frac{M_{s_3}}{M_2}\left[Y_2\left(x_{s_3}\right) - \frac{l_{s_3}Y_2(x_\beta)}{l_\beta}\right]s^2 & 0 & s^2 + 2\overline{\zeta_2\omega_2}s + \overline{\omega_2^2} + \frac{Y_2(x_\beta)}{M_2 l_\beta}g_2 \end{vmatrix} = 0 \quad (42)$$

At BO the maximum frequency error for Eq. 42 is 0.2 percent.

2. η_1 Numerator

The approximation for the three slosh zeros of the η_1 numerator is a 3-by-3 characteristic equation:

$$
\begin{vmatrix}
\left\{1 + \frac{M_{s_1} Y_1(x_{s_1})}{Y_1(x_\beta)}\left[\frac{1}{M} + \frac{l_{s_1} l_\beta}{I}\right] - M_{s_1} a_{11}\right\} s^2 + 2\zeta_{s_1}\omega_{s_1} s + \omega_{s_1}^2 & \left\{\frac{Y_1(x_{s_2})}{Y_1(x_\beta)}\left[\frac{1}{M} + \frac{l_{s_1} l_\beta}{I}\right] - a_{12}\right\} M_{s_2} s^2 & \left\{\frac{Y_1(x_{s_3})}{Y_1(x_\beta)}\left[\frac{1}{M} + \frac{l_{s_1} l_\beta}{I}\right] - a_{13}\right\} M_{s_3} s^2 \\
\left\{\frac{Y_1(x_{s_1})}{Y_1(x_\beta)}\left[\frac{1}{M} + \frac{l_{s_2} l_\beta}{I}\right] - a_{12}\right\} M_{s_1} s^2 & \left\{1 + \frac{M_{s_2} Y_1(x_{s_2})}{Y_1(x_\beta)}\left[\frac{1}{M} + \frac{l_{s_2} l_\beta}{I}\right] - M_{s_2} a_{22}\right\} s^2 + 2\zeta_{s_2}\omega_{s_2} s + \omega_{s_2}^2 & \left\{\frac{Y_1(x_{s_3})}{Y_1(x_\beta)}\left[\frac{1}{M} + \frac{l_{s_2} l_\beta}{I}\right] - a_{23}\right\} M_{s_3} s^2 \\
\left\{\frac{Y_1(x_{s_1})}{Y_1(x_\beta)}\left[\frac{1}{M} + \frac{l_{s_3} l_\beta}{I}\right] - a_{13}\right\} M_{s_1} s^2 & \left\{\frac{Y_1(x_{s_2})}{Y_1(x_\beta)}\left[\frac{1}{M} + \frac{l_{s_3} l_\beta}{I}\right] - a_{23}\right\} M_{s_2} s^2 & \left\{1 + \frac{M_{s_3} Y_1(x_{s_3})}{Y_1(x_\beta)}\left[\frac{1}{M} + \frac{l_{s_3} l_\beta}{I}\right] - M_{s_3} a_{33}\right\} s^2 + 2\zeta_{s_3}\omega_{s_3} s + \omega_{s_3}^2
\end{vmatrix} = 0 \qquad (43)
$$

In the denominator approximations (Eq. 18 or 20) the slosh coupling depended on a_{ij}, which is proportional to the distance of one slosh mass from the center of percussion of a second slosh mass. In the above η_1 numerator there is an additional term, $\left[1/M + (l_{s_j} l_\beta)/I\right]$, which is proportional to the distance of a slosh mass from the center of percussion of the gimbaled engines.

As shown in Appendix G, the zeros obtained from Eq. 43 are quite accurate for all flight conditions. Only one frequency is in error by greater than 1 percent and that is the second slosh at Max Q (1.3 percent).

3. Higher Bending Numerators

The approximation for the slosh and first bending zeros of the higher bending numerators (η_2, η_3, and η_4) is quite complicated. It is necessary to include a dynamic correction for rigid-body, three slosh, and two bending modes. The characteristic equation can be reduced to a 4-by-4 which can be written as:

$$
\begin{vmatrix}
\left\{1 + \frac{M_{s_1} Y_1(x_{s_1})}{Y_1(x_\beta)}\left[\frac{1}{M} + \frac{l_{s_1} l_\beta}{I}\right] - M_{s_1} a_{11}\right\} s^2 + 2\zeta_{s_1}\omega_{s_1} s + \omega_{s_1}^2 & \left\{\frac{Y_1(x_{s_2})}{Y_1(x_\beta)}\left[\frac{1}{M} + \frac{l_{s_1} l_\beta}{I}\right] - a_{12}\right\} M_{s_2} s^2 & \left\{\frac{Y_1(x_{s_3})}{Y_1(x_\beta)}\left[\frac{1}{M} + \frac{l_{s_1} l_\beta}{I}\right] - a_{13}\right\} M_{s_3} s^2 & Y_1(x_{s_1}) s^2 \\
\left\{\frac{Y_1(x_{s_1})}{Y_1(x_\beta)}\left[\frac{1}{M} + \frac{l_{s_2} l_\beta}{I}\right] - a_{12}\right\} M_{s_1} s^2 & \left\{1 + \frac{M_{s_2} Y_1(x_{s_2})}{Y_1(x_\beta)}\left[\frac{1}{M} + \frac{l_{s_2} l_\beta}{I}\right] - M_{s_2} a_{22}\right\} s^2 + 2\zeta_{s_2}\omega_{s_2} s + \omega_{s_2}^2 & \left\{\frac{Y_1(x_{s_3})}{Y_1(x_\beta)}\left[\frac{1}{M} + \frac{l_{s_2} l_\beta}{I}\right] - a_{23}\right\} M_{s_3} s^2 & Y_1(x_{s_2}) s^2 \\
\left\{\frac{Y_1(x_{s_1})}{Y_1(x_\beta)}\left[\frac{1}{M} + \frac{l_{s_3} l_\beta}{I}\right] - a_{13}\right\} M_{s_1} s^2 & \left\{\frac{Y_1(x_{s_2})}{Y_1(x_\beta)}\left[\frac{1}{M} + \frac{l_{s_3} l_\beta}{I}\right] - a_{23}\right\} M_{s_2} s^2 & \left\{1 + \frac{M_{s_3} Y_1(x_{s_3})}{Y_1(x_\beta)}\left[\frac{1}{M} + \frac{l_{s_3} l_\beta}{I}\right] - M_{s_3} a_{33}\right\} s^2 + 2\zeta_{s_3}\omega_{s_3} s + \omega_{s_3}^2 & Y_1(x_{s_3}) s^2 \\
\left[Y_1(x_{s_1}) - \frac{Y_1(x_{s_1}) Y_1(x_\beta)}{Y_1(x_\beta)}\right]\frac{M_{s_1}}{M_1} s^2 & \left[Y_1(x_{s_2}) - \frac{Y_1(x_{s_2}) Y_1(x_\beta)}{Y_1(x_\beta)}\right]\frac{M_{s_2}}{M_1} s^2 & \left[Y_1(x_{s_3}) - \frac{Y_1(x_{s_3}) Y_1(x_\beta)}{Y_1(x_\beta)}\right]\frac{M_{s_3}}{M_1} s^2 & s^2 + 2\overline{\zeta_1}\overline{\omega_1} s + \overline{\omega}_1^2 - \frac{c_{1_1} M_1 Y_1(x_\beta)}{M_1 Y_1(x_\beta)}
\end{vmatrix} = 0 \quad (44)
$$

where $i = 2, 3, 4$

The accuracy of the zeros obtained from Eq. 44 is quite good. Out of 36 cases (four zeros x three numerators x three flight conditions) only three have errors greater than 1 percent, and all these occur in the η_4 numerator. Of these three, one is the third slosh at BO (6 percent error); this will be reduced to 0.1 percent by using a third slosh and first and second bending approximation to be given next. The other

Slosh and First Bending Zeros, Higher Bending Numerators (contd)

two errors are 2.1 and 2.2 percent; no attempt to further reduce these will be made because of the relative unimportance of the η_4 numerator.

At BO the third slosh plus first and second bending zeros for the η_4 numerator can be approximated by considering these modes with a dynamic correction for the rigid body. The characteristic equation can be written as:

$$\begin{vmatrix} \left\{1 + \frac{M_{s_3} Y_4(x_{s_3})}{Y_4(x_\beta)}\left[\frac{1}{M} + \frac{l_{s_3} l_\beta}{I}\right] - M_{s_3} a_{33}\right\} s^2 + 2\zeta_{s_3}\omega_{s_3} s + \omega_{s_3}^2 & Y_1(x_{s_3}) s^2 + \frac{c_{41} M_4}{Y_4(x_\beta)}\left[\frac{1}{M} + \frac{l_{s_3} l_\beta}{I}\right] & Y_2(x_{s_3}) s^2 + \frac{c_{42} M_4}{Y_4(x_\beta)}\left[\frac{1}{M} + \frac{l_{s_3} l_\beta}{I}\right] \\ - \frac{\bar{g} M_{s_3} Y_4'(x_{s_3})}{Y_4(x_\beta)}\left[\frac{1}{M} + \frac{l_{s_3} l_\beta}{I}\right] & & \\ \frac{M_{s_3}}{M_1}\left[Y_1(x_{s_3}) - \frac{Y_1(x_\beta) Y_4(x_{s_3})}{Y_4(x_\beta)}\right] s^2 + \frac{\bar{g} M_{s_3}}{M_1} \frac{Y_1(x_\beta) Y_4'(x_{s_3})}{Y_4(x_\beta)} & s^2 + 2\overline{\zeta_1\omega_1} s + \bar{\omega}_1^2 - \frac{c_{41} M_4 Y_1(x_\beta)}{M_1 Y_4(x_\beta)} & 0 \\ \frac{M_{s_3}}{M_2}\left[Y_2(x_{s_3}) - \frac{Y_2(x_\beta) Y_4(x_{s_3})}{Y_4(x_\beta)}\right] s^2 + \frac{\bar{g} M_{s_3}}{M_2} \frac{Y_2(x_\beta) Y_4'(x_{s_3})}{Y_4(x_\beta)} & 0 & s^2 + 2\overline{\zeta_2\omega_2} s + \bar{\omega}_2^2 - \frac{c_{42} M_4 Y_2(x_\beta)}{M_2 Y_4(x_\beta)} \end{vmatrix} = 0 \quad (45)$$

The three zeros given by Eq. 45 have errors of less than 1 percent.

D. HIGHER BENDING ZEROS

1. φ Numerator

The approximation for the higher bending (η_2, η_3, and η_4) zeros of the φ numerator is similar to that used for the denominator. Basically, a dynamic correction for the slosh masses is applied. The characteristic equation for the η_i zero is (see Appendix H for the derivation):

$$\left\{1 - \sum_{j=1}^{3} \frac{M_{s_j} Y_i\left(x_{s_j}\right)}{M_i} \left[Y_i\left(x_{s_j}\right) - \frac{Y_i(x_\beta) l_{s_j}}{l_\beta}\right]\right\} s^2$$

$$+ 2\overline{\zeta_i \omega_i} s + \overline{\omega}_i^2 + \frac{Y_i(x_\beta)}{M_i l_\beta} g_i = 0 \qquad (46)$$

where $i = 2, 3, 4$

Equation 46 amounts to correcting both the ith mode generalized mass and stiffness. The zeros obtained from Eq. 46 are quite good; only two frequency errors are greater than 1 percent — η_4 zero at Max Q (1.4 percent) and η_2 zero at BO (2.9 percent). The error in the η_2 zero at BO is reduced to 0.2 percent by using the third slosh mass plus first and second bending approximation of Eq. 42.

2. η_1 Numerator

The approximation for the η_1 numerator is similar to that above, i.e.,

$$\left\{1 - \sum_{j=1}^{3} \frac{M_{s_j} Y_i\left(x_{s_j}\right)}{M_i} \left[Y_i\left(x_{s_j}\right) - \frac{Y_1\left(x_{s_j}\right) Y_i(x_\beta)}{Y_1(x_\beta)}\right]\right\} s^2$$

$$+ 2\overline{\zeta_i \omega_i} s + \overline{\omega}_i^2 - c_{1i} \frac{M_1 Y_i(x_\beta)}{M_i Y_1(x_\beta)} = 0 \qquad (47)$$

where $i = 2, 3, 4$

Of the zeros obtained from Eq. 47, again only two have errors greater than 1 percent — η_4 zero at Max Q (1.4 percent) and η_2 zero at BO (1.1 percent) The error in the η_2 zero at BO is reduced to 0.6 percent by using the third slosh plus first and second bending approximation given in Appendix G, Eq. G-5).

3. Higher Bending Numerators

The two higher bending zeros of the η_2, η_3, or η_4 numerator can be approximated by generalizing Eq. 47. The η_i zero of the η_k numerator is approximated by:

$$\left\{1 - \sum_{j=1}^{3} \frac{M_{s_j} Y_i(x_{s_j})}{M_i} \left[Y_i(x_{s_j}) - \frac{Y_k(x_{s_j}) Y_i(x_\beta)}{Y_k(x_\beta)}\right]\right\} s^2$$

$$+ 2\overline{\zeta_i \omega_i} s + \overline{\omega}_i^2 - c_{ki} \frac{M_k Y_i(x_\beta)}{M_i Y_k(x_\beta)} = 0 \qquad (48)$$

$$\text{where} \quad i \neq k$$

$$i, k = 2, 3, 4$$

Equation 48 works very well for the η_2 and η_3 numerators, in which all the frequency errors are less than 1 percent. For the η_4 numerator the η_2 zero at BO has a 5.9 percent error, but this can be reduced to 0.3 percent by using the third slosh plus first and second bending approximation of Eq. 45. The other zeros of the η_4 numerator have errors less than 3 percent, and no attempt was made to reduce these because of the relatively low importance of the η_4 numerator.

E. LEAD COEFFICIENTS

The approximation for the lead coefficient of the φ numerator, A_φ, will be discussed in some detail. The approximations for the η_i numerators are then straightforward variations.

The φ numerator of the complete 11-by-11 matrix, as noted earlier, is equal to $K_1 \omega_E^2$ times the 9-by-9 determinant (the first nine rows and columns of the 11-by-11 with the negative of the β column substituted for the φ column). The contributions of the 9-by-9 to the lead coefficient will be approximated by multiplying the lead coefficients from each of the submatrices used to approximate various zeros, i.e.,

$$A_\varphi \doteq K_1\omega_E^2 \frac{C}{I}\left(M_E l_E l_\beta - I_E\right)$$

$$\times \left[\begin{array}{l}\text{lead coefficient of 4-by-4 determinant used}\\ \text{for slosh and first bending zeros, Eq. 41}\end{array}\right]$$

$$\times \prod_{i=2}^{4}\left\{1 - \sum_{j=1}^{3}\frac{M_{s_j}Y_i(x_{s_j})}{M_i}\left[Y_i(x_{s_j}) - \frac{Y_i(x_\beta)l_{s_j}}{l_\beta}\right]\right\} \quad (49)$$

Several points about this approximation may need clarification.

The $C(M_E l_E l_\beta - I_E)/I$ term is obtained directly from the β column. Since we are considering the φ numerator we use the s^2 coefficient in the φ row of the β column, i.e., the diagonal term.

A second point is that the contribution of the slosh and η_i zeros must be the lead coefficient of the 4-by-4 of Eq. 41 and not the 7-by-7 of Eq. G-1. In the 7-by-7 the β diagonal term is l_β/I, which has already been accounted for in Eq. 49 in the $C(M_E l_E l_\beta - I_E)/I$ term. Therefore, if Eq. G-1 is to be used, the whole β column should be multiplied by I/l_β to reduce the diagonal term to 1. In writing the 7-by-7 this was not done because it would have been confusing to the reader. It was accomplished, in effect, when the determinant was reduced to a 4-by-4. Likewise, in Eq. G-1 the static correction for the second bending mode should be written so it does not affect the lead coefficient.

The final point is that the lead coefficient from the rigid-body modes is unity and therefore does not appear explicitly in Eq. 49.

By similar developments we find that the lead coefficients of the bending numerators can be approximated by:

$$A_{\eta_1} \doteq K_1\omega_E^2 \frac{C}{M_1}\left[M_E l_E Y_1(x_\beta) - I_E Y_1'(x_\beta)\right]$$

$$\times \left[\begin{array}{l}\text{lead coefficient of 3-by-3 determinant}\\ \text{used for slosh zeros, Eq. 43}\end{array}\right]$$

$$\times \prod_{i=2}^{4}\left\{1 - \sum_{j=1}^{3}\frac{M_{s_j}Y_i(x_{s_j})}{M_i}\left[Y_i(x_{s_j}) - \frac{Y_1(x_{s_j})Y_i(x_\beta)}{Y_1(x_\beta)}\right]\right\} \quad (50)$$

$$A_{\eta_k} \doteq K_1 \omega_E^2 \frac{C}{M_k} \left[M_E l_E Y_k(x_\beta) - I_E Y_k'(x_\beta) \right]$$

$$\times \begin{bmatrix} \text{lead coefficient of 4-by-4 determinant used} \\ \text{for slosh and first bending zeros, Eq. 44} \end{bmatrix}$$

$$\times \prod_{\substack{i=2 \\ i \neq k}}^{4} \left\{ 1 - \sum_{j=1}^{3} \frac{M_{s_j} Y_i(x_{s_j})}{M_i} \left[Y_i(x_{s_j}) - \frac{Y_k(x_{s_j}) Y_i(x_\beta)}{Y_k(x_\beta)} \right] \right\} \quad (51)$$

The approximate and exact lead coefficients are summarized in Table II. The approximations are quite good, with only one error greater than 2 percent. The η_4 numerator coefficient has a 6 percent error at Max Q, but considering the relative unimportance of η_4 this is entirely satisfactory.

TABLE II

SUMMARY OF NUMERATOR LEAD COEFFICIENTS

NUMERATOR	UNITS	FLIGHT CONDITION								
		Lift-Off			Max Q			Burnout		
		Exact	Approx.	Error	Exact	Approx.	Error	Exact	Approx.	Error
φ	m^2/sec^3	-958.37	-968.63	+1.1	-1054.1	-1064.4	+0.9	-5805.3	-5851.9	+0.8
η_1	$(m/sec)^3$	37,896	38,523	+1.6	38,546	38,925	+1.0	448,920	450,170	+0.3
η_2	$(m/sec)^3$	45,444	45,830	+0.8	57,803	58,486	+1.2	278,210	277,770	-0.2
η_3	$(m/sec)^3$	46,838	47,005	+0.4	68, 743	68,469	+0.4	47,266	47,225	-0.1
η_4	$(m/sec)^3$	20,845	20,839	-0.03	11 ,884	12,593	+6.0	37,504	36,957	-1.5

$$\text{Error} = \frac{\text{Approximate}-\text{Exact}}{\text{Exact}} \times 100$$

SECTION V

SUMMARY

Approximate expressions for the transfer function factors of a large highly flexible boost vehicle have been derived. The resulting approximations have been evaluated and compared with exact values for the Marshall Space Flight Center Model Vehicle No. 2. The approximations include the vehicle transfer function poles (or characteristic roots), numerator zeros for motion quantities sensed by attitude or rate gyros, and lead (or gain) coefficients. The numerator approximations provide the first step in determining approximate expressions for gyro output transfer function numerators.

The approximations have been developed to:

- Provide the control system designer with physical insights to the basic dynamic characteristics of the vehicle
- Assist the designer in performing simplified, yet meaningful, preliminary synthesis studies
- Assist the designer in evaluating the effects of deliberate variations, or possible uncertainties, in vehicle dynamic characteristics

Accordingly, various levels of approximation have been presented and discussed for each of the dynamic modes. The approximate expressions indicate the coupling terms that must be included according to modes of interest, level of accuracy desired, and flight condition. The basic approach has been to include all contributing factors within the immediate vicinity (frequency) of the mode of interest plus static or dynamic corrections for those modes outside the region of interest. The resulting approximations for Model Vehicle No. 2 are of the form:

- Rigid-body poles — Two degrees of freedom (attitude and translation) plus a static correction for the first bending mode
- Slosh and first bending poles — Four degrees of freedom* (displacements of the three slosh masses and the first

*The cross-coupling among these four modes is unusually large for Model Vehicle No. 2 because they all lie in a very narrow frequency band.

bending deflection) plus dynamic corrections for the rigid-body modes and static corrections for higher bending modes

- Higher bending poles — One degree of freedom (ith bending mode deflection) plus dynamic corrections for the slosh modes
- Actuator and actuator-nozzle compliance poles — Two degrees of freedom (positions of actuator output and nozzle) plus dynamic corrections for rigid-body, slosh, and bending modes

The method of obtaining approximate zeros is comparably simple.

For Model Vehicle No. 2 at three flight conditions, the approximate expressions have been shown to provide transfer function factors which are generally within 5 percent of exact factors obtained from the complete 11-by-11 matrix (containing all coupling terms). Where appropriate, approximations good to within 1 percent also are presented for situations where greater accuracy may be desired, e.g., slosh mode poles and zeros. Similar accuracy should be obtained for other boost vehicles of the general class represented by the MSFC Model Vehicle No. 2. For considerably different vehicles it may be necessary to modify the approximate expressions presented here. Nevertheless, the same approach can be used and a thorough understanding of the material in this report will enable the reader to make the appropriate changes.

The following observations, made during this study, are indicative of the physical insights to coupling effects provided by the approximations:

Rigid-Body Modes

The primary effect of vehicle flexibility is to alter the aerodynamic characteristics of the vehicle. The principal contribution arises from the first bending mode. The next largest contribution comes from the third bending mode, but is comparatively small.

Slosh and First Bending Modes

1. For Model Vehicle No. 2, two slosh modes involve strong cross-coupling among all three slosh masses; the third slosh and first bending modes involve strong coupling among two slosh masses and the first bending mode.
2. Slosh masses couple through the finite inertia of the vehicle. The degree of cross-coupling depends on a

center-of-percussion concept: cross-coupling between slosh mass "a" and slosh mass"b" is proportional to the distance between mass "b" and the center of percussion for a force applied at the location of mass "a".

3. The coupling between a slosh mass and a bending mode depends on the ratio of slosh mass to generalized bending mode mass, the magnitude of the bending mode shape at the slosh mass location, and the separation between the uncoupled frequencies of the slosh mass and bending mode.

4. Because of the strong coupling among the slosh masses in this vehicle, it is possible to increase the damping of all slosh modes without baffling all the fuel tanks. Thus it may be possible to take advantages of this coupling and, through selective location of baffles, to reduce the amount of baffling required.

Higher Bending Modes

1. The dynamic correction for the slosh masses amounts to removing the slosh masses from the generalized bending mode mass. The reduction in bending mode mass accounts for the commonly observed increase in the coupled frequency (e.g., Ref. 5).

2. This correction is required because the slosh masses do not respond at the higher bending mode frequencies and hence remain nearly fixed in inertial space.

In addition to physical understanding, the approximations provide ready means of assessing, by inspection or relatively simple computation, the consequences of variations in vehicle dynamic characteristics. They also may be employed to generate vehicle dynamic models appropriate at the preliminary analysis and synthesis level without requiring access to large scale digital or analog computer facilities.

APPENDIX A

EQUATIONS OF MOTION FOR A DYNAMICALLY SIMPLE BOOSTER

The objectives of this appendix are to

- Illustrate the separation of the equations of motion into trim and perturbation components
- Develop a simpler alternate approach for deriving the perturbation equations

These goals can be obtained by considering a dynamically simple booster in which the effects of engine mass, fuel slosh, and body bending modes are neglected.

As shown in Fig. 2 (page 6), the vehicle perturbed position with respect to inertial coordinates is given by

$$\bar{R}_{IC} = \bar{R}_{ID} + X\bar{i}_x + Z\bar{i}_z \tag{A-1}$$

The angular velocity of the XYZ coordinates is

$$\bar{\Omega} = \Omega\bar{i}_y = -\left(\dot{\theta} + \frac{V_N \sin\theta}{R_{ID}}\right)\bar{i}_y \tag{A-2}$$

Therefore the linear velocity and acceleration of the booster are

$$\begin{aligned}\dot{\bar{R}}_{IC} &= V_N\bar{i}_x + \dot{X}\bar{i}_x + \dot{Z}\bar{i}_z + \bar{\Omega} \times (X\bar{i}_x + Z\bar{i}_z) \\ &= (V_N + \dot{X} + \Omega Z)\bar{i}_x + (\dot{Z} - \Omega X)\bar{i}_z \end{aligned} \tag{A-3}$$

$$\begin{aligned}\ddot{\bar{R}}_{IC} &= (\dot{V}_N + \ddot{X} + \dot{\Omega}Z + \Omega\dot{Z})\bar{i}_x + (\ddot{Z} - \dot{\Omega}X - \Omega\dot{X})\bar{i}_x \\ &\qquad + \bar{\Omega} \times \left[(V_N + \dot{X} + \Omega Z)\bar{i}_x + (\dot{Z} - \Omega X)\bar{i}_z\right] \\ &= (\dot{V}_N + \ddot{X} + \dot{\Omega}Z + 2\Omega\dot{Z} - \Omega^2 X)\bar{i}_x + (-\Omega V_N + \ddot{Z} - \dot{\Omega}X - 2\Omega\dot{X} - \Omega^2 Z)\bar{i}_z \end{aligned} \tag{A-4}$$

The angular acceleration is $(\dot{\Omega} - \ddot{\varphi}_1)\bar{i}_y$.

Neglecting the effects of engine mass, the external forces and moments on the vehicle can be written (see Fig. A-1):

$$F_x = -Mg \cos\theta - N_\alpha \alpha_1 \sin\varphi_1 + \left[\left(\frac{F-C}{F}\right)T - X_a\right] \cos\varphi_1 + \frac{CT}{F} \cos(\beta_1 + \varphi_1) \qquad \text{(A-5)}$$

$$F_z = Mg \sin\theta + N_\alpha \alpha_1 \cos\varphi_1 + \left[\left(\frac{F-C}{F}\right)T - X_a\right] \sin\varphi_1 + \frac{CT}{F} \sin(\beta_1 + \varphi_1) \qquad \text{(A-6)}$$

$$M_y = -l_{CP} N_\alpha \alpha_1 - l_\beta \frac{CT}{F} \sin\beta_1 \qquad \text{(A-7)}$$

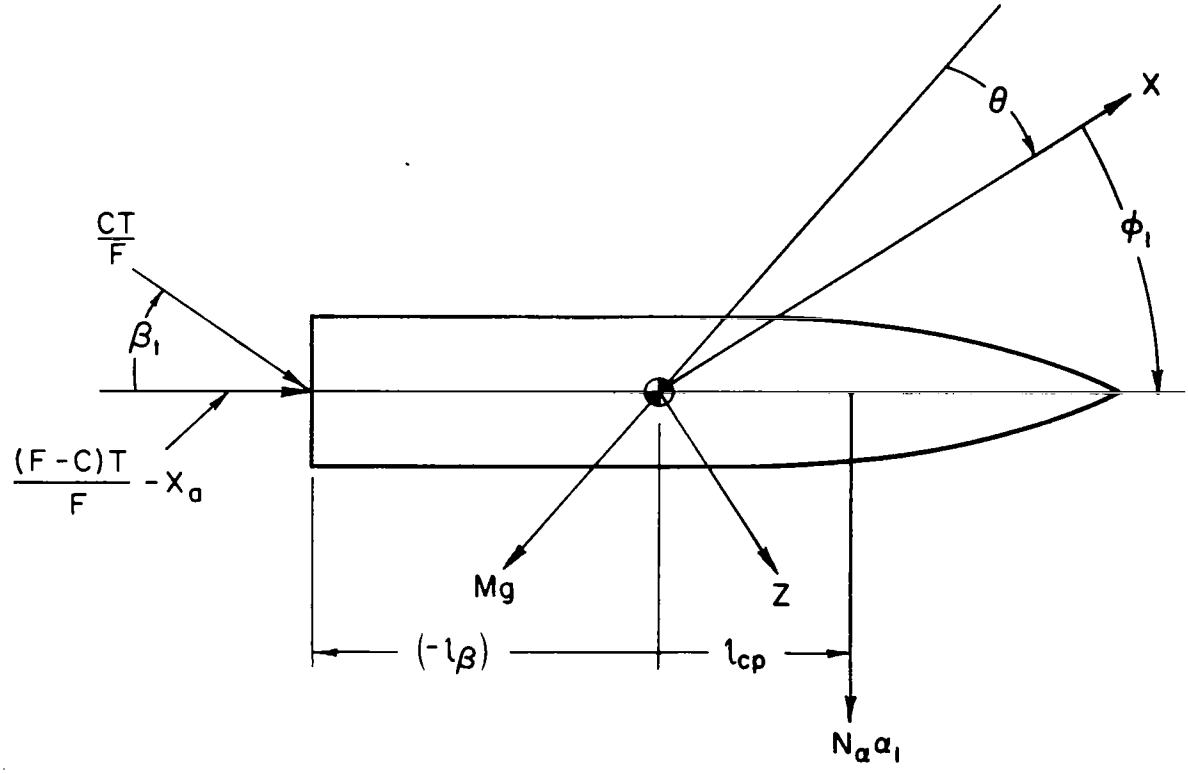

Figure A-1. External Forces on Simple Booster

Combining Eqs. A-4 to A-7 with the assumptions

1. Vehicle mass and moment of inertia are constant
2. Angles φ_1 and β_1 are small, i.e., small angle approximations for trigonometric functions can be used
3. Product $\varphi_1\alpha_1$ is negligible

the complete equations of motion can be written:

$$T - X_a - Mg\cos\theta = M(\dot{V}_N + \ddot{X} + \dot{\Omega}Z + 2\Omega\dot{Z} - \Omega^2 X) \qquad \text{(A-8)}$$

$$(T - X_a)\varphi_1 + \frac{CT}{F}\beta_1 + N_\alpha\alpha_1 + Mg\sin\theta = M(-\Omega V_N + \ddot{Z} - \dot{\Omega}X - 2\Omega\dot{X} - \Omega^2 Z) \qquad \text{(A-9)}$$

$$l_{CP}N_\alpha\alpha_1 + l_\beta\frac{CT}{F}\beta_1 = I(\ddot{\varphi}_1 - \dot{\Omega}) \qquad \text{(A-10)}$$

An additional equation which relates the angle of attack, α_1, to the other variables is also required. The inertial velocity of the booster is given by Eq. A-3. Allowing for a wind of velocity $\bar{W}_1$, with components W_{1_X} and W_{1_Z}, the vehicle velocity relative to the air mass is given by (see Fig. A-2):

$$\bar{V}_{air} = (V_N + \dot{X} + \Omega Z - W_{1_X})\bar{\imath}_X + (\dot{Z} - \Omega X - W_{1_Z})\bar{\imath}_Z \qquad \text{(A-11)}$$

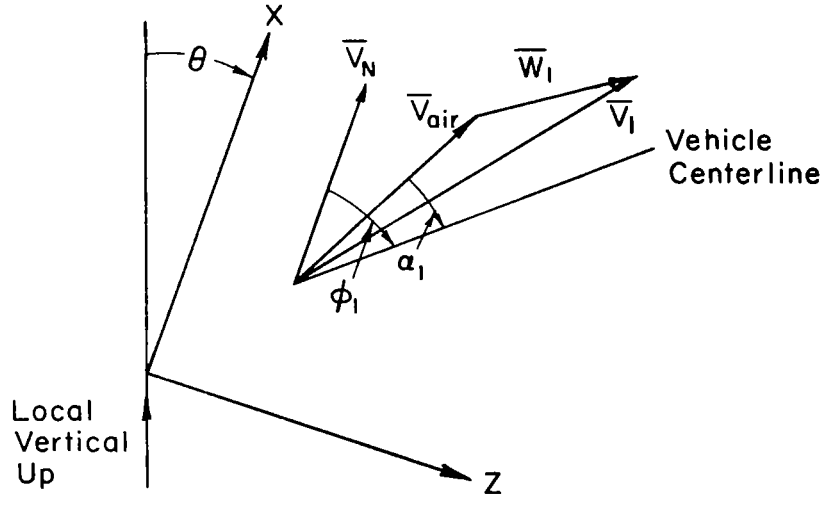

Figure A-2. Components of Angle of Attack

Thus the angle of attack is

$$\alpha_1 = \varphi_1 - \tan^{-1} \frac{\dot{Z} - \Omega X - W_{1_Z}}{V_N + \dot{X} + \Omega Z - W_{1_X}} \tag{A-12}$$

Neglecting relatively small terms, using the small angle approximation, and introducing the substitution

$$w_1 = W_{1_Z} \tag{A-13}$$

reduces Eq. A-12 to

$$\alpha_1 = \varphi_1 + \frac{w_1 - \dot{Z}}{V_N} \tag{A-14}$$

The complete equations of motion can now be separated into trim and perturbation components by separating α_1, β_1, φ_1, and w_1 into nominal components (α_N, β_N, φ_N, and w_N) and perturbation components (α, β, φ, and w).

$$\begin{aligned} \alpha_1 &= \alpha_N + \alpha & \varphi_1 &= \varphi_N + \beta \\ \beta_1 &= \beta_N + \beta & w_1 &= w_N + w \end{aligned} \tag{A-15}$$

The resulting sets of equations are shown below.

Trim Equations

$$T - X_a - Mg \cos \theta = M\dot{V}_N \tag{A-16}$$

$$(T - X_a)\varphi_N + \frac{CT}{F} \beta_N + N_\alpha \alpha_N + Mg \sin \theta = -M\Omega V_N \tag{A-17}$$

$$l_{CP} N_\alpha \alpha_N + l_\beta \frac{CT}{F} \beta_N = I\ddot{\varphi}_N \tag{A-18}$$

$$\alpha_N = \varphi_N + \frac{w_N}{V_N} \tag{A-19}$$

$$\Omega = -\left(\dot{\theta} + \frac{V_N \sin \theta}{R_{ID}}\right) \tag{A-20}$$

$$\dot{R}_{ID} = V_N \cos \theta \tag{A-21}$$

Perturbation Equations

$$0 = \ddot{X} + \dot{\Omega} Z + 2\Omega \dot{Z} - \Omega^2 X \tag{A-22}$$

$$(T - X_a)\varphi + \frac{CT}{F} \beta + N_\alpha \alpha = M(\ddot{Z} - \dot{\Omega} X - 2\Omega \dot{X} - \Omega^2 Z) \tag{A-23}$$

$$l_{CP} N_\alpha \alpha + l_\beta \frac{CT}{F} \beta = I(\ddot{\varphi} - \dot{\Omega}) \tag{A-24}$$

$$\alpha = \varphi + \frac{w - \dot{Z}}{V_N} \tag{A-25}$$

The trim equations define motion during a "perfect" launch, i.e., flight along the nominal trajectory. Solution of the trim equations for some given β_N and w_N yields the time histories of V_N, θ, Ω, R_{ID}, α_N, and φ_N.

The perturbation equations describe vehicle motion with respect to the XYZ coordinates. Since the maximum values of Ω and $\dot{\Omega}$ are on the order of 0.01 rad/sec and 0.0002 rad/sec^2, respectively, these terms affect the very low frequency motions of the vehicle wherein other slow variations, such as vehicle mass and moment of inertia, must also be considered. Consequently, for the study of vehicle attitude control, bending, and fuel slosh the Ω and $\dot{\Omega}$ terms can be neglected.

Additional simplifications result if the nominal trajectory is restricted to a no-wind, gravity turn trajectory. Then

$$\alpha_N = \beta_N = \varphi_N = w_N = 0 \tag{A-26}$$

and α, β, and φ become total, physically measurable quantities. Thus for a nominal no-wind, gravity turn trajectory the equations become:

Trim Equations

$$T - X_a - Mg \cos \theta = M\dot{V}_N \tag{A-27}$$

$$g \sin \theta = -\Omega V_N \tag{A-28}$$

$$\Omega = -\left(\dot{\theta} + \frac{V_N \sin \theta}{R_{ID}}\right) \tag{A-29}$$

$$\dot{R}_{ID} = V_N \cos \theta \tag{A-30}$$

Perturbation Equations

$$X = 0 \tag{A-31}$$

$$(T - X_a)\varphi + \frac{CT}{F}\beta + N_\alpha \alpha = M\ddot{Z} \tag{A-32}$$

$$l_{CP} N_\alpha \alpha + l_\beta \frac{CT}{F}\beta = I\ddot{\varphi} \tag{A-33}$$

$$\alpha = \varphi + \frac{w - \dot{Z}}{V_N} \tag{A-34}$$

where the Ω and $\dot{\Omega}$ terms have been omitted from the perturbation equations as discussed above.

The perturbation equations could also be obtained by:

1. Assuming the XYZ coordinates to be inertial
2. Suppressing the X degree of freedom
3. Omitting the gravity force, Mg
4. Adding an artificial gravity force, $-\bar{g}M\bar{1}_x$, where $\bar{g} = (T - X_a)/M$

The approach indicated by these last four steps is used in Appendix B to derive the equations of motion for an elastic booster with fuel slosh. The above approach could be modified for a nominal trajectory other than no-wind, gravity turn, but it would then be necessary to add an artificial lateral gravity force due to the nonzero α_N, β_N, and φ_N.

APPENDIX B

DERIVATION OF PERTURBATION EQUATIONS FOR FLEXIBLE BOOSTER WITH FUEL SLOSH

The perturbation equations of motion for a flexible booster wherein the effects of fuel slosh and rocket engine inertial reaction forces are included are fearsome things to derive unless energy methods (via Lagrange's equation) are employed. Even then, derivation is somewhat tedious.

To begin, Lagrange's equation is:

$$\frac{d}{dt}\left(\frac{\partial T}{\partial \dot{q}_i}\right) - \frac{\partial T}{\partial q_i} + \frac{\partial D}{\partial \dot{q}_i} + \frac{\partial V}{\partial q_i} = Q_i \quad , \quad i = 1, 2, \cdots, n \qquad \text{(B-1)}$$

The q_i are the generalized coordinates of the system under analysis. We assume that any displacement of the system can be expressed in terms of a set of n discrete generalized coordinates. The generalized forces, Q_i, are obtained from the expression for the virtual work resulting when external forces act through a virtual displacement, δq_i, in each of the generalized coordinate directions.

$$\delta W_e = \sum_{i=1}^{n} Q_i \delta q_i \qquad \text{(B-2)}$$

T is the kinetic energy of the system (with respect to inertial space), V is the potential energy stored in the system, and D is a dissipation function which accounts for internal damping in the system. Throughout this analysis, "frozen" values of all system parameters are employed to evaluate short term dynamic response and all angles except θ are assumed small.

Degrees of freedom, or generalized coordinates, used are Z, φ, z_{s_j}, η_i, β, and β_a. All symbols are defined in the list of symbols.

1. KINETIC ENERGY

We shall now proceed to write the expressions for the kinetic energy for all components of the total system. The kinetic energy of the empty airframe, without propellants or rocket engines, is (see Fig. B-1):

$$T_A = \frac{1}{2}\int_L M_A'\left[\dot{Z} + (x-x_{cg})\dot{\varphi} + \sum_{i=1}^{\infty} Y_i(x)\dot{\eta}_i\right]^2 dx + \frac{1}{2}\int_L I_A'\left[\dot{\varphi} + \sum_{i=1}^{\infty} Y_i'(x)\dot{\eta}_i\right]^2 dx \quad \text{(B-3)}$$

Using the spring mass analogy for fuel slosh, the kinetic energy of the propellant in the jth tank is (see Fig. B-2):

$$T_{s_j} = \frac{1}{2} M_{o_j}\left[\dot{Z} + l_{o_j}\dot{\varphi} + \sum_{i=1}^{\infty} Y_i\left(x_{o_j}\right)\dot{\eta}_i\right]^2 + \frac{1}{2} I_{o_j}\left[\dot{\varphi} + \sum_{i=1}^{\infty} Y_i'\left(x_{o_j}\right)\dot{\eta}_i\right]^2 + \frac{1}{2} M_{s_j}\left[\dot{Z} + l_{s_j}\dot{\varphi} + \sum_{i=1}^{\infty} Y_i\left(x_{s_j}\right)\dot{\eta}_i + \dot{z}_{s_j}\right]^2 \quad \text{(B-4)}$$

With the aid of Fig. B-3 we see that the kinetic energy of the rocket engines is

$$T_E = \frac{1}{2} CM_E\left[\dot{Z} + l_\beta\dot{\varphi} + \sum_{i=1}^{\infty} Y_i(x_\beta)\dot{\eta}_i - l_E\dot{\psi}\right]^2 + \frac{1}{2} CI_{E_{CG}}\dot{\psi}^2 + \frac{1}{2}(F-C)M_E\left[\dot{Z} + (l_\beta - l_E)\dot{\varphi} + \sum_{i=1}^{\infty} Y_i(x_\beta)\dot{\eta}_i - l_E\sum_{i=1}^{\infty} Y_i'(x_\beta)\dot{\eta}_i\right]^2 + \frac{1}{2}(F-C)I_{E_{CG}}\left[\dot{\varphi} + \sum_{i=1}^{\infty} Y_i'(x_\beta)\dot{\eta}_i\right]^2 \quad \text{(B-5)}$$

where ψ is given by:

$$\psi = \varphi + \sum_{i=1}^{\infty} Y_i'(x_\beta)\eta_i + \beta \quad \text{(B-6)}$$

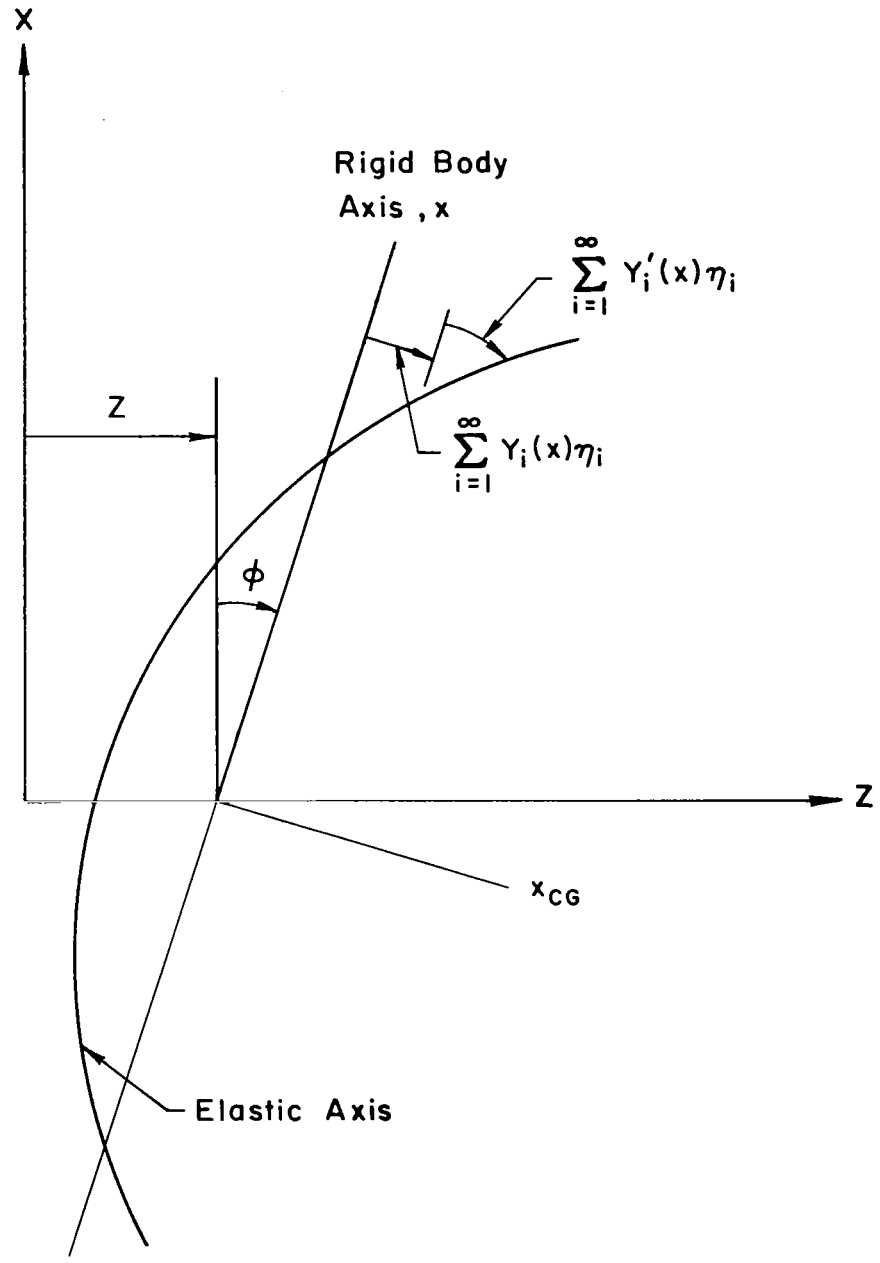

Figure B-1. Elastic Axis

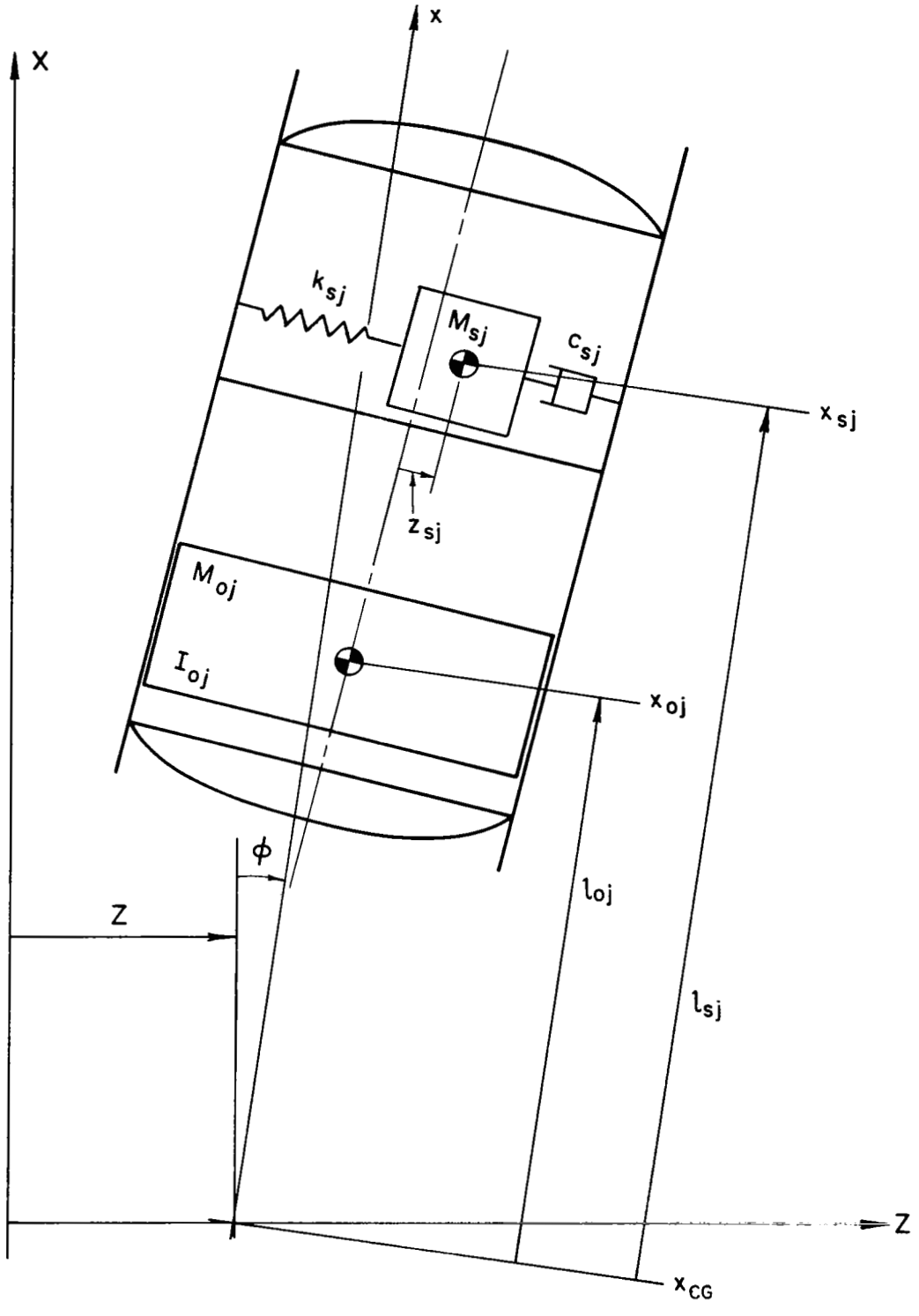

Figure B-2. Propellant Model for jth Tank

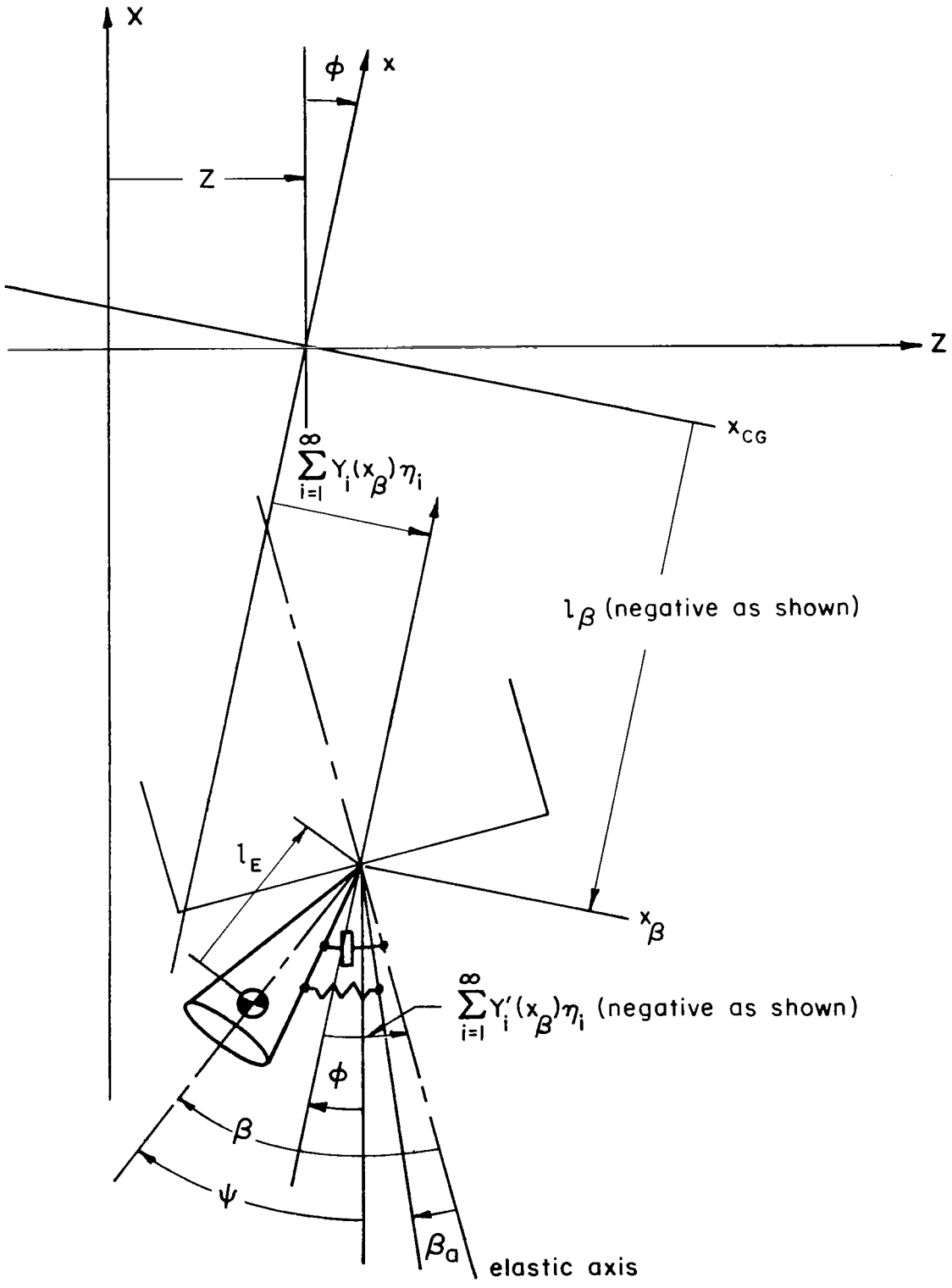

Figure B-3. Engine Model

Upon substituting the expression for $\dot{\psi}$ into the expression for T_E, we obtain:

$$T_E = \frac{1}{2} CM_E \left[\dot{Z} + (l_\beta - l_E)\dot{\phi} + \sum_{i=1}^{\infty} Y_i(x_\beta)\dot{\eta}_i - l_E \sum_{i=1}^{\infty} Y_i'(x_\beta)\dot{\eta}_i - l_E\dot{\beta}\right]^2$$

$$+ \frac{1}{2} CI_{E_{CG}} \left[\dot{\phi} + \sum_{i=1}^{\infty} Y_i'(x_\beta)\dot{\eta}_i + \dot{\beta}\right]^2$$

$$+ \frac{1}{2} (F-C)M_E \left[\dot{Z} + (l_\beta - l_E)\dot{\phi} + \sum_{i=1}^{\infty} Y_i(x_\beta)\dot{\eta}_i - l_E \sum_{i=1}^{\infty} Y_i'(x_\beta)\dot{\eta}_i\right]^2$$

$$+ \frac{1}{2} (F-C)I_{E_{CG}} \left[\dot{\phi} + \sum_{i=1}^{\infty} Y_i'(x_\beta)\dot{\eta}_i\right]^2 \qquad \text{(B-7)}$$

The kinetic energy of the total system is given by the sum of T_A, $\sum_j T_{s_j}$, and T_E.

2. POTENTIAL ENERGY

We shall now write the expression for the potential energy for all components of the total system. From Fig. B-4 we see that the potential energy due to the deflection of the empty airframe in the $\bar{g}$ acceleration field is:*

$$V_A = -\int_L \bar{g} M_A' \left[(x - x_{CG})\frac{\varphi^2}{2} + \varphi \sum_{i=1}^{\infty} Y_i(x)\eta_i\right] dx \qquad \text{(B-8)}$$

Potential energy is also stored in the structure because of the elastic deformations. This potential energy is:

$$V_B = \frac{1}{2} \sum_{i=1}^{\infty} \int_L \left[M' Y_i^2(x) + I' Y_i'^2(x)\right] dx\, \omega_i^2\, \eta_i^2 \qquad \text{(B-9)}$$

*Note that the displacement $\sum_{i=1}^{\infty} Y_i(x)\eta_i$ is <u>defined</u> to be perpendicular to the x axis.

where M' and I' are, respectively, the running <u>total</u> mass and running <u>total</u> section moment of inertia for the system. Since the generalized masses of the bending modes are given by

$$M_i = \int_L \left[M' Y_i^2(x) + I' Y_i'^2(x) \right] dx \qquad \text{(B-10)}$$

Eq. B-9 can be written as

$$V_B = \frac{1}{2} \sum_{i=1}^{\infty} M_i \omega_i^2 \eta_i^2 \qquad \text{(B-11)}$$

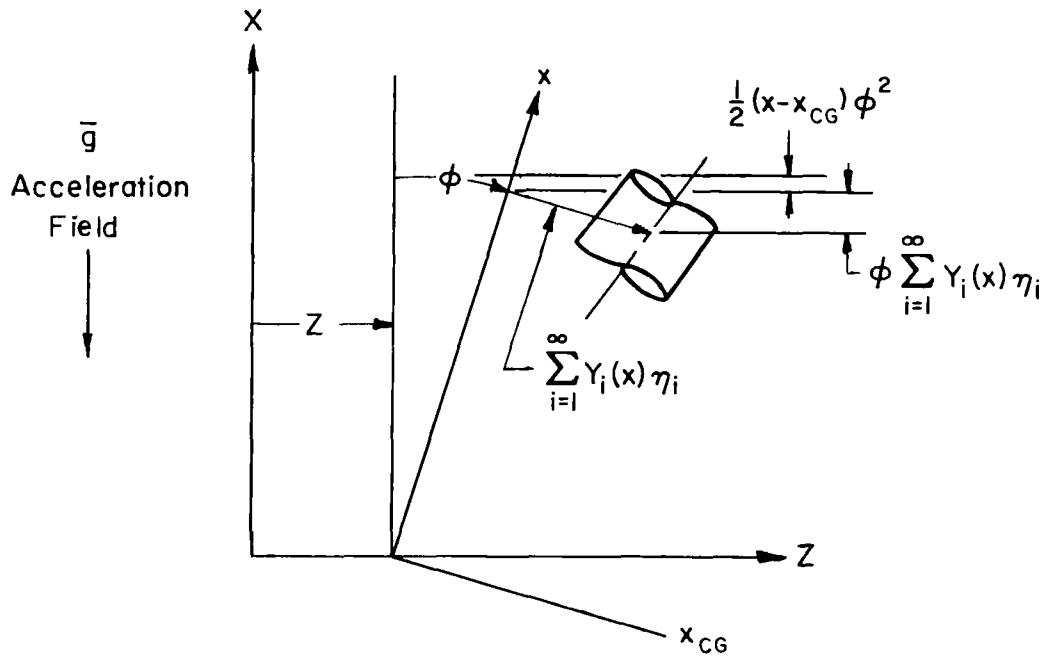

Figure B-4. Deflection of Empty Airframe in an Acceleration Field

We next consider the potential energy of the jth propellant tank. From Fig. B-5 we see that the potential energy is:

$$V_{s_j} = \frac{1}{2} k_{s_j} z_{s_j}^2 - \frac{1}{2} \bar{g} M_{s_j} l_{s_j} \varphi^2$$

$$- \bar{g} M_{s_j} z_{s_j} \left[\varphi + \sum_{i=1}^{\infty} Y_i'(x_{s_j}) \eta_i \right] - \bar{g} M_{s_j} \varphi \sum_{i=1}^{\infty} Y_i(x_{s_j}) \eta_i$$

$$- \frac{1}{2} \bar{g} M_{o_j} l_{o_j} \varphi^2 - \bar{g} M_{o_j} \varphi \sum_{i=1}^{\infty} Y_i(x_{o_j}) \eta_i \qquad \text{(B-12)}$$

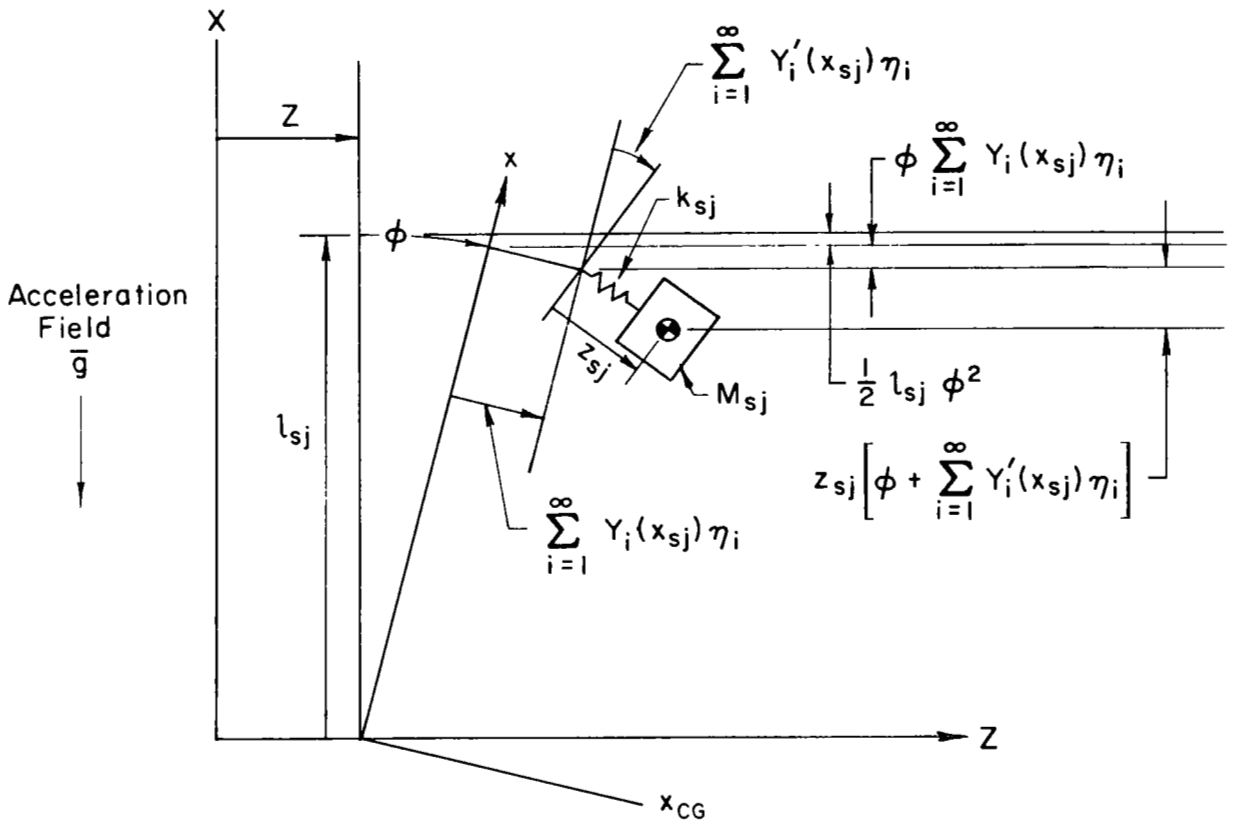

Figure B-5. Deflection of Propellant Mass in an Acceleration Field

However,

$$k_{s_j} = M_{s_j}\omega_{s_j}^2 \tag{B-13}$$

Then,

$$V_{s_j} = \frac{1}{2} M_{s_j}\omega_{s_j}^2 z_{s_j}^2 - \frac{1}{2} \bar{g}M_{s_j} l_{s_j}\varphi^2 - \bar{g}M_{s_j} z_{s_j}\left[\varphi + \sum_{i=1}^{\infty} Y_i'(x_{s_j})\eta_i\right]$$

$$- \bar{g}M_{s_j}\varphi \sum_{i=1}^{\infty} Y_i(x_{s_j})\eta_i - \frac{1}{2} \bar{g}M_{o_j} l_{o_j}\varphi^2$$

$$- \bar{g}M_{o_j}\varphi \sum_{i=1}^{\infty} Y_i(x_{o_j})\eta_i \tag{B-14}$$

The final potential energy contribution is that from the engines, which can be written:

$$V_E = \frac{1}{2} CK_L(\beta - \beta_a)^2 - \frac{1}{2} \bar{g}FM_E l_\beta \varphi^2 - \bar{g}FM_E\varphi \sum_{i=1}^{\infty} Y_i(x_\beta)\eta_i$$

$$+ \frac{1}{2} \bar{g}CM_E l_E \psi^2 + \frac{1}{2} \bar{g}(F - C)M_E l_E\left[\varphi + \sum_{i=1}^{\infty} Y_i'(x_\beta)\eta_i\right]^2 \tag{B-15}$$

The first term on the right side of Eq. B-15 is the potential energy stored in the spring connecting β and β_a (actuator–nozzle compliance). The second and third terms are due to the motion of the gimbal point in the X direction (see Fig. B-4). The last two terms account for the relative X motions between the gimbal point and the engine cg's. Substituting the identity

$$\omega_E^2 = \frac{K_L}{I_E} \tag{B-16}$$

and the definition of ψ, Eq. B-6, into Eq. B-15 gives us

$$V_E = \frac{1}{2} CI_E \omega_E^2 (\beta - \beta_a)^2 - \frac{1}{2} \bar{g} F M_E l_\beta \varphi^2$$

$$- \bar{g} F M_E \varphi \sum_{i=1}^{\infty} Y_i(x_\beta)\eta_i + \frac{1}{2} CM_E l_E \left[\varphi + \sum_{i=1}^{\infty} Y_i'(x_\beta)\eta_i + \beta\right]^2$$

$$+ \frac{1}{2} \bar{g}(F-C) M_E l_E \left[\varphi + \sum_{i=1}^{\infty} Y_i'(x_\beta)\eta_i\right]^2 \qquad \text{(B-17)}$$

The total potential energy is $V_A + V_B + \sum_j V_{s_j} + V_E$.

3. DISSIPATION FUNCTIONS

The dissipation functions for the various components can be simply written in terms of damping ratios and natural frequencies, i.e.,

$$D_A = \frac{1}{2} \sum_i M_i \omega_i (2\zeta_i) \dot{\eta}_i^2 \qquad \text{(B-18)}$$

$$D_{s_j} = \frac{1}{2} M_{s_j} \omega_{s_j} (2\zeta_{s_j}) \dot{z}_{s_j}^2 \qquad \text{(B-19)}$$

$$D_E = \frac{1}{2} CI_E \omega_E (2\zeta_E) \dot{\beta}^2 \qquad \text{(B-20)}$$

For the engines the damping forces are assumed to be in the gimbals.

4. GENERALIZED FORCES

Finally, we shall write the expressions for the generalized forces due to thrust and aerodynamic terms. Aerodynamic contributions to the generalized forces are assumed proportional to local angle of attack of the booster airframe. The expression for the local angle of attack is:

$$\alpha(x) = \varphi + \sum_{i=1}^{\infty} Y_i'(x)\eta_i - \frac{1}{V_N}\left[\dot{Z} + (x - x_{cg})\dot{\Phi} + \sum_{i=1}^{\infty} Y_i(x)\dot{\eta}_i - w\right] \qquad \text{(B-21)}$$

From Fig. B-6 we see that the Z generalized force is:

$$
\begin{aligned}
Q_Z &= \frac{CT}{F}\left[\varphi + \sum_{i=1}^{\infty} Y_i'(x_\beta)\eta_i + \beta\right] \\
&+ \left[(F-C)\,\frac{T}{F} - X_a\right]\left[\varphi + \sum_{i=1}^{\infty} Y_i'(x_\beta)\eta_i\right] \\
&+ qS \int_L \frac{\partial C_{Z_\alpha}}{\partial x}\,\alpha(x)\,dx \\
&= \frac{CT}{F}\,\beta + (T - X_a)\left[\varphi + \sum_{i=1}^{\infty} Y_i'(x_\beta)\eta_i\right] + N_\alpha\left(\varphi - \frac{\dot{Z}}{V_N} + \frac{w}{V_N}\right) \\
&- \frac{N_{\dot{\varphi}}}{V_N}\,\dot{\varphi} + \sum_{i=1}^{\infty}\left(N_{\eta_i}\eta_i - N_{\dot{\eta}_i}\,\frac{\dot{\eta}_i}{V_N}\right) \qquad \text{(B-22)}
\end{aligned}
$$

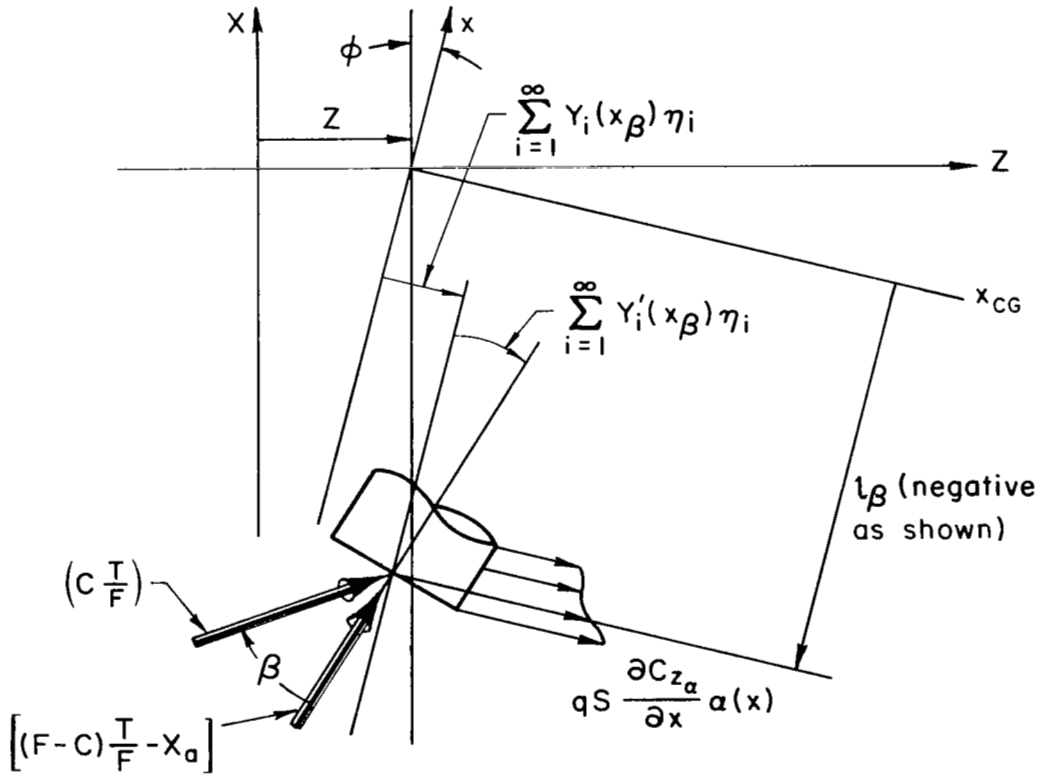

Figure B-6. Generalized Forces

where

$$N_\alpha = qS \int_L \frac{\partial C_{Z_\alpha}}{\partial x}\, dx \tag{B-23}$$

$$N_{\dot{\varphi}} = qS \int_L \frac{\partial C_{Z_\alpha}}{\partial x}\, (x - x_{CG})\, dx \tag{B-24}$$

$$N_{\eta_i} = qS \int_L \frac{\partial C_{Z_\alpha}}{\partial x}\, Y_i'(x)\, dx \tag{B-25}$$

$$N_{\dot{\eta}_i} = qS \int_L \frac{\partial C_{Z_\alpha}}{\partial x}\, Y_i(x)\, dx \tag{B-26}$$

From Fig. B-6 we also see that the φ generalized force is:

$$\begin{aligned} Q_\varphi &= \frac{CT}{F}\, l_\beta \left[\beta + \sum_{i=1}^{\infty} Y_i'(x_\beta)\eta_i\right] + \left[(F-C)\,\frac{T}{F} - X_a\right] l_\beta \sum_{i=1}^{\infty} Y_i'(x_\beta)\eta_i \\ &\quad - (T - X_a) \sum_{i=1}^{\infty} Y_i(x_\beta)\eta_i + qS \int_L \frac{\partial C_{Z_\alpha}}{\partial x}\, (x - x_{CG})\alpha(x)\, dx \\ &= \frac{CT}{F}\, l_\beta \beta + (T - X_a) l_\beta \sum_{i=1}^{\infty} Y_i'(x_\beta)\eta_i \\ &\quad - (T - X_a) \sum_{i=1}^{\infty} Y_i(x_\beta)\eta_i + M_\alpha \left(\varphi + \frac{w - \dot{Z}}{V_N}\right) \\ &\quad - M_{\dot{\varphi}}\, \frac{\dot{\varphi}}{V_N} + \sum_{i=1}^{\infty} \left[M_{\eta_i}\eta_i - M_{\dot{\eta}_i}\, \frac{\dot{\eta}_i}{V_N}\right] \end{aligned} \tag{B-27}$$

where

$$M_\alpha = qS \int_L \frac{\partial C_{Z_\alpha}}{\partial x}\, (x - x_{CG})\, dx \tag{B-28}$$

$$M_{\dot{\varphi}} = qS \int_L \frac{\partial C_{Z_\alpha}}{\partial x}\, (x - x_{CG})^2\, dx \tag{B-29}$$

$$M_{\eta_i} = qS \int_L \frac{\partial C_{Z_\alpha}}{\partial x}\, (x - x_{CG}) Y_i'(x)\, dx \tag{B-30}$$

$$M_{\dot{\eta}_i} = qS \int_L \frac{\partial C_{Z_\alpha}}{\partial x}\, (x - x_{CG}) Y_i(x)\, dx \tag{B-31}$$

There is no z_{s_j} generalized force. The η_i generalized force is, again referring to Fig. B-6,

$$Q_{\eta_i} = \frac{CT}{F}\left[\sum_{i=1}^{\infty} Y_i'(x_\beta)\eta_i + \beta\right]Y_i(x_\beta) + \left[(F-C)\frac{T}{F} - X_a\right]Y_i(x_\beta)\sum_{i=1}^{\infty} Y_i'(x_\beta)\eta_i$$

$$+ qS\int_L \frac{\partial C_{Z_\alpha}}{\partial x} Y_i(x)\alpha(x)\,dx$$

$$= \frac{CT}{F} Y_i(x_\beta)\beta + \underline{(T-X_a)Y_i(x_\beta)\sum_{i=1}^{\infty} Y_i'(x_\beta)\eta_i} + N_{\dot{\eta}_i}\left(\varphi + \frac{w-\dot{Z}}{V_N}\right)$$

$$- M_{\dot{\eta}_i}\frac{\dot{\varphi}}{V_N} + \sum_{k=1}^{\infty}\left[N_{\eta_{ik}}\eta_k - N_{\dot{\eta}_{ik}}\frac{\dot{\eta}_k}{V_N}\right] \qquad \text{(B-32)}$$

If preferred, the underlined term may be omitted per the discussion of page 10.

where

$$N_{\eta_{ik}} = qS\int_L \frac{\partial C_{Z_\alpha}}{\partial x} Y_i(x)Y_k'(x)\,dx \qquad \text{(B-33)}$$

$$N_{\dot{\eta}_{ik}} = qS\int_L \frac{\partial C_{Z_\alpha}}{\partial x} Y_i(x)Y_k(x)\,dx \qquad \text{(B-34)}$$

The β and β_a generalized forces are zero.

5. GENERALIZED MASSES AND ORTHOGONALITY RELATIONSHIPS

In applying Lagrange's equation to the flexible booster, great simplifications result from the use of generalized masses and the orthogonality relationships given below. The total system mass, or Z generalized mass, is:

$$M = \int_L M_A'\,dx + \sum_j \left(M_{o_j} + M_{s_j}\right) + FM_E \qquad \text{(B-35)}$$

The total system moment of inertia, or φ generalized mass, is:

$$I = \int_L \left[M_A'(x-x_{CG})^2 + I_A'\right] dx + \sum_j \left(M_{o_j} l_{o_j}^2 + I_{o_j} + M_{s_j} l_{s_j}^2\right)$$

$$+ FM_E(l_\beta - l_E)^2 + FI_{E_{CG}} \qquad \text{(B-36)}$$

The ith bending (η_i) generalized mass is:

$$M_i = \int_L \left[M_A' Y_i^2(x) + I_A' Y_i'^2(x)\right] dx$$

$$+ \sum_j \left[M_{o_j} Y_i^2\left(x_{o_j}\right) + I_{o_j} Y_i'^2\left(x_{o_j}\right) + M_{s_j} Y_i^2\left(x_{s_j}\right)\right]$$

$$+ FM_E\left[Y_i(x_\beta) - l_E Y_i'(x_\beta)\right]^2 + FI_{E_{CG}} Y_i'^2(x_\beta) \qquad \text{(B-37)}$$

From the definition of x_{CG} as the system center of gravity when β and z_{s_j} are constrained to zero, we have:

$$\int_L M_A'(x-x_{CG})\, dx + \sum_j \left(M_{o_j} l_{o_j} + M_{s_j} l_{s_j}\right) + FM_E(l_\beta - L_E) = 0 \qquad \text{(B-38)}$$

From the orthogonality of rigid-body translation to the ith bending mode, or the requirement that the bending mode does not move the system CG, we have

$$\int_L M_A' Y_i(x)\, dx + \sum_j \left[M_{o_j} Y_i\left(x_{o_j}\right) + M_{s_j} Y_i\left(x_{s_j}\right)\right]$$

$$+ FM_E\left[Y_i(x_\beta) - l_E Y_i'(x_\beta)\right] = 0 \qquad \text{(B-39)}$$

The orthogonality of rigid-body rotation to the ith bending mode gives:

$$\int_L \left[M_A'(x-x_{CG})Y_i(x) + I_A'Y_i'(x)\right] dx$$

$$+ \sum_j \left[M_{o_j} l_{o_j} Y_i(x_{o_j}) + I_{o_j} Y_i'(x_{o_j}) + M_{s_j} l_{s_j} Y_i(x_{s_j})\right]$$

$$+ FM_E(l_\beta - l_E)\left[Y_i(x_\beta) - l_E Y_i'(x_\beta)\right] + FI_{E_{CG}} Y_i'(x_\beta) = 0 \qquad \text{(B-40)}$$

Finally, the orthogonality of the ith bending mode to the kth bending mode gives:

$$\int_L \left[M_A'Y_i(x)\, Y_k(x) + I_A'Y_i'(x)Y_k'(x)\right] dx$$

$$+ \sum_j \left[M_{o_j} Y_i(x_{o_j}) Y_k(x_{o_j}) + I_{o_j} Y_i'(x_{o_j}) Y_k'(x_{o_j}) + M_{s_j} Y_i(x_{s_j}) Y_k(x_{s_j})\right]$$

$$+ FM_E\left[Y_i(x_\beta) - l_E Y_i'(x_\beta)\right]\left[Y_k(x_\beta) - l_E Y_k'(x_\beta)\right]$$

$$+ FI_{E_{CG}} Y_i'(x_\beta) Y_k'(x_\beta) = 0 \qquad \text{(B-41)}$$

where $i \neq k$

6. EFFECTS OF OFF-ELASTIC-AXIS ENGINE LOCATIONS

The above development has considered all engines to be located on the elastic axis. The effects of off-elastic-axis locations are generally small, but may be accounted for by modifying the generalized mass and orthogonality conditions to include the change in mass distribution. For example, the moment of inertia is increased by the product of the mass of the engines times the square of their distance from the elastic axis. The net result is a slight numerical change in the moment of inertia and the bending mode generalized masses, but no change in the form of the equations of motion.

7. SUMMARY OF EQUATIONS OF MOTION

In applying Lagrange's equation to the flexible booster, the kinetic energy terms become inertial reaction forces in the equations of motion. Potential energy terms become forces developed in distributed or lumped springs, or become forces developed by deforming the system in an acceleration field. Dissipation function terms become viscous damping forces. Generalized forces are the components in the generalized coordinate directions of the thrust and aerodynamic forces and moments applied to the total system.

The resultant equations of motion are summarized below.* The origin of each term is easily traced to its causal physical effects via the coefficients and the diagrams used for the derivation of the equations of motion.

Z Force Equation

$$M\ddot{Z} + \sum_j M_{s_j}\ddot{z}_{s_j} - CM_E l_E \ddot{\beta} - (T - X_a)\left[\varphi + \sum_{i=1}^{\infty} Y_i'(x_\beta)\eta_i\right] - \frac{CT}{F}\beta - N_\alpha\left(\varphi + \frac{w - \dot{Z}}{V_N}\right) + \frac{N_{\dot{\varphi}}\dot{\varphi}}{V_N} - \sum_{i=1}^{\infty}\left(N_{\eta_i}\eta_i - N_{\dot{\eta}_i}\frac{\dot{\eta}_i}{V_N}\right) = 0 \quad \text{(B-42)}$$

φ Moment Equation

$$I\ddot{\varphi} + \sum_j M_{s_j} l_{s_j}\ddot{z}_{s_j} + C\left\{-M_E l_E l_\beta + I_E\right\}\ddot{\beta} - \bar{g}\sum_j M_{s_j} z_{s_j} + \bar{g}CM_E l_E \beta + (T - X_a)\left[-l_\beta \sum_{i=1}^{\infty} Y_i'(x_\beta)\eta_i + \sum_{i=1}^{\infty} Y_i(x_\beta)\eta_i\right] - \frac{CT}{F} l_\beta \beta - M_\alpha\left(\varphi + \frac{w - \dot{Z}}{V_N}\right) + M_{\dot{\varphi}}\frac{\dot{\varphi}}{V_N} - \sum_{i=1}^{\infty}\left(M_{\eta_i}\eta_i - M_{\dot{\eta}_i}\frac{\dot{\eta}_i}{V_N}\right) = 0 \quad \text{(B-43)}$$

*The generalized mass and orthogonality relationships of Eqs. B-35 through B-41 have been used to greatly simplify the resultant equations.

jth Sloshing Mode Equation

$$\ddot{z}_{s_j} + 2\zeta_{s_j}\omega_{s_j}\dot{z}_{s_j} + \omega_{s_j}^2 z_{s_j} + \ddot{Z} + l_{s_j}\ddot{\varphi} + \sum_{i=1}^{\infty} Y_i\left(x_{s_j}\right)\ddot{\eta}_i - \bar{g}\varphi - \bar{g}\sum_{i=1}^{\infty} Y_i'\left(x_{s_j}\right)\eta_i = 0 \quad \text{(B-44)}$$

ith Bending Mode Equation

$$M_i\left(\ddot{\eta}_i + 2\zeta_i\omega_i\dot{\eta}_i + \omega_i^2\eta_i\right) - \frac{CT}{F}Y_i(x_\beta)\beta + \bar{g}CM_E l_E Y_i'(x_\beta)\beta + C\left[I_E Y_i'(x_\beta) - M_E l_E Y_i(x_\beta)\right]\ddot{\beta} + \sum_j M_{s_j}Y_i\left(x_{s_j}\right)\ddot{z}_{s_j} - \bar{g}\sum_j M_{s_j}Y_i'\left(x_{s_j}\right)z_{s_j} + \bar{g}FM_E l_E Y_i'(x_\beta)\sum_{i=1}^{\infty} Y_i'(x_\beta)\eta_i - \underline{(T-X_a)Y_i(x_\beta)\sum_{i=1}^{\infty} Y_i'(x_\beta)\eta_i} - N_{\dot{\eta}_i}\left(\varphi + \frac{w-\dot{Z}}{V_N}\right) + M_{\dot{\eta}_i}\frac{\dot{\varphi}}{V_N} - \sum_{k=1}^{\infty}\left(N_{\eta_{ik}}\eta_k - N_{\dot{\eta}_{ik}}\frac{\dot{\eta}_k}{V_N}\right) = 0 \quad \text{(B-45)}$$

If preferred, the underlined term may be omitted per the discussion of page 10.

Engine Deflection Equation

$$\ddot{\beta} + 2\zeta_E\omega_E\dot{\beta} + \omega_E^2\beta - \omega_E^2\beta_a + \ddot{\varphi} + \sum_{i=1}^{\infty} Y_i'(x_\beta)\ddot{\eta}_i - \frac{M_E l_E}{I_E}\left[\ddot{Z} + l_\beta\ddot{\varphi} + \sum_{i=1}^{\infty} Y_i(x_\beta)\ddot{\eta}_i\right] + \frac{M_E l_E}{I_E}\bar{g}\left[\varphi + \sum_{i=1}^{\infty} Y_i'(x_\beta)\eta_i + \beta\right] = 0 \quad \text{(B-46}$$

Angular Motion Sensed by a Gyro

$$\varphi_G = \varphi + \sum_{i=1}^{\infty} Y_i'(x_G)\eta_i \tag{B-47}$$

Lateral Acceleration Sensed by an Accelerometer

$$\ddot{z}_A = \ddot{Z} + l_A\ddot{\varphi} + \sum_{i=1}^{\infty} Y_i(x_A)\ddot{\eta}_i - \bar{g}\left[\varphi + \sum_{i=1}^{\infty} Y_i'(x_A)\eta_i\right] \tag{B-48}$$

Angle of Attack Sensed by a Forward Vane

For vane on a boom of length l_V which is attached to the booster at x_α:

$$\alpha_V = \alpha(x_\alpha) - \frac{l_V}{V_N}\left[\dot{\varphi} + \sum_{i=1}^{\infty} Y_i'(x_\alpha)\dot{\eta}_i\right] \tag{B-49}$$

Note that the above equations are for the inputs to the various sensors; that is, nonideal sensor effects are not included.

8. ACTUATOR EQUATION

The above equations consider the deflection of the control engines in terms of the actual engine angle, β, and the output of the actuator, β_a. To fully complete the equations an additional expression is required to relate the commanded engine angle, β_c, with β and β_a. The following approximates the actuator by a first-order lag.

The flow rate into the actuator, Q, is given by:

$$Q = K_1(\beta_c - \beta_a) - K_3\frac{f}{A} \tag{B-50}$$

where

K_1 = actuator open-loop gain

β_c = commanded β

f = load on actuator

K_3 = valve pressure feedback gain

A = effective actuator area

An alternate expression for the flow rate is obtained from volumetric considerations.

$$Q = \left(A \dot{\beta}_a + \frac{\dot{f}}{K_0} \right) \tag{B-51}$$

where K_0 = effective hydraulic spring constant

The actuator load is given by:

$$f = K_L(\beta_a - \beta) \tag{B-52}$$

where K_L = effective spring constant of β_a to β compliance

Combining the above gives the final actuator equation:

$$A\left(1 + \frac{K_L}{K_0}\right)\dot{\beta}_a + \left(K_1 + \frac{K_3 K_L}{A}\right)\beta_a - \frac{AK_L}{K_0}\dot{\beta} - \frac{K_3 K_L}{A}\beta = K_1\beta_c \tag{B-53}$$

APPENDIX C

APPROXIMATIONS FOR RIGID-BODY POLES

The complete equations of motion can be written in matrix form as

$$[A]\{x\} = \{\delta\} \tag{C-1}$$

where $[A]$ represents the matrix of stability derivatives and "s" terms

$\{x\}$ represents the column matrix of coordinates

$\{\delta\}$ represents the column matrix of inputs

It will be assumed that two rigid-body equations of motion are represented by the first two rows in the matrices of Eq. C-1. The matrices can then be partitioned so that the coordinates for the rigid-body degrees of freedom, x_1, and the coordinates for the nonrigid-body degrees of freedom, x_2, are in separate partitions, as shown in Eq. C-2 (Ref. 9).

$$\left[\begin{array}{c|c} A_1 & A_2 \\ \hline A_3 & A_4 \end{array}\right] \left\{\begin{array}{c} x_1 \\ \hline x_2 \end{array}\right\} = \left\{\begin{array}{c} \delta_1 \\ \hline \delta_2 \end{array}\right\} \tag{C-2}$$

Expanding Eq. C-2 gives the rigid-body equations

$$[A_1]\{x_1\} + [A_2]\{x_2\} = \{\delta_1\} \tag{C-3}$$

and the "elastic mode" equations

$$[A_3]\{x_1\} + [A_4]\{x_2\} = \{\delta_2\} \tag{C-4}$$

Solving Eq. C-4 for $\{x_2\}$ gives

$$\{x_2\} = [A_4]^{-1}\left[\{\delta_2\} - [A_3]\{x_1\}\right] \tag{C-5}$$

which can now be substituted into Eq. C-3 to eliminate the elastic mode coordinates from the rigid-body equations. Making this substitution and rearranging terms gives

$$\left[\left[A_1\right] - \left[A_2\right]\left[A_4\right]^{-1}\left[A_3\right]\right]\{x_1\} = \{\delta_1\} - \left[A_2\right]\left[A_4\right]^{-1}\{\delta_2\} \quad \text{(C-6)}$$

Equation C-6 is the desired form of the rigid-body equations of motion. As a result of eliminating the elastic mode coordinates, the stability derivatives $\left[A_1\right]$ are seen to be modified by the aeroelastic correction matrix

$$\left[Q\right] \equiv \left[A_2\right]\left[A_4\right]^{-1}\left[A_3\right] \quad \text{(C-7)}$$

The aeroelastic contribution is a direct result of the coupling among the various degrees of freedom. The coupling that influences the rigid-body mode characteristics is due primarily to aerodynamic loads created by the various "elastic" effects. Because the slosh degrees of freedom do not directly affect the aerodynamic loads on the booster, it is assumed that the slosh equations may be neglected. Similarly, because the engine degrees of freedom have a negligible effect on the aerodynamic loads, it is assumed that the engine equations may also be neglected. This leaves the rigid-body and body-bending equations to be considered.

For practical reasons a quasi-static correction is desired. To achieve this, the derivatives of the bending mode coordinates in the rigid-body equations are neglected, leaving only the static deflection terms to add to the rigid-body terms. This has been found to be a valid simplification when only rigid-body modes are of interest (Refs. 9, 10) and is effected by discarding the "s" terms in $\left[A_2\right]$ and $\left[A_4\right]$. It is pointed out that although it is a virtual necessity to neglect the "s" terms in $\left[A_2\right]$ and $\left[A_4\right]$ at this point in the derivation (they would later be found to be unimportant terms if they were retained), to further simplify the computations it is assumed that the "s" terms in $\left[A_3\right]$ can also be neglected. These assumptions will be validated by the numerical results shortly.

With the "s" terms neglected in $[A_2]$, $[A_3]$, and $[A_4]$, the aeroelastic correction matrix (Eq. C-7) is simply a matrix of constants. It has been found that the small off-diagonal terms of $[A_4]$, which represent cross-coupling among the bending modes, can be neglected. Then the correction matrix can be written:

$$
Q = \begin{bmatrix}
-\bar{g}Y_1'(x_\beta) - \dfrac{N_{\eta_1}}{M} & -\bar{g}Y_2'(x_\beta) - \dfrac{N_{\eta_2}}{M} & \cdots \\
\dfrac{-M_{\eta_1} + \bar{g}M\left[Y_1(x_\beta) - l_\beta Y_1'(x_\beta)\right]}{I} & \dfrac{-M_{\eta_2} + \bar{g}M\left[Y_2(x_\beta) - l_\beta Y_2'(x_\beta)\right]}{I} & \cdots
\end{bmatrix}
$$

$$
\times \begin{bmatrix}
\bar{\omega}_1^2 & 0 & \cdots \\
0 & \bar{\omega}_2^2 & \cdots \\
\vdots & \vdots & \\
\end{bmatrix}^{-1}
\times \begin{bmatrix}
\dfrac{N\dot{\eta}_1}{M_1 V_N} & \dfrac{-N\dot{\eta}_1}{M_1} \\
\dfrac{N\dot{\eta}_2}{M_2 V_N} & \dfrac{-N\dot{\eta}_2}{M_2} \\
\vdots & \vdots
\end{bmatrix}
$$

$$
= \begin{bmatrix}
-\sum \dfrac{N\dot{\eta}_i}{M_i V_N \bar{\omega}_i^2}\left[\bar{g}Y_i'(x_\beta) + \dfrac{N_{\eta_i}}{M}\right] & \sum \dfrac{N\dot{\eta}_i}{M_i \bar{\omega}_i^2}\left[\bar{g}Y_i'(x_\beta) + \dfrac{N_{\eta_i}}{M}\right] \\
\sum \dfrac{N\dot{\eta}_i}{IM_i V_N \bar{\omega}_i^2}\left\{-M_{\eta_i} + \bar{g}M\left[Y_i(x_\beta) - l_\beta Y_i'(x_\beta)\right]\right\} & -\sum \dfrac{N\dot{\eta}_i}{IM_i \bar{\omega}_i^2}\left\{-M_{\eta_i} + \bar{g}M\left[Y_i(x_\beta) - l_\beta Y_i'(x_\beta)\right]\right\}
\end{bmatrix}
\qquad \text{(C-8)}
$$

Comparing Eq. C-8 with $[A_1]$, given below, we see that the aeroelastic corrections amount to changes in the aerodynamic derivatives N_α and M_α.

$$[A_1] = \begin{bmatrix} s + \frac{N_\alpha}{MV_N} & \frac{N_{\dot{\Phi}}}{MV_N} s - \bar{g} - \frac{N_\alpha}{M} \\ \frac{M_\alpha}{IV_N} & s^2 + \frac{M_{\dot{\Phi}}}{IV_N} s - \frac{M_\alpha}{I} \end{bmatrix} \tag{C-9}$$

The corrected rigid-body matrix can then be written as

$$[\bar{A}_1] = \begin{bmatrix} s + \frac{\bar{N}_\alpha}{MV_N} & \frac{N_{\dot{\Phi}}}{MV_N} s - \bar{g} - \frac{\bar{N}_\alpha}{M} \\ \frac{\bar{M}_\alpha}{IV_N} & s^2 + \frac{M_{\dot{\Phi}}}{IV_N} s - \frac{\bar{M}_\alpha}{I} \end{bmatrix} \tag{C-10}$$

where

$$\bar{N}_\alpha = N_\alpha + \sum_{i=1}^{\infty} \frac{N_{\dot{\eta}_i}}{M_i \bar{\omega}_i^2} \left[\bar{g} M Y_i'(x_\beta) + N_{\eta_i} \right] \tag{C-11}$$

$$\bar{M}_\alpha = M_\alpha + \sum_{i=1}^{\infty} \frac{N_{\dot{\eta}_i}}{M_i \bar{\omega}_i^2} \left\{ M_{\eta_i} + \bar{g} M \left[l_\beta Y_i'(x_\beta) - Y_i(x_\beta) \right] \right\} \tag{C-12}$$

To illustrate the magnitude of the corrections, let us consider Model Vehicle No. 2 at the Max Q flight condition. Considering the four bending modes used for Model Vehicle No. 2, the various terms of Eq. C-11 and Eq. C-12 would be:

$$\bar{N}_\alpha = (1.4681 - 0.1962 - 0.0201 - 0.0415 + 0.0056) \times 10^6 \text{ kg} \tag{C-13}$$

$$\bar{M}_\alpha = (17.48 + 7.79 + 0.14 + 1.89 + 0.07) \times 10^6 \text{ kg-m} \tag{C-14}$$

From Eqs. C-13 and C-14 we see that the most important aeroelastic correction is a substantial increase in M_α (static instability is increase

There is also an appreciable correction to N_α. For both derivatives the major contribution is from the first bending mode and this term is more than four times the next largest one, which comes from the third bending mode. In subsequent numerical evaluations only the effects of the first bending mode on $\bar{N}_\alpha$ and $\bar{M}_\alpha$ will be included.

The approximate characteristic equation for the rigid-body roots is obtained directly from Eq. C-10:

$$\left|\bar{A}_1\right| = s^3 + s^2\left(\frac{\bar{N}_\alpha}{MV_N} + \frac{M_{\dot{\varphi}}}{IV_N}\right) + s\left(\frac{-M_\alpha}{I} + \frac{\bar{N}_\alpha M_{\dot{\varphi}} - N_{\dot{\varphi}}\bar{M}_\alpha}{MIV_N^2}\right) + \bar{g}\,\frac{M_\alpha}{IV_N} = 0 \qquad \text{(C-15)}$$

The rigid-body roots can be found by numerically factoring the cubic of Eq. C-15; however, literal approximate factors can also be derived. Equation C-15 can be written as follows:

$$\begin{aligned}\left|\bar{A}_1\right| &= \left(s + p_z\right)\left(s + p_{\varphi_1}\right)\left(s + p_{\varphi_2}\right) \\ &= s^3 + s^2\left(p_z + p_{\varphi_1} + p_{\varphi_2}\right) + s\left(p_z p_{\varphi_1} + p_z p_{\varphi_2} + p_{\varphi_1} p_{\varphi_2}\right) + p_z p_{\varphi_1} p_{\varphi_2}\end{aligned} \qquad \text{(C-16)}$$

For a statically stable vehicle ($\bar{M}_\alpha < 0$) the two real φ roots generally combine into a complex pair. In that case it is simpler to substitute

$$2\zeta_\varphi \omega_\varphi = p_{\varphi_1} + p_{\varphi_2} \qquad \text{(C-17)}$$

$$\omega_\varphi^2 = p_{\varphi_1} p_{\varphi_2} \qquad \text{(C-18)}$$

into Eq. C-16. Usually $|p_{\varphi_1} p_{\varphi_2}| \gg |p_z(p_{\varphi_1} + p_{\varphi_2})|$ or for a complex pair $\omega_\varphi \gg |2\zeta_\varphi p_z|$, so that p_z can be approximated by the ratio of the last two coefficients of Eq. C-15, i.e.,

$$p_z \doteq \frac{\bar{g}\,\dfrac{M_\alpha}{IV_N}}{\dfrac{-\bar{M}_\alpha}{I} + \dfrac{\bar{N}_\alpha M_{\dot{\varphi}} - N_{\dot{\varphi}}\bar{M}_\alpha}{MIV_N^2}} \qquad \text{(C-19)}$$

Since it is generally true that

$$\left|M_\alpha\right| \gg \left|\frac{\bar{N}_\alpha M_{\dot{\varphi}} - N_{\dot{\varphi}}\bar{M}_\alpha}{MV_N^2}\right|$$

Eq. C-19 may be further simplified to

$$p_z \doteq \frac{-\bar{g}}{V_N} \tag{C-20}$$

Equating the remaining terms of Eqs. C-15 and C-16, we find

$$\left.\begin{array}{c} p_{\varphi_1} + p_{\varphi_2} \\ \text{or} \\ 2\zeta_\varphi\omega_\varphi \end{array}\right\} \begin{array}{l} \doteq \dfrac{M_{\dot{\varphi}}}{IV_N} + \dfrac{\bar{N}_\alpha}{MV_N} - p_z \\ \\ \doteq \dfrac{M_{\dot{\varphi}}}{IV_N} + \dfrac{\bar{N}_\alpha}{MV_N} + \dfrac{\bar{g}}{V_N} \end{array} \tag{C-21}$$

$$\left.\begin{array}{c} p_{\varphi_1} p_{\varphi_2} \\ \text{or} \\ \omega_\varphi^2 \end{array}\right\} \doteq \frac{-\bar{M}_\alpha}{I} \tag{C-22}$$

For a statically unstable vehicle ($\bar{M}_\alpha > 0$) a further simplification for the φ roots results if

$$\left|\frac{\bar{M}_\alpha}{I}\right| \gg \left[\frac{M_{\dot{\varphi}}}{IV_N} + \frac{\bar{N}_\alpha}{MV_N} + \frac{\bar{g}}{V_N}\right]^2$$

i.e.,

$$p_{\varphi_1} \doteq -\sqrt{\frac{\bar{M}_\alpha}{I}} + \frac{1}{2}\left(\frac{M_{\dot{\varphi}}}{IV_N} + \frac{\bar{N}_\alpha}{MV_N} + \frac{\bar{g}}{V_N}\right) \tag{C-23}$$

$$p_{\varphi_2} \doteq \sqrt{\frac{\bar{M}_\alpha}{I}} + \frac{1}{2}\left(\frac{M_{\dot{\varphi}}}{IV_N} + \frac{\bar{N}_\alpha}{MV_N} + \frac{\bar{g}}{V_N}\right) \tag{C-24}$$

Using the Model Vehicle No. 2 dynamic characteristics, the rigid-body poles obtained from the approximations derived above are compared, in Table C-I, with the exact values from the 11-by-11 matrix of Fig. 3. This comparison illustrates three important points:

- Adequate simple approximations for the rigid-body roots are available.
- During periods of high dynamic pressure, the aeroelastic correction can greatly improve the accuracy.
- When the conditions of validity are satisfied, the literal factors give adequate results. The relatively large errors for burnout are because ω_φ is only eight times $|2\zeta_\varphi p_z|$.

TABLE C-I

COMPARISON OF EXACT AND APPROXIMATE RIGID-BODY ROOTS

FLIGHT CONDITION	PARAMETER	EXACT VALUE	CUBIC (EQ. C-15) APPROXIMATION WITHOUT AEROELASTIC CORRECTION[1]	ERROR[2]	CUBIC (EQ. C-15) APPROXIMATION WITH AEROELASTIC CORRECTION[1]	ERROR[2]	LITERAL FACTORS[3]	ERROR[2]
Lift-off	p_z (sec^{-1})	0	0					
	p_{φ_1} (sec^{-1})	0	0	NA	NA	NA	NA	NA
	p_{φ_2} (sec^{-1})	0	0					
Max Q	p_z (sec^{-1})	−0.04202	−0.04288	2.0	−0.04202	0	−0.04048	−3.7
	p_{φ_1} (sec^{-1})	−0.2786	−0.2178	−22	−0.2730	−2.0	−0.2769	−0.6
	p_{φ_2} (sec^{-1})	0.3644	0.3017	−17	0.3547	−2.7	0.3571	−2.0
Burnout	p_z (sec^{-1})	−0.01428	−0.01412	−1.1			−0.01631	14.2
	ζ_φ	0.176	0.184				0.228	
	$\zeta_\varphi\omega_\varphi$ (rad/sec)	0.00717	0.00711	−0.8	NA	NA	0.00820	14.4
	ω_φ (rad/sec)	0.04073	0.03866	−5.1			0.03597	−11.7

[1] Aeroelastic correction is applied only at Max Q; $N_{\dot{\eta}_1}$ was assumed zero at LO and BO.

[2] Error = $\left[(\text{Approximate}-\text{Exact})/\text{Exact}\right] \times 100$.

[3] Literal factors are Eq. C-20 and Eqs. C-21, C-22 (BO), or C-23, C-24 (Max Q).

APPENDIX D

APPROXIMATIONS FOR SLOSH AND BENDING MODE POLES

As a starting point for the examination of slosh and bending modes we will compare the exact and the uncoupled solutions for the example vehicle. Table D-I summarizes the values of the slosh and bending modes as obtained from various types of approximations at each of the three flight conditions. Focusing attention on the first three columns, the first column lists the "exact" values — the roots obtained from the complete 11-degree-of-freedom matrix as given in Fig. 3. The "uncoupled" values (second column) include no coupling effects. The "diagonal" values (third column) include all terms in the 11-by-11 principal diagonal wherein the slosh mode frequencies are identical to the uncoupled values, but bending modes include self-coupling terms,* i.e.,

$$s^2 + \left(2\zeta_i\omega_i + \frac{N\eta_{ii}}{M_i V_N}\right)s + \omega_i^2 + \frac{1}{M_i}\left[-N\eta_{ii} + \tilde{g}FM_E l_E Y_i'^2(x_\beta) - \underline{\tilde{g}MY_i'(x_\beta)Y_i(x_\beta)}\right] = s^2 + 2\overline{\zeta_i\omega_i}s + \overline{\omega_i}^2 \quad \text{(D-1)}$$

Examination of Table D-I shows that the diagonal terms generally give adequate approximations of the damping ratios, but that the frequencies can have as much as a 10 percent error. In other words, the cross-couplings primarily affect the modal frequencies rather than the dampings. It is also noted that the second, third, and fourth bending mode frequencies are always greater than the slosh mode frequencies, and that the diagonal approximations for these bending frequencies are always low.

The next level of approximation is to add the cross-coupling of the slosh modes through the rigid-body modes or, in other words, to add a dynamic correction to the slosh modes for the rigid-body modes. This gives us the following approximate equations of motion:

*The underlined term may be omitted as discussed on page 10.

$$\begin{bmatrix} 1 & 0 & \frac{M_{s_1}}{M}s^2 & \frac{M_{s_2}}{M}s^2 & \frac{M_{s_3}}{M}s^2 \\ 0 & 1 & \frac{M_{s_1}l_{s_1}}{I}s^2 & \frac{M_{s_2}l_{s_2}}{I}s^2 & \frac{M_{s_3}l_{s_3}}{I}s^2 \\ 1 & l_{s_1} & s^2+2\zeta_{s_1}\omega_{s_1}s+\omega_{s_1}^2 & 0 & 0 \\ 1 & l_{s_2} & 0 & s^2+2\zeta_{s_2}\omega_{s_2}s+\omega_{s_2}^2 & 0 \\ 1 & l_{s_3} & 0 & 0 & s^2+2\zeta_{s_3}\omega_{s_3}s+\omega_{s_3}^2 \end{bmatrix} \begin{Bmatrix} \ddot{z} \\ \ddot{\varphi} \\ z_{s_1} \\ z_{s_2} \\ z_{s_3} \end{Bmatrix} = 0 \quad \text{(D-2)}$$

Equation D-2 can be reduced to the following characteristic equation for the coupled slosh modes:

$$\begin{bmatrix} s^2\left(1-\frac{M_{s_1}}{M}-\frac{M_{s_1}l_{s_1}^2}{I}\right) + 2\zeta_{s_1}\omega_{s_1}s+\omega_{s_1}^2 & -s^2\left(\frac{M_{s_2}}{M}+\frac{M_{s_2}l_{s_1}l_{s_2}}{I}\right) & -s^2\left(\frac{M_{s_3}}{M}+\frac{M_{s_3}l_{s_1}l_{s_3}}{I}\right) \\ -s^2\left(\frac{M_{s_1}}{M}+\frac{M_{s_1}l_{s_1}l_{s_2}}{I}\right) & s^2\left(1-\frac{M_{s_2}}{M}-\frac{M_{s_2}l_{s_2}^2}{I}\right) + 2\zeta_{s_2}\omega_{s_2}s+\omega_{s_2}^2 & -s^2\left(\frac{M_{s_3}}{M}+\frac{M_{s_3}l_{s_2}l_{s_3}}{I}\right) \\ -s^2\left(\frac{M_{s_1}}{M}+\frac{M_{s_1}l_{s_1}l_{s_3}}{I}\right) & -s^2\left(\frac{M_{s_2}}{M}+\frac{M_{s_2}l_{s_2}l_{s_3}}{I}\right) & s^2\left(1-\frac{M_{s_3}}{M}-\frac{M_{s_3}l_{s_3}^2}{I}\right) + 2\zeta_{s_3}\omega_{s_3}s+\omega_{s_3}^2 \end{bmatrix} = 0 \quad \text{(D-3}$$

The characteristic roots obtained from Eq. D-3 are listed in Table D-I under the heading "Three Slosh."

TABLE D-I

COMPARISON OF EXACT AND APPROXIMATE ROOTS

(a) Lift-Off

MODE	EXACT	UNCOUPLED	DIAGONAL	THREE SLOSH	THREE SLOSH + η_1	THREE SLOSH + $\eta_1(\eta_2)$	THREE SLOSH + $\eta_1(\eta_2,\eta_3)$	BENDING (SLOSH)
First slosh								
ζ	0.0045	0.0050	0.0050	0.0048	0.0044	0.0043	0.0045	
ω	2.030	2.136	2.136	2.209	2.000	2.008	2.018	
ω error ...		5.2	5.2	8.8	-1.5	-1.1	-0.6	
Second slosh								
ζ	0.0050	0.0050	0.0050	0.0050	0.0050	0.0051	0.0050	
ω	2.132	2.136	2.136	2.126	2.145	2.115	2.136	
ω error ...		0.2	0.2	-0.3	0.6	-0.8	0.2	
Third slosh								
ζ	0.0052	0.0050	0.0050	0.0055	0.0052	0.0051	0.0051	
ω	2.221	2.136	2.136	2.228	2.213	2.236	2.194	
ω error ...		-3.8	-3.8	0.3	-0.4	0.7	-1.2	
First bending								
ζ	0.0054	0.0050	0.0046		0.0057	0.0057	0.0055	
ω	2.607	2.156	2.350		2.700	2.684	2.608	
ω error ...		-17.3	-9.8		3.6	3.0	0.04	
Second bending								
ζ	0.0048	0.0050	0.0049					0.0049
ω	5.289	5.062	5.185					5.257
ω error ...		-4.3	-2.0					-0.6
Third bending								
ζ	0.0049	0.0050	0.0050					0.0051
ω	9.188	8.783	8.872					9.151
ω error ...		-4.4	-3.4					-0.4
Fourth bending								
ζ	0.0050	0.0050	0.0050					0.0050
ω	12.58	12.36	12.39					12.54
ω error ...		-1.7	-1.5					-0.3

ω in rad/sec ; error = $\left[(\text{approximate}-\text{exact})/\text{exact}\right] \times 100$

Table D-I (Continued)

(b) Max Q

MODE	EXACT	UNCOUPLED	DIAGONAL	THREE SLOSH	THREE SLOSH + η_1	THREE SLOSH + $\eta_1(\eta_2)$	BENDING (SLOSH)	
First slosh								
ζ	0.0050	0.0050	0.0050	0.0050	0.0051	0.0050		
ω	2.750	2.765	2.765	2.776	2.777	2.776		
ω error ...		0.6	0.6	1.0	1.0	1.0		
Second slosh								
ζ	0.0057	0.0050	0.0050	0.0055	0.0054	0.0055		
ω	3.047	2.765	2.765	3.050	3.048	3.046		
ω error ...		-9.2	-9.2	0.1	0.03	-0.03		
Third slosh								
ζ	0.0087	0.0050	0.0050	0.0052	0.0092	0.0086		
ω	3.131	2.827	2.827	2.882	3.184	3.153		
ω error ...		-9.7	-9.7	-8.0	1.7	0.7		
First bending								
ζ	0.0141	0.0050	0.0159		0.0125	0.0126		
ω	2.234	2.319	2.407		2.268	2.243		
ω error ...		3.8	7.8		1.5	0.4		
Second bending								
ζ	0.0084	0.0050	0.0088				0.0091	
ω	6.022	5.645	5.739				5.921	
ω error ...		-6.3	-4.7				-1.7	
Third bending								
ζ	0.0071	0.0050	0.0070				0.0075	
ω	9.944	9.184	9.299				9.886	
ω error ...		-7.6	-6.5				-0.6	
Fourth bending								
ζ	0.0064	0.0050	0.0068				0.0070	
ω	12.89	12.50	12.45				12.72	
ω error ...		-3.0	-3.4				-1.3	

ω in rad/sec ; error = $\left[(\text{approximate}-\text{exact})/\text{exact}\right] \times 100$

Table D-I (Concluded)

(c) Burnout

MODE	EXACT	UNCOUPLED	DIAGONAL	THREE SLOSH	THREE SLOSH + η_1	THREE SLOSH + η_1 (η_2)	BENDING (SLOSH)	THIRD SLOSH + η_1 + η_2
First slosh								
ζ	0.0048	0.0050	0.0050	0.0050	0.0049	0.0049		
ω	3.680	3.581	3.581	3.605	3.692	3.683		
ω error ...		−2.7	−2.7	−2.0	0.3	0.1		
Second slosh								
ζ	0.0043	0.0050	0.0050	0.0051	0.0050	0.0051		
ω	4.027	3.770	3.770	3.815	4.076	4.033		
ω error ...		−6.4	−6.4	−5.3	1.2	0.2		
Third slosh								
ζ	0.0051	0.0050	0.0050	0.0053	0.0054	0.0051		0.0051
ω	4.951	4.712	4.712	4.980	5.059	5.053		4.914
ω error ...		−4.8	−4.8	0.6	2.2	2.1		−0.7
First bending								
ζ	0.0039	0.0050	0.0039		0.0042	0.0042		0.0041
ω	3.409	2.915	3.727		3.424	3.401		3.607
ω error ...		−14.5	9.3		0.4	−0.2		5.8
Second bending								
ζ	0.0028	0.0050	0.0047				0.0049	0.0050
ω	7.419	6.592	6.951				7.105	7.318
ω error ...		−11.1	−6.3				−4.2	−1.4
Third bending								
ζ	0.0046	0.0050	0.0050				0.0051	
ω	11.86	11.71	11.77				11.63	
ω error ...		−1.3	−0.8				−1.9	
Fourth bending								
ζ	0.0053	0.0050	0.0050				0.0050	
ω	24.99	24.86	24.90				25.01	
ω error ...		−0.5	−0.4				0.1	

ω in rad/sec ; error = $\left[(\text{approximate}-\text{exact})/\text{exact}\right] \times 100$

For the three flight conditions, this relatively simple equation gives the frequencies of two modes within 2 percent. The frequency for the third mode has a sizable error. From the study of the MRR it would appear that the primary source of this error is the coupling with the first bending mode.

The principal source of slosh–bending coupling occurs through inertial rather than aerodynamic or thrust terms. Consequently our next approximation is to solve for the three slosh and first bending modes simultaneously using the following characteristic equation:

$$\begin{vmatrix} & & & s^2 Y_1(x_{s_1}) \\ & S_3 & & s^2 Y_1(x_{s_2}) \\ & & & s^2 Y_1(x_{s_3}) \\ \hline \frac{M_{s_1} Y_1(x_{s_1})}{M_1} s^2 & \frac{M_{s_2} Y_1(x_{s_2})}{M_1} s^2 & \frac{M_{s_3} Y_1(x_{s_3})}{M_1} s^2 & s^2 + 2\overline{\zeta_1 \omega_1} s + \bar{\omega}_1^2 \end{vmatrix} = 0 \quad \text{(D-4)}$$

where S_3 is the 3-by-3 matrix of Eq. D-3. The characteristic roots obtained from Eq. D-13 are listed in Table D-I under the heading "Three Slosh + η_1."

The addition of the first bending mode has greatly reduced frequency errors in general, but a 3.6 percent error remains in the first bending mode at LO. It was felt that this error was probably due to the effects of higher bending modes. Therefore a static correction was applied to the η_1 equation for the effects of the second bending mode. This results in the following characteristic equation:*

*In the body of the report the determinant is written with the fifth row divided by $\bar{\omega}_2^2$. This is done to avoid confusion in subsequent expressions for the denominator lead coefficient.

$$
\begin{vmatrix}
 & & & s^2 Y_1(x_{s_1}) & 0 \\
 & S_3 & & s^2 Y_1(x_{s_2}) & 0 \\
 & & & s^2 Y_1(x_{s_3}) & 0 \\
\hline
\frac{M_{s_1} Y_1(x_{s_1})}{M_1} s^2 & \frac{M_{s_2} Y_1(x_{s_2})}{M_1} s^2 & \frac{M_{s_3} Y_1(x_{s_3})}{M_1} s^2 & s^2 + 2\overline{\zeta_1 \omega_1} s + \overline{\omega}_1^2 & c_{12} \\
\frac{M_{s_1} Y_2(x_{s_1})}{M_2} s^2 & \frac{M_{s_2} Y_2(x_{s_2})}{M_2} s^2 & \frac{M_{s_3} Y_2(x_{s_3})}{M_2} s^2 & c_{21} & \overline{\omega}_2^2
\end{vmatrix} = 0 \quad \text{(D-5)}
$$

where $$c_{ij} = \frac{1}{M_i} \left\{ -N_{\eta_{ij}} + \tilde{g} Y_j'(x_\beta) \left[F M_E l_E Y_i'(x_\beta) - M Y_i(x_\beta) \right] \right\} \quad \text{(D-6)}$$

Equation D-5 can be reduced to a 4-by-4 determinant that is identical to Eq. D-4 except for the last row, which becomes

$$
s^2 M_{s_1} \left[\frac{Y_1(x_{s_1})}{M_1} - \frac{c_{12}}{\overline{\omega}^2} \frac{Y_2(x_{s_1})}{M_2} \right] \quad s^2 M_{s_2} \left[\frac{Y_1(x_{s_2})}{M_2} - \frac{c_{12}}{\overline{\omega}^2} \frac{Y_2(x_{s_2})}{M_2} \right] \quad s^2 M_{s_3} \left[\frac{Y_1(x_{s_3})}{M_1} - \frac{c_{12}}{\overline{\omega}^2} \frac{Y_2(x_{s_3})}{M_2} \right] \quad s^2 + 2\overline{\zeta_1 \omega_1} s + \overline{\omega}_1^2 - \frac{c_{12} c_{21}}{\overline{\omega}_2^2}
$$

The characteristic roots obtained from this equation are listed in Table D-I under the heading "Three Slosh + $\eta_1 (\eta_2)$."

Now there are only two frequency errors greater than 2 percent — the third slosh mode at BO and the first bending mode at LO. The error in the third slosh mode at BO will be discussed later. The error in the first bending mode at LO may be reduced by including a static correction for the third bending mode. This is accomplished by adding a sixth row to the 5-by-5 determinant of Eq. D-5,

$$
\frac{M_{s_1}}{M_3} Y_3(x_{s_1}) s^2 \quad \frac{M_{s_2}}{M_3} Y_3(x_{s_2}) s^2 \quad \frac{M_{s_3}}{M_3} Y_3(x_{s_3}) s^2 \quad c_{31} \quad c_{32} \quad \overline{\omega}_3^2
$$

and a sixth column,

$$0 \qquad 0 \qquad 0 \qquad c_{13} \qquad c_{23} \qquad \bar{\omega}_3^2$$

The characteristic roots obtained from this equation are listed in Table D-Ia under the heading "Three Slosh + $\eta_1(\eta_2, \eta_3)$."

With this correction the accuracy for all four modes at LO is very good; maximum error is 1.2 percent. Thus it appears that, with the exception of the third slosh at BO, accuracies on the order of 1 percent or better can be obtained for the sloshing and first bending modes by including only the inertial coupling terms and static corrections for the higher bending modes.

Approximations for the second, third, and fourth bending modes are obtained by adding a dynamic correction for the slosh modes. This correction is discussed in Section III-C. The resultant characteristic equation (Eq. 23) gives the approximate roots listed in Table D-I under the heading "Bending (Slosh)." Except for the second bending mode at BO, the frequency errors are all less than 2 percent. The relatively poor accuraty at BO for the second bending and third slosh is caused by the small (50 percent) frequency separation of these modes.

The coupling between the third slosh mode and the second bending mode at BO is also discussed in Section III-C. The approximation derived there (Eq. 25) includes the third slosh mass plus the first and second bending modes with a dynamic correction for the rigid-body modes. Roots obtained from this approximation are listed in Table D-Ic under "Third Slosh + η_1 + η_2." Note that this gives good results for the third slosh and second bending modes, but that for the first bending mode we have to use the "Three Slosh + $\eta_1(\eta_2)$" approximation.

APPENDIX E

APPROXIMATIONS FOR ACTUATOR POLES

The coupled modes to be considered here are the first-order lag, p_a, of the actuator and the second-order mode, ω_a, of the compliance in the actuator–nozzle connection. As a first approximation we will neglect the rigid-body and bending contributions to the engine deflection equations. This leaves the lower right 2-by-2 submatrix of the original 11-by-11, i.e.,

$$\begin{bmatrix} s^2 + 2\zeta_E\omega_E s + \omega_E^2 + \frac{\bar{g}M_E l_E}{I_E} & -\omega_E^2 \\ \frac{-AK_L}{K_0}\,s - \frac{K_3K_L}{A} & \frac{A(K_0+K_L)}{K_0}\,s + K_1 + \frac{K_3K_L}{A} \end{bmatrix} \begin{Bmatrix} \beta \\ \beta_a \end{Bmatrix} = 0 \quad \text{(E-1)}$$

which yields a cubic characteristic equation:

$$\frac{A(K_0+K_L)}{K_0}\,s^3 + \left[2\zeta_E\omega_E\frac{A(K_0+K_L)}{K_0} + K_1 + \frac{K_3K_L}{A}\right]s^2 + \left[2\zeta_E\omega_E\left(K_1 + \frac{K_3K_L}{A}\right) + \omega_A^2 A + \frac{\bar{g}M_E l_E}{I_E}\frac{A(K_0+K_L)}{K_0}\right]s + \omega_E^2 K_1 + \frac{\bar{g}M_E l_E}{I_E}\left(K_1 + \frac{K_3K_L}{A}\right) = 0 \quad \text{(E-2)}$$

In Eq. E-2 only $\bar{g}$ varies throughout the flight. Since the terms involving $\bar{g}$ are quite small, this approximation gives roots which change slightly with flight condition. The roots obtained from Eq. E-2 are compared with the exact values from the complete 11-by-11 matrix in Table E-I under the heading "Cubic." The worst errors occur at BO where the first-order lag is off by 4 percent and the second-order frequency is off by 12 percent. While these errors are relatively large compared to those obtained for other modes, the approximations are probably satisfactory for preliminary analyses (a more accurate approximation will be derived shortly).

TABLE E-I

ACCURACY OF ACTUATOR APPROXIMATIONS

FLIGHT CONDITION	PARAMETER	EXACT	CUBIC	LITERAL	CUBIC (RB, η_i)
Lift-off	p_a (sec^{-1})	14.56	14.66	14.04	14.63
	ζ_a	0.0984	0.0982	0.1028	0.0973
	ω_a (rad/sec)	47.04	46.15	47.09	47.14
	p_a error*		0.7	-3.6	0.5
	ω_a error*		-1.9	0.1	0.2
Max Q	p_a (sec^{-1})	14.52	14.66	14.04	14.62
	ζ_a	0.0986	0.0980	0.1028	0.0967
	ω_a (rad/sec)	47.53	46.18	47.09	47.64
	p_a error*		1.0	-3.3	0.7
	ω_a error*		-2.8	-0.9	0.2
Burnout	p_a (sec^{-1})	14.14	14.69	14.04	14.52
	ζ_a	0.0979	0.0977	0.1028	0.0918
	ω_a (rad/sec)	52.50	46.26	47.09	53.39
	p_a error*		3.9	-0.7	2.7
	ω_a error*		-11.9	-10.3	1.7

*Error = [(Approximate-Exact)/Exact] × 100

In general, the roots of Eq. E-2 may be approximated via the factoring method of Appendix C; the real root is obtained from the ratio of the last two coefficients. Dropping small terms, the literal expression becomes

$$p_a \doteq \frac{\omega_E^2 K_1}{\omega_E^2 A} = \frac{K_1}{A} \tag{E-3}$$

The second-order then is approximated by

$$\omega_a^2 \doteq \omega_E^2 \left(\frac{K_0}{K_0 + K_L}\right) \tag{E-4}$$

$$2\zeta_a\omega_a \doteq 2\zeta_E\omega_E + \left(K_1 + \frac{K_3 K_L}{A}\right)\left(\frac{K_0}{A(K_0 + K_L)}\right) - \frac{K_1}{A}$$

$$\doteq 2\zeta_E\omega_E + \frac{K_L}{A}\frac{\left(\frac{K_0 K_3}{A} - K_1\right)}{(K_0 + K_L)} \tag{E-5}$$

Note that the term containing $\bar{g}$ is among the small terms dropped, hence the above values are independent of flight condition. The resulting approximations are listed in Table E-I under the heading "Literal." The fact that the maximum error obtained with these "approximations to an approximation" is less than that obtained from factoring the cubic is purely coincidental.

A more accurate approximation is obtained for these modes by including a dynamic correction for the rigid-body and bending modes. The procedure is identical to that used in correcting the second to fourth bending modes for the slosh masses. The dynamic correction changes only the upper left element in Eq. E-1. It becomes

$$\left\{1 - \frac{C}{I_E}\left[\frac{(M_E l_E)^2}{M} + \frac{(I_E - M_E l_E l_\beta)^2}{I} + \sum_i \frac{\left[I_E Y_i'(x_\beta) - M_E l_E Y_i(x_\beta)\right]^2}{M_i}\right]\right\} s^2$$

$$+ 2\zeta_E\omega_E s + \omega_E^2 + \frac{\bar{g} M_E l_E}{I_E}$$

The approximate roots with these corrections are listed in Table E-I under "Cubic (RB, η_i)." The errors in p_a and ω_a are greatly reduced. Maximum errors still occur at BO, but are not only 2.7 and 1.7 percent for p_a and ω_a.

Obviously, conditions of validity for the application of Eqs. E-3 through E-5 involve the relative magnitudes of terms in the exact equations of motion. However, in general, $\omega_a^2 \gg 2\zeta_a\omega_a p_a$ which allows the direct approximation of roots via Eqs. E-3 through E-5. If this inequality is not valid, the roots must be obtained by factoring Eq. E-2. Further, Eqs. E-3 through E-5 require the dynamic correction to be small:

$$\frac{C}{I_E}\left\{\frac{(M_E l_E)^2}{M} + \frac{(I_E - M_E l_E l_\beta)^2}{I} + \sum_i \frac{\left[I_E Y_i'(x_\beta) - M_E l_E Y_i(x_\beta)\right]^2}{M_i}\right\} \ll 1$$

This inequality is not so general as is indicated by the effect the dynamic correction has at BO. Note, however, that the major contribution of this correction is easily included in Eq. E-4 when appropriate, i.e.,

$$\omega_a^2 \doteq \left(\frac{K_O}{K_O + K_L}\right)\left[\frac{\omega_E^2}{1 - \frac{C}{I_E}\left\{\frac{(M_E l_E)^2}{M} + \frac{(I_E - M_E l_E l_\beta)^2}{I} + \sum_i \frac{\left[I_E Y_i'(x_\beta) - M_E l_E Y_i(x_\beta)\right]^2}{M_i}\right\}}\right] \tag{E-6}$$

Equation E-6 results in an error similar to that indicated in Table E-I under "Cubic (RB, η_i)."

APPENDIX F

APPROXIMATIONS FOR RIGID-BODY ZEROS

1. $\dot{Z}$ NUMERATOR

Considering only the $\dot{Z}$ and φ equations, the characteristic equation for the φ zeros of the $\dot{Z}$ numerator can be written as:

$$\begin{vmatrix} 1 & \frac{N_{\dot{\varphi}}}{MV_N}s - \bar{g} - \frac{N_\alpha}{M} \\ \frac{Ml_\beta}{I} & s^2 + \frac{M_{\dot{\varphi}}}{IV_N}s - \frac{M_\alpha}{I} \end{vmatrix} = 0 \qquad \text{(F-1)}$$

or

$$s^2 + \frac{1}{IV_N}\left(M_{\dot{\varphi}} - l_\beta N_{\dot{\varphi}}\right)s + \frac{l_\beta(\bar{g}M + N_\alpha) - M_\alpha}{I} = 0 \qquad \text{(F-2)}$$

In Eq. F-1 only the thrust portions of the static terms in the β column have been retained, and the column has been normalized to unity on the main diagonal. This normalization is done to avoid confusion in the expressions for the numerator lead coefficients.

The approximate zeros obtained from Eq. F-1 are listed in Table F-I under "Rigid Body." The maximum error is 14.6 percent. To reduce the errors we add a static correction for the first bending mode using the same technique employed for the denominator. The characteristic equation with the static correction is given in Section IV (Eq. 35). The zeros obtained from it are listed in Table F-I under "Rigid Body (η_1)." The maximum error is now reduced to 5 percent, which is acceptable since the closure of a load relief loop will be relatively insensitive to the exact location of these zeros.

TABLE F-I

RIGID-BODY ZEROS OF $\dot{Z}$ NUMERATOR

FLIGHT CONDITION	ZERO (sec^{-1})	EXACT	RIGID BODY	ERROR*	RIGID BODY (η_1)	ERROR*
Lift-off	z_{φ_1}	-0.8689	-0.8055	-7.3	-0.8608	-0.9
	z_{φ_2}	0.8693	0.8055	-7.3	0.8608	-1.0
Max Q	z_{φ_1}	-1.089	-1.058	-2.8	-1.056	-3.0
	z_{φ_2}	1.123	1.094	-2.6	1.092	-2.7
Burnout	z_{φ_1}	-2.126	-1.857	-12.7	-2.233	5.0
	z_{φ_2}	2.128	1.857	-14.6	2.233	4.9

*Error = [(Approximate-Exact)/Exact] × 100

2. φ NUMERATOR

Considering only the $\dot{Z}$ and φ equations, the characteristic equation for the Z zero of the φ numerator is:

$$\begin{vmatrix} s + \frac{N_\alpha}{MV_N} & \frac{I}{Ml_\beta} \\ \frac{M_\alpha}{IV_N} & 1 \end{vmatrix} = 0 \qquad \text{(F-3)}$$

or

$$s + \frac{1}{MV_N}\left(N_\alpha - \frac{M_\alpha}{l_\beta}\right) = 0 \qquad \text{(F-4)}$$

At LO both the complete equations and Eq. F-4 give a zero at the origin. At Max Q the exact value is 0.01369 sec^{-1} and the approximation is 0.01390 sec^{-1}, an error of 1.5 percent. The error at BO is -2.4 percent, the exact value is 0.780×10^{-4} sec^{-1}, and the approximation is 0.762×10^{-4} sec^{-1}. This is more than adequate accuracy for this zero.

3. η_i NUMERATOR

For the rigid-body zeros of the η_i numerator we start by including the rigid-body modes and the static effects of the ith bending mode. This gives a characteristic equation of

$$\begin{vmatrix} s + \frac{N_\alpha}{MV_N} & \frac{N_{\dot\Phi}}{MV_N} s - \bar{g} - \frac{N_\alpha}{M} & \frac{M_i}{MY_i(x_\beta)} \\ \frac{M_\alpha}{IV_N} & s^2 + \frac{M_{\dot\Phi}}{IV_N} s - \frac{M_\alpha}{I} & \frac{M_i l_\beta}{IY_i(x_\beta)} \\ \frac{N_{\dot\eta_i}}{M_i V_N} & \frac{-N_{\dot\eta_i}}{M_i} & 1 \end{vmatrix} = 0 \qquad \text{(F-5)}$$

The zeros obtained from Eq. F-5 are listed* in Table F-II under "Rigid Body." The results for the η_1 numerator are satisfactory, but there are large errors for the other numerators.

By analogy with the denominator approximations, the next step is to add a static correction for the first bending mode. This correction adds a fourth row and column to Eq. F-5 (see Eq. 38, Section IV, for the complete determinant). The zeros obtained with the correction are listed in Table F-IIa under "Rigid Body (η_1)." The errors at Max Q have been greatly reduced. The largest one is now an acceptable 8 percent.

The static correction for the first bending mode has little effect at BO because the aerodynamic derivatives M_{η_i}, $N_{\dot\eta_i}$, and N_{η_i} were assumed zero in the exact solution. By process of elimination it appeared that the only cause of the large errors at BO could be the third slosh mass (the other two slosh masses are very small at BO). Consequently a static correction for the third slosh mass was added to Eq. F-5 (see Eq. 39,

*As noted in Section IV, all three zeros are at the origin for the LO condition.

Section IV). For this case we found that it was necessary to retain the s term in the $\dot{Z}$ column and the $l_{s_3}s^2$ term in the φ column.

TABLE F-II

RIGID-BODY ZEROS OF η_i NUMERATORS

(a) Maximum Q

NUMERATOR	ZERO		EXACT	RIGID BODY	ERROR*	RIGID BODY (η_1)	ERROR*
η_1	z_z	(sec^{-1})	-0.04112	-0.04097	-0.4		
	z_{φ_1}	(sec^{-1})	-0.4714	-0.4609	-2.2		
	z_{φ_2}	(sec^{-1})	0.5683	0.5345	-5.9		
η_2	z_z	(sec^{-1})	-0.04156	-0.04185	0.7	-0.04226	1.7
	z_{φ_1}	(sec^{-1})	-0.2585	-0.2888	11.9	-0.2541	-1.8
	z_{φ_2}	(sec^{-1})	0.3118	0.3698	18.8	0.3365	7.9
η_3	z_z	(sec^{-1})	-0.04098	-0.04092	-0.1	-0.04093	-0.1
	z_{φ_1}	(sec^{-1})	-0.4897	-0.4816	-1.6	-0.4812	-1.7
	z_{φ_2}	(sec^{-1})	0.5728	0.5542	-3.3	0.5538	-3.3
η_4	z_z	(sec^{-1})	-0.04022	-0.03817	-5.0	-0.03934	-2.2
	ζ_φ		0.0297	0.1661		0.1169	
	ω_φ	(rad/sec)	0.4061	0.2572	-37.0	0.3877	-4.5

*Error = [(Approximate-Exact)/Exact] x 100

The results obtained with the slosh correction are listed in Table F-IIb under "Rigid Body (z_{s_3})." The maximum error has now been reduced to 6 percent.

Table F-II (contd)

(b) Burnout

NUMERATOR	ZERO		EXACT	RIGID BODY	ERROR*	RIGID BODY (η_1)	ERROR*
η_1	z_z	(sec^{-1})	-0.01411	-0.01412	0.1	-0.01413	0.1
	ζ_φ		0.1838	0.1837		0.1833	
	ω_φ	(rad/sec)	0.03864	0.03866	0.1	0.03875	0.3
η_2	z_z	(sec^{-1})	-0.01423	-0.01412	-0.7	-0.01421	-0.1
	ζ_φ		0.1786	0.1837		0.1796	
	ω_φ	(rad/sec)	0.04007	0.03866	-3.7	0.03979	-0.7
η_3	z_z	(sec^{-1})	-0.01448	-0.01412	-2.5	-0.01439	-0.6
	ζ_φ		0.1662	0.1837		0.1704	
	ω_φ	(rad/sec)	0.04381	0.03866	-11.7	0.04248	-3.0
η_4	z_z	(sec^{-1})	-0.01484	-0.01412	-4.8	-0.01469	-1.0
	ζ_φ		0.1467	0.1837		0.1546	
	ω_φ	(rad/sec)	0.05086	0.03866	-24.9	0.04780	-6.0

*Error = [(Approximate-Exact)/Exact] × 100

APPENDIX G

APPROXIMATIONS FOR SLOSH AND FIRST BENDING ZEROS

1. φ NUMERATOR

The most complete approximation for the slosh and first bending zeros starts with a 7-by-7 determinant which includes:

- Dynamic correction for Z
- Control characteristics in φ column
- Three slosh modes
- First bending mode
- Static correction for second bending mode

This 7-by-7 determinant is given by:

$$
\begin{vmatrix}
1 & \frac{1}{M} & \frac{M_{s_1}}{M}s^2 & \frac{M_{s_2}}{M}s^2 & \frac{M_{s_3}}{M}s^2 & 0 & 0 \\
0 & \frac{l_\beta}{I} & \frac{M_{s_1}l_{s_1}}{I}s^2 & \frac{M_{s_2}l_{s_2}}{I}s^2 & \frac{M_{s_3}l_{s_3}}{I}s^2 & \frac{M_{\dot\eta_1}}{IV_N}s - \frac{g_1}{I} & -\frac{g_2}{I} \\
1 & 0 & s^2 + 2\zeta_{s_1}\omega_{s_1}s + \omega_{s_1}^2 & 0 & 0 & Y_1(x_{s_1})s^2 & 0 \\
1 & 0 & 0 & s^2 + 2\zeta_{s_2}\omega_{s_2}s + \omega_{s_2}^2 & 0 & Y_1(x_{s_2})s^2 & 0 \\
1 & 0 & 0 & 0 & s^2 + 2\zeta_{s_3}\omega_{s_3}s + \omega_{s_3}^2 & Y_1(x_{s_3})s^2 & 0 \\
0 & \frac{Y_1(x_\beta)}{M_1} & \frac{M_{s_1}Y_1(x_{s_1})}{M_1}s^2 & \frac{M_{s_2}Y_1(x_{s_2})}{M_1}s^2 & \frac{M_{s_3}Y_1(x_{s_3})}{M_1}s^2 & s^2 + 2\overline{\zeta_1}\omega_1 s + \overline{\omega_1}^2 & c_{12} \\
0 & \frac{Y_2(x_\beta)}{M_2} & \frac{M_{s_1}Y_2(x_{s_1})}{M_2}s^2 & \frac{M_{s_2}Y_2(x_{s_2})}{M_2}s^2 & \frac{M_{s_3}Y_2(x_{s_3})}{M_2}s^2 & c_{21} & \overline{\omega}_2^2
\end{vmatrix} = 0 \qquad \text{(G-1)}
$$

The reason for including the $M_{\dot\eta_1}$, g_1, and g_2 terms is discussed in Section IV.

To reduce the 7-by-7 of Eq. G-1 to the 5-by-5 given in Section IV (Eq. 40), the first two rows and columns of Eq. G-1 are eliminated. In making this reduction the contributions of the $M_{\dot\eta_1}$, g_1, and g_2 terms to the slosh rows were neglected. The $M_{\dot\eta_1}$ and g_1 contributions are neglected since they are generally smaller than the $Y_1(x_{s_j})s^2$ terms. The g_2

contributions are neglected since we only desire a second bending mode correction to the first bending mode.

Before evaluating the complete 5-by-5 of Eq. 40, several simpler approximations were tried. By considering the first three diagonal terms we have the individual slosh zeros with dynamic corrections for the rigid-body modes. The resulting zeros are listed in Table G-I under "Individual Slosh." As might be expected, the results are unsatisfactory; frequency errors are as large as 5 percent.

The next level of approximation was to include the slosh cross-coupling by retaining the first three rows and columns of Eq. 40. The results are listed in Table G-I under "Three Slosh." Errors as large as 5 percent remain.

Next, the first bending mode was added by using the first four rows and columns. The results, listed under "Three Slosh + η_1" were better, but there were still several errors of 2.3 percent.

In the final approximation, the complete 5-by-5 determinant, a static correction to the first bending mode for the second bending mode is included. The results, listed under "Three slosh + $\eta_1(\eta_2)$," are quite good. The only error greater than 1 percent is the third slosh zero at BO.

The problem with this zero is the same one we had with the pole; its frequency is too close to that of the second bending mode. Consequently we must have a separate BO approximation. This approximation includes the third slosh, first and second bending modes with rigid-body dynamic corrections, i.e., Eq. G-2.

Equation G-2 is reduced to the 3-by-3 of Eq. 42 by eliminating the first two rows and columns. In the reduction the c_{ij} terms are dropped and only the contributions of the g_i terms to the diagonal elements are retained. The reasons for these simplifications are: (a) The $Y_i(x_{s3})s^2$ terms are larger than the g_i contributions, and (b) we are mainly interested in the coupling of the first and second bending modes with the third slosh, not the first to second bending coupling. As shown in Table G-1, under "Third Slosh + η_1 + η_2," Eq. 42 gives very good results for all three zeros.

TABLE G-I

SLOSH AND FIRST BENDING ZEROS OF φ NUMERATOR

(a) Lift-Off

ZERO	EXACT	INDIVIDUAL SLOSH	THREE SLOSH	THREE SLOSH + η_1	THREE SLOSH + $\eta_1(\eta_2)$	THIRD SLOSH + η_1 + η_2
First slosh						
ζ	0.028	0.0050	0.0083	0.028	0.027	
ω	2.140	2.147	2.136	2.140	2.139	
ω error		0.4	-0.2	0	0	
Second slosh						
ζ	-0.018	0.0052	0.0017	-0.018	-0.017	
ω	2.140	2.185	2.136	2.145	2.140	
ω error		2.1	-0.2	0.2	0	
Third slosh						
ζ	0.0050	0.0052	0.0053	0.0049	0.0049	
ω	2.141	2.188	2.253	2.145	2.145	
ω error		2.2	5.1	0.2	0.2	
First bending						
ζ	0.0053			0.0055	0.0053	
ω	2.417			2.424	2.425	
ω error				0.3	0.3	
(b) Max Q						
First slosh						
ζ	0.0040	0.0050	-0.0085	0.0044	0.020	
ω	2.750	2.763	2.748	2.749	2.765	
ω error		0.5	-0.1			
Second slosh						
ζ	0.0053	0.0051	0.010	0.0050	-0.011	
ω	2.764	2.838	2.804	2.777	2.768	
ω error		2.7	1.5	0.5	0.2	
Third slosh						
ζ	0.0066	0.0053	0.014	0.0067	0.0066	
ω	3.081	2.922	2.995	3.079	3.071	
ω error		-5.1	-2.8	-0.1	-0.3	
First bending						
ζ	0.022			0.020	0.021	
ω	2.142			2.175	2.159	
ω error				1.5	0.8	
(c) Burnout						
First slosh						
ζ	0.0051	0.0050	0.0050	0.00020	0.0052	
ω	3.567	3.582	3.582	3.668	3.567	
ω error		0.4	0.4	2.8	0	
Second slosh						
ζ	0.0050	0.0050	0.0050	0.0100	0.0050	
ω	3.750	3.774	3.774	3.676	3.749	
ω error		0.6	0.6	-2.0	0	
Third slosh						
ζ	0.0050	0.0052	0.0052	0.0054	0.0054	0.0051
ω	4.918	4.933	4.934	5.056	5.044	4.925
ω error		0.3	0.3	2.7	2.6	0.1
First bending						
ζ	0.0041			0.0040	0.0040	0.0041
ω	3.474			3.470	3.478	3.466
ω error				-0.1	0.1	-0.2
Second bending						
ζ	0.0053					0.0054
ω	7.103					7.116
ω error						0.2

ω in rad/sec ; error = [(approximate-exact)/exact] × 100

$$\begin{vmatrix} 1 & \frac{1}{M} & \frac{M_{s_3}}{M} s^2 & 0 & 0 \\ 0 & \frac{l_\beta}{I} & \frac{M_{s_3} l_{s_3}}{I} s^2 & \frac{-g_1}{I} & \frac{-g_2}{I} \\ 1 & 0 & s^2 + 2\zeta_{s_3}\omega_{s_3} s + \omega_{s_3}^2 & Y_1\left(x_{s_3}\right)s^2 & Y_2\left(x_{s_3}\right)s^2 \\ 0 & \frac{Y_1(x_\beta)}{M_1} & \frac{M_{s_3} Y_1\left(x_{s_3}\right)}{M_1} s^2 & s^2 + 2\overline{\zeta_1\omega_1} s + \overline{\omega}_1^2 & c_{12} \\ 0 & \frac{Y_2(x_\beta)}{M_2} & \frac{M_{s_3} Y_2\left(x_{s_3}\right)}{M_2} s^2 & c_{21} & s^2 + 2\overline{\zeta_2\omega_2} s + \overline{\omega}_2^2 \end{vmatrix} = 0 \qquad \text{(G-2)}$$

2. η_1 NUMERATOR

Starting with the three slosh masses and their coupling through the rigid-body modes, the approximate characteristic equation is:

$$\begin{vmatrix} 1 & 0 & \frac{M_{s_1}}{M} s^2 & \frac{M_{s_2}}{M} s^2 & \frac{M_{s_3}}{M} s^2 & \frac{1}{M} \\ 0 & 1 & \frac{M_{s_1} l_{s_1}}{I} s^2 & \frac{M_{s_2} l_{s_2}}{I} s^2 & \frac{M_{s_3} l_{s_3}}{I} s^2 & \frac{l_\beta}{I} \\ 1 & l_{s_1} & s^2 + 2\zeta_{s_1}\omega_{s_1} s + \omega_{s_1}^2 & 0 & 0 & 0 \\ 1 & l_{s_2} & 0 & s^2 + 2\zeta_{s_2}\omega_{s_2} s + \omega_{s_2}^2 & 0 & 0 \\ 1 & l_{s_3} & 0 & 0 & s^2 + 2\zeta_{s_3}\omega_{s_3} s + \omega_{s_3}^2 & 0 \\ 0 & 0 & \frac{M_{s_1}}{M_1} Y_1\left(x_{s_1}\right)s^2 & \frac{M_{s_2}}{M_1} Y_1\left(x_{s_2}\right)s^2 & \frac{M_{s_3} Y_1\left(x_{s_3}\right)}{M_1} s^2 & \frac{Y_1(x_\beta)}{M_1} \end{vmatrix} = 0 \qquad \text{(G-3)}$$

This can be reduced to the 3-by-3 determinant of Eq. 43 by eliminating the first two and the sixth rows and columns.

As a first approximation we consider just the diagonal elements of Eq. 43. The resulting zeros, listed in Table G-II under "Individual Slosh," have relatively large errors, up to 5 percent. Using the complete 3-by-3 determinant greatly reduces the errors. The zeros, listed under "Three Slosh," have only one error greater than 1 percent and that is 1.3 percent.

Although a special solution for the third slosh zero at burnout does not appear necessary, the previous techniques of using the third slosh mass plus first and second bending is employed here. The characteristic equation in this case is:

$$\begin{vmatrix} 1 & 0 & \frac{M_{s_3}}{M} s^2 & \frac{1}{M} & 0 \\ 0 & 1 & \frac{M_{s_3} l_{s_3}}{I} s^2 & \frac{l_\beta}{I} & 0 \\ 1 & l_{s_3} & s^2 + 2\zeta_{s_3}\omega_{s_3} s + \omega_{s_3}^2 & 0 & Y_2(x_{s_3}) s^2 \\ 0 & 0 & \frac{M_{s_3}}{M_1} Y_1(x_{s_3}) s^2 & \frac{Y_1(x_\beta)}{M_1} & c_{12} \\ 0 & 0 & \frac{M_{s_3}}{M_2} Y_2(x_{s_3}) s^2 & \frac{Y_2(x_\beta)}{M_2} & s^2 + 2\overline{\zeta_2\omega_2} s + \overline{\omega_2^2} \end{vmatrix} = 0 \qquad \text{(G-4)}$$

which can be reduced to the 2-by-2 of Eq. G-5 by eliminating the first, second, and fourth rows and columns. The resulting zeros are listed in Table G-IIc under "Third Slosh + η_1 + η_2." The error in the third slosh zero is slightly reduced, to 0.7 percent, and the second bending error is 0.6 percent.

TABLE G-II

SLOSH ZEROS OF η_1 NUMERATOR

(a) Lift-Off

ZERO	EXACT	INDIVIDUAL SLOSH	THREE SLOSH	THIRD SLOSH + η_1 + η_2
First slosh				
ζ	0.0077	0.0050	0.0050	
ω	2.136	2.155	2.138	
ω error		1.0	0.1	
Second slosh				
ζ	0.0023	0.0051	0.0050	
ω	2.136	2.197	2.141	
ω error		2.9	0.3	
Third slosh				
ζ	0.0053	0.0050	0.0053	
ω	2.267	2.186	2.263	
ω error		-3.6	-0.2	
(b) Max Q				
First slosh				
ζ	0.0087	0.0049	0.0050	
ω	2.774	2.791	2.766	
ω error		0.6	-0.3	
Second slosh				
ζ	0.0014	0.0054	0.0050	
ω	2.774	2.838	2.810	
ω error		2.3	1.3	
Third slosh				
ζ	0.0056	0.0051	0.0055	
ω	3.065	2.916	3.051	
ω error		-5.0	-0.5	
(c) Burnout				
First slosh				
ζ	0.0050	0.0050	0.0050	
ω	3.583	3.582	3.582	
ω error		0	0	
Second slosh				
ζ	0.0050	0.0048	0.0050	
ω	3.781	3.775	3.780	
ω error		-0.2	0	
Third slosh				
ζ	0.0050	0.0051	0.0053	0.0052
ω	4.992	5.033	5.037	4.955
ω error		0.8	0.9	-0.7
Second bending				
ζ	0.0052			0.0052
ω	6.716			6.759
ω error				0.6

$$\begin{vmatrix} \left\{1 + \frac{M_{s_3} Y_1(x_{s_3})}{Y_1(x_\beta)}\left[\frac{1}{M} + \frac{l_{s_3} l_\beta}{I}\right] - a_{33} M_{s_3}\right\} s^2 + 2\zeta_{s_3}\omega_{s_3} s + \omega_{s_3}^2 & Y_2(x_{s_3}) s^2 + \frac{c_{12} M_1}{Y_1(x_\beta)}\left[\frac{1}{M} + \frac{l_{s_3} l_\beta}{I}\right] \\ \frac{M_{s_3}}{M_2}\left[Y_2(x_{s_3}) - \frac{Y_1(x_{s_3}) Y_2(x_\beta)}{Y_1(x_\beta)}\right] s^2 & s^2 + 2\overline{\zeta_2\omega_2} s + \overline{\omega_2}^2 - \frac{c_{12} M_1 Y_2(x_\beta)}{M_2 Y_1(x_\beta)} \end{vmatrix} = 0 \quad \text{(G-5)}$$

3. HIGHER BENDING NUMERATORS

To approximate the slosh and first bending zeros of the higher bending (η_2, η_3, or η_4) numerators, it is necessary to include a dynamic correction for the rigid-body modes, the three slosh, and two bending modes. This results in a 7-by-7 determinant, Eq. G-6.

$$\begin{vmatrix} 1 & 0 & \frac{M_{s_1}}{M} s^2 & \frac{M_{s_2}}{M} s^2 & \frac{M_{s_3}}{M} s^2 & 0 & \frac{1}{M} \\ 0 & 1 & \frac{M_{s_1} l_{s_1}}{I} s^2 & \frac{M_{s_2} l_{s_2}}{I} s^2 & \frac{M_{s_3} l_{s_3}}{I} s^2 & 0 & \frac{l_\beta}{I} \\ 1 & l_{s_1} & s^2 + 2\zeta_{s_1}\omega_{s_1} s + \omega_{s_1}^2 & 0 & 0 & Y_1(x_{s_1}) s^2 & 0 \\ 1 & l_{s_2} & 0 & s^2 + 2\zeta_{s_2}\omega_{s_2} s + \omega_{s_2}^2 & 0 & Y_1(x_{s_2}) s^2 & 0 \\ 1 & l_{s_3} & 0 & 0 & s^2 + 2\zeta_{s_3}\omega_{s_3} s + \omega_{s_3}^2 & Y_1(x_{s_3}) s^2 & 0 \\ 0 & 0 & \frac{M_{s_1} Y_1(x_{s_1})}{M_1} s^2 & \frac{M_{s_2} Y_1(x_{s_2})}{M_1} s^2 & \frac{M_{s_3} Y_1(x_{s_3})}{M_1} s^2 & s^2 + 2\overline{\zeta_1\omega_1} s + \overline{\omega_1}^2 & \frac{Y_1(x_\beta)}{M_1} \\ 0 & 0 & \frac{M_{s_1} Y_i(x_{s_1})}{M_i} s^2 & \frac{M_{s_2} Y_i(x_{s_2})}{M_i} s^2 & \frac{M_{s_3} Y_i(x_{s_3})}{M_i} s^2 & c_{i1} & \frac{Y_i(x_\beta)}{M_i} \end{vmatrix} = 0 \quad \text{(G-6}$$

where $i = 2, 3, 4$

Equation G-6 can be reduced to the 4-by-4 of Eq. 44 by eliminating the first, second, and seventh rows and columns.

The simplest approximation from Eq. 44 is to consider only the first three diagonal terms. The resulting zeros are listed in Tables G-III, G-IV, and G-V under "Individual Slosh." The errors are generally quite large and are completely unacceptable.

By including the first three rows and columns of Eq. 44, the effects of slosh cross-coupling are added. The results, listed under "Three Slosh," are somewhat better but the errors are still too large.

The results from the complete 4-by-4 are listed under "Three Slosh + η_1." The results are very good in general, with only three frequency errors greater than 1 percent and these all occur in the η_4 numerator. Improved approximations for the cases of 2.2 and 2.1 percent errors will not be considered, but the 6 percent error in the third slosh zero at BO can be reduced.

For BO we again consider a special approximation involving a dynamic correction for rigid-body modes, third slosh, first and second bending. The resulting characteristic equation for the η_4 numerator is:

$$
\begin{vmatrix}
1 & 0 & \frac{M_{s_3}}{M}s^2 & 0 & 0 & \frac{1}{M} \\
0 & 1 & \frac{M_{s_3}l_{s_3}}{I}s^2 & 0 & 0 & \frac{l_\beta}{I} \\
1 & l_{s_3} & s^2+2\zeta_{s_3}\omega_{s_3}s+\omega_{s_3}^2 & Y_1(x_{s_3})s^2 & Y_2(x_{s_3})s^2 & 0 \\
0 & 0 & \frac{M_{s_3}Y_1(x_{s_3})}{M_1}s^2 & s^2+2\overline{\zeta_1\omega_1}s+\overline{\omega_1^2} & 0 & \frac{Y_1(x_\beta)}{M_1} \\
0 & 0 & \frac{M_{s_3}Y_2(x_{s_3})}{M_2}s^2 & 0 & s^2+2\overline{\zeta_2\omega_2}s+\overline{\omega_2^2} & \frac{Y_2(x_\beta)}{M_2} \\
0 & 0 & \frac{M_{s_3}}{M_4}\left[Y_4(x_{s_3})s^2-\bar{g}Y_4'(x_{s_3})\right] & c_{41} & c_{42} & \frac{Y_4(x_\beta)}{M_4}
\end{vmatrix} = 0 \qquad \text{(G-7)}
$$

TABLE G-III

SLOSH AND FIRST BENDING ZEROS OF η_2 NUMERATOR

(a) Lift-Off

ZERO	EXACT	INDIVIDUAL SLOSH	THREE SLOSH	THREE SLOSH + η_1
First slosh				
ζ	0.0050	0.0050	0.0049	0.0050
ω	2.138	2.166	2.112	2.131
ω error		1.4	-1.2	-0.3
Second slosh				
ζ	0.0052	0.0051	0.0051	0.0052
ω	2.220	2.199	2.188	2.218
ω error		-0.9	-1.5	-0.1
Third slosh				
ζ	0.0055	0.0046	0.0053	0.0057
ω	2.427	2.190	2.263	2.429
ω error		-9.8	-6.8	0.1
First bending				
ζ	0.0046			0.0047
ω	1.993			1.999
ω error				0.3
(b) Max Q				
First slosh				
ζ	0.0050	0.0051	0.0050	0.0050
ω	2.768	2.807	2.765	2.765
ω error		1.4	-0.1	-0.1
Second slosh				
ζ	0.0075	0.0053	0.0051	0.0078
ω	2.961	2.944	2.856	2.975
ω error		-0.6	-3.5	0.5
Third slosh				
ζ	0.0050	0.0052	0.0055	0.0041
ω	3.055	2.920	3.068	3.033
ω error		-4.4	0.4	-0.8
First bending				
ζ	0.026			0.018
ω	1.995			2.011
ω error				0.8
(c) Burnout				
First slosh				
ζ	0.0050	0.0050	0.0050	0.0050
ω	3.589	3.584	3.583	3.586
ω error		-0.1	-0.2	-0.1
Second slosh				
ζ	0.0051	0.0050	0.0050	0.0051
ω	3.815	3.797	3.793	3.817
ω error		-0.5	-0.6	0.1
Third slosh				
ζ	0.0053	0.0055	0.0054	0.0053
ω	5.036	5.039	5.109	5.044
ω error		0.1	1.5	0.2
First bending				
ζ	0.0050			0.0050
ω	2.913			2.913
ω error				0

ω in rad/sec ; error = $\left[(\text{approximate}-\text{exact})/\text{exact}\right] \times 100$

TABLE G-IV

SLOSH AND FIRST BENDING ZEROS OF η_3 NUMERATOR

(a) Lift-Off

ZERO	EXACT	INDIVIDUAL SLOSH	THREE SLOSH	THREE SLOSH + η_1
First slosh				
ζ	0.0050	0.0051	0.0050	0.0050
ω	2.136	2.181	2.143	2.142
ω error		2.1	0.3	0.3
Second slosh				
ζ	0.0052	0.0051	0.012	0.0052
ω	2.210	2.190	2.214	2.218
ω error		-0.9	0.2	0.4
Third slosh				
ζ	0.0060	0.0051	-0.0020	0.0060
ω	2.626	2.197	2.214	2.607
ω error		-20.0	-16.0	-0.8
First bending				
ζ	0.0046			0.0045
ω	1.920			1.915
ω error				-0.3
(b) Max Q				
First slosh				
ζ	0.0050	0.0051	0.0050	0.0050
ω	2.766	2.823	2.768	2.769
ω error		2.1	0.1	0.1
Second slosh				
ζ	0.0052	0.0054	0.0055	0.0054
ω	3.053	2.995	3.045	3.051
ω error		-1.9	-0.3	-0.1
Third slosh				
ζ	0.0069	0.0052	0.0052	0.0087
ω	3.196	2.909	2.926	3.192
ω error		-9.0	-8.5	-0.1
First bending				
ζ	0.012			0.015
ω	2.096			2.115
ω error				0.9
(c) Burnout				
First slosh				
ζ	0.0050	0.0050	0.0050	0.0050
ω	3.596	3.587	3.585	3.591
ω error		-0.3	-0.3	-0.1
Second slosh				
ζ	0.0053	0.0051	0.0050	0.0053
ω	3.882	3.824	3.817	3.898
ω error		-1.4	-1.7	0.4
Third slosh				
ζ	0.0054	0.0054	0.0054	0.0053
ω	5.014	5.107	5.130	5.046
ω error		1.9	2.3	0.6
First bending				
ζ	0.0050			0.0049
ω	2.866			2.890
ω error				0.8

ω in rad/sec ; error = $\left[\text{(approximate-exact)/exact}\right] \times 100$

TABLE G-V

SLOSH AND FIRST BENDING ZEROS OF η_{l_4} NUMERATOR

(a) Lift-Off

ZERO	EXACT	INDIVIDUAL SLOSH	THREE SLOSH	THREE SLOSH + η_1	THIRD SLOSH + η_1 + η_2
First slosh					
ζ	0.0050	0.0047	0.0050	0.0050	
ω	2.132	2.194	2.136	2.137	
ω error		3.0	0.2	0.3	
Second slosh					
ζ	0.0052	0.0051	0.021	0.0050	
ω	2.210	2.175	2.216	2.212	
ω error		-1.6	0.3	0.1	
Third slosh					
ζ	0.0062	0.0051	-0.011	0.0062	
ω	2.658	2.197	2.216	2.669	
ω error		-17.4	-16.6	0.4	
First bending					
ζ	0.0044			0.0044	
ω	1.906			1.898	
ω error				-0.4	
(b) Max Q					
First slosh					
ζ	0.0050	0.0051	0.0050	0.0050	
ω	2.764	2.837	2.765	2.766	
ω error		2.7	0	0.1	
Second slosh					
ζ	0.0053	0.0054	0.030	0.0050	
ω	3.047	2.989	2.985	3.038	
ω error		-1.9	-2.1	-0.3	
Third slosh					
ζ	0.011	0.0051	-0.020	0.0095	
ω	3.210	2.900	2.985	3.279	
ω error		-9.7	-7.0	2.2	
First bending					
ζ	0.033			0.017	
ω	1.862			1.865	
ω error				0.2	
(c) Burnout					
First slosh					
ζ	0.0050	0.0050	0.0050	0.0050	
ω	3.606	3.597	3.591	3.596	
ω error		-0.3	-0.4	-0.3	
Second slosh					
ζ	0.0058	0.0051	0.0057	0.0057	
ω	4.097	3.915	3.953	4.012	
ω error		-4.5	-3.5	-2.1	
Third slosh					
ζ	0.0050	0.0053	0.0054	0.0054	0.0051
ω	4.781	4.766	4.738	5.108	4.786
ω error		-0.3	-0.9	6.0	0.1
First bending					
ζ	0.0047			0.0049	0.0052
ω	2.724			2.720	2.700
ω error				-0.2	-0.9
Second bending					
ζ	0.0057				0.0055
ω	7.245				7.225
ω error					-0.3

ω in rad/sec ; error = $\left[\text{(approximate-exact)/exact}\right] \times 100$

An unusual feature of Eq. G-7 is the inclusion of the $\bar{g}Y_4'(x_{s_3})$ term. In general, $|Y_i(x_{s_j})s^2| \gg |\bar{g}Y_i'(x_{s_j})|$ at slosh mode frequencies so the $\bar{g}$ term is neglected; however, this inequality does not hold for the fourth bending and third slosh mass at burnout. Consequently, the $\bar{g}$ term was included.

The cross-coupling of first and second bending through c_{12} and c_{21} is small so these terms were neglected. The c_{41} and c_{42} terms were retained because the diagonally opposite elements, $Y_1(x_\beta)/M_1$ and $Y_2(x_\beta)/M_2$, are relatively large.

Equation G-7 is reduced to the 3-by-3 of Eq. 45 by eliminating the first, second, and sixth rows and columns. In the reduction process, c_{41} and c_{42} cross-coupling terms between the first and second bending modes are developed but were dropped from Eq. 45 because their effects are small. The zeros obtained from Eq. 45 are listed in Table G-Vc under "Third Slosh + η_1 + η_2." The errors for all three zeros are less than 1 percent.

4. EFFECT OF APPROXIMATIONS ON POLE–ZERO SEPARATION

The most critical requirement for any slosh approximation is to adequately represent the pole–zero separations. A relative large error in both the pole and zero is acceptable if the separation is accurate. It is also important to note that approximating a +1 percent separation by −1 percent is much worse than approximating a 10 percent separation by 12 percent. In the first case the error is apt to make the difference between closed-loop stability and instability, but not in the second case.

To judge the adequacy of the slosh approximations presented here, the pole–zero separations given by the various approximations* are compared with the exact separations in Table G-VI. A detailed examination of the table gives the following conclusions with respect to MSFC Model Vehicle No. 2:

*The pole approximations used in Table G-VI are those listed under the same headings in Appendix D.

- The first and second slosh modes are adequately approximated at all flight conditions by including a dynamic correction for rigid-body modes, the third slosh and first bending modes, and a static correction for the second bending mode, the "Three Slosh + $\eta_1(\eta_2)$" approximation. This approximation also gives very good results for the first bending mode.

- The "Three Slosh + $\eta_1(\eta_2)$" approximation is adequate for the third slosh mode at LO and Max Q; at BO it is necessary to include a dynamic correction for rigid-body modes and the third slosh, first and second bending modes, the "Third Slosh + η_1 + η_2" approximation.

These rather complex approximations for the slosh modes are the result of the unusual characteristics of Model Vehicle No. 2, i.e., three slosh and one bending mode in a narrow frequency range. For characteristics more typical of current boosters, such as only two slosh modes and those well separated from any bending modes, much simpler approximations should be apparent from the material presented in this report.

TABLE G-VI

SLOSH MODE POLE–ZERO SEPARATIONS

(a) First Slosh Mode at Lift-Off

NUMERATOR	POLE–ZERO SEPARATION					
	Three Slosh	Three Slosh + η_1	Three Slosh + $\eta_1(\eta_2)$	Three Slosh + $\eta_1(\eta_2, \eta_3)$	Three Slosh + η_1 + η_2	Exact
φ	-3.3	7.0	6.5	6.0*		5.4
η_1	-3.2	6.9*	6.5*	6.0*		5.2
η_2	-4.4	6.5	6.1*	5.6*		5.3
η_3	-3.0	7.1	6.7*	6.2*		5.2
η_4	-3.3	6.9	6.4*	5.9*		5.0
(b) First Slosh Mode at Max Q						
φ	-1.0	-1.0	-0.4			0
η_1	-0.4	-0.4*	-0.4*			0.8
η_2	-0.4	-0.4	-0.4*			0.6
η_3	-0.3	-0.3	-0.3*			0.6
η_4	-0.4	-0.4	-0.4*			0.5
(c) First Slosh Mode at Burnout						
φ	-0.6	-0.7	-3.1			-3.1
η_1	-0.6	-3.0*	-2.7*			-2.6
η_2	-0.6	-2.9	-2.6*			-2.5
η_3	-0.6	-2.7	-2.5*			-2.3
η_4	-0.4	-2.6	-2.4*			-2.0

*Same zero approximation used as in previous column.

$$\text{Separation} = \frac{\text{Frequency of zero} - \text{frequency of pole}}{\text{Frequency of pole}} \times 100$$

Table G-VI (Continued)

(d) Second Slosh Mode at Lift-Off

NUMERATOR	POLE-ZERO SEPARATION					
	Three Slosh	Three Slosh + η_1	Three Slosh + $\eta_1(\eta_2)$	Three Slosh + $\eta_1(\eta_2, \eta_3)$	Third Slosh + η_1 + η_2	Exact
φ	0.5	0	1.2	0.2*		0.4
η_1	0.7	−0.2*	1.2*	0.2*		0.2
η_2	2.9	3.4	4.9*	3.8*		4.1
η_3	4.1	3.4	4.9*	3.8*		3.7
η_4	4.2	3.1	4.6*	3.5*		3.7
(e) Second Slosh Mode at Max Q						
φ	−8.1	−8.9	−9.1			−9.3
η_1	−7.9	−7.8*	−7.8*			−9.0
η_2	−6.3	−2.4	−2.3*			−2.8
η_3	−0.2	0.1	0.2*			0.2
η_4	−2.1	−0.3	−0.3*			0
(f) Second Slosh Mode at Burnout						
φ	−1.1	−9.8	−7.0			−6.9
η_1	−0.9	−7.3*	−6.3*			−6.1
η_2	−0.6	−6.4	−5.4*			−5.3
η_3	0	−4.4	−3.4*			−3.6
η_4	3.6	−1.6	−0.5*			1.7

Table G-VI (Concluded)

(g) Third Slosh Mode at Lift-Off

NUMERATOR	POLE–ZERO SEPARATION					
	Three Slosh	Three Slosh + η_1	Three Slosh + $\eta_1(\eta_2)$	Three Slosh + $\eta_1(\eta_2, \eta_3)$	Third Slosh + η_1 + η_2	Exact
φ	1.1	−3.1	−4.1	−2.3*		−3.4
η_1	1.6	2.2*	1.2*	3.1*		2.1
η_2	1.6	9.7	8.6*	10.7*		9.3
η_3	−0.6	17.8	16.6*	18.8*		18.2
η_4	−0.5	20.6	19.3*	21.6*		19.7
(h) Third Slosh Mode at Max Q						
φ	3.9	−3.3	−2.6			−1.6
η_1	5.9	−4.2*	−3.2*			−2.1
η_2	6.5	−4.8	−3.8*			−2.4
η_3	1.5	0.3	1.2*			2.1
η_4	3.6	3.0	4.0*			2.5
(i) Third Slosh Mode at Burnout						
φ	−0.9	−0.1	−0.2		0.2	−0.7
η_1	1.1	−0.4*	−0.3*		0.8	0.8
η_2	2.6	−0.3	−0.2*		2.6*	1.7
η_3	3.0	−0.3	−0.1*		2.7*	1.3
η_4	−4.9	1.0	1.1*		−2.6	−3.5

APPENDIX H

APPROXIMATIONS FOR HIGHER BENDING ZEROS

1. φ NUMERATOR

For the higher bending (η_2, η_3, and η_4) zeros of the φ numerator we use an approximation similar to that employed for the denominator, i.e., a dynamic correction for the slosh masses. The characteristic equation for the η_i zero can then be written as

$$\begin{vmatrix} \frac{l_\beta}{I} & \frac{M_{s_1} l_{s_1}}{I} & \frac{M_{s_2} l_{s_2}}{I} & \frac{M_{s_3} l_{s_3}}{I} & \frac{-g_i}{I} \\ 0 & 1 & 0 & 0 & Y_i(x_{s_1})\, s^2 \\ 0 & 0 & 1 & 0 & Y_i(x_{s_2})\, s^2 \\ 0 & 0 & 0 & 1 & Y_i(x_{s_3})\, s^2 \\ \frac{Y_i(x_\beta)}{M_i} & \frac{M_{s_1} Y_i(x_{s_1})}{M_i} & \frac{M_{s_2} Y_i(x_{s_2})}{M_i} & \frac{M_{s_3} Y_i(x_{s_3})}{M_i} & s^2 + 2\overline{\zeta_i \omega_i} s + \overline{\omega_i^2} \end{vmatrix} = 0 \quad \text{(H-1)}$$

where $i = 2, 3, 4$

The g_i term is included here because the diagonally opposite term, $Y_i(x_\beta)/M_i$, represents a direct control input to the bending equation.

The reduction of Eq. H-1 to a quadratic equation in s, Eq. 46, is straightforward. The zeros obtained from Eq. 46 are listed in Table H-I. The results are generally good except for the η_2 zero at BO which is better approximated by the third slosh mass plus first and second bending, Eq. 42.

TABLE H-I

HIGHER BENDING ZEROS OF φ NUMERATOR

ZERO	LIFT-OFF		MAX Q		BURNOUT	
	Exact	Approx.	Exact	Approx.	Exact	Approx.
Second bending						
ζ	0.0050	0.0049	0.0070	0.0068	0.0053	0.0050
ω	5.169	5.163	5.783	5.763	7.103	6.901
ω error		-0.1		-0.3		-2.9
Third bending						
ζ	0.0053	0.0052	0.0083	0.0081	0.0050	0.0050
ω	9.275	9.260	9.795	9.809	11.80	11.76
ω error		-0.2		0.1		-0.3
Four bending						
ζ	0.0052	0.0050	0.0062	0.0066	0.0051	0.0050
ω	12.71	12.63	12.98	12.80	24.96	24.99
ω error		-0.6		-1.4		0.1

ω in rad/sec ; error = $\left[(\text{approximate}-\text{exact})/\text{exact}\right] \times 100$

2. η_1 NUMERATOR

The basic approximation is quite similar to that used above. The approximate characteristic equation is

$$\begin{vmatrix} 1 & 0 & 0 & 0 & Y_i(x_{s_1})s^2 \\ 0 & 1 & 0 & 0 & Y_i(x_{s_2})s^2 \\ 0 & 0 & 1 & 0 & Y_i(x_{s_3})s^2 \\ \frac{M_{s_1}Y_1(x_{s_1})}{M_1} & \frac{M_{s_2}Y_1(x_{s_2})}{M_1} & \frac{M_{s_3}Y_1(x_{s_3})}{M_1} & \frac{Y_1(x_\beta)}{M_1} & c_{1i} \\ \frac{M_{s_1}Y_i(x_{s_1})}{M_i} & \frac{M_{s_2}Y_i(x_{s_2})}{M_i} & \frac{M_{s_3}Y_i(x_{s_3})}{M_i} & \frac{Y_i(x_\beta)}{M_i} & s^2 + 2\overline{\zeta_i\omega_i}s + \overline{\omega_i}^2 \end{vmatrix} = 0 \quad \text{(H-2)}$$

The reduction of Eq. H-2 to a quadratic in s, Eq. 47, is again straightforward.

The zeros obtained from Eq. 47 are listed in Table H-II. Only two errors are greater than 1 percent and the maximum error is 1.4 percent. The 1.1 percent error in the η_2 zero at BO is reduced to 0.6 percent by using the third slosh plus first and second bending approximation of Eq. G-5.

TABLE H-II

HIGHER BENDING ZEROS OF η_1 NUMERATOR

ZERO	LIFT-OFF		MAX Q		BURNOUT	
	Exact	Approx.	Exact	Approx.	Exact	Approx.
Second bending						
ζ	0.0050	0.0050	0.012	0.0097	0.0052	0.0050
ω	5.072	5.065	5.393	5.348	6.716	6.641
ω error		−0.1		−0.9		−1.1
Third bending						
ζ	0.0053	0.0052	0.0064	0.0054	0.0050	0.0050
ω	9.241	9.216	9.849	9.890	11.74	11.75
ω error		−0.3		0.4		0.1
Fourth bending						
ζ	0.0052	0.0051	0.0070	0.0076	0.0051	0.0051
ω	12.72	12.62	12.91	12.73	24.99	25.00
ω error		−0.9		−1.4		0

ω in rad/sec ; error = $\left[(\text{approximate}-\text{exact})/\text{exact}\right] \times 100$

3. HIGHER BENDING NUMERATORS

As noted in Section IV, the approximation for the η_2, η_3, and η_4 numerators can be obtained by generalizing Eq. H-2 or Eq. 47. The zeros obtaining from the resulting characteristic equation, Eq. 48, are listed in Tables H-III, H-IV, and H-V. The largest error (5.9 percent) occurs in the η_2 zero of the η_4 numerator, but it can be reduced to 0.3 percent by using the third slosh plus first and second bending approximation of Eq. 45. There are two errors in the η_4 numerator which are in the 2 to 3 percent range; all other errors are less than 1 percent.

TABLE H-III

HIGHER BENDING ZEROS OF η_2 NUMERATOR

ZERO	LIFT-OFF		MAX Q		BURNOUT	
	Exact	Approx.	Exact	Approx.	Exact	Approx.
Third bending						
ζ	0.0052	0.0051	0.0087	0.0075	0.0050	0.0050
ω	9.043	9.001	9.415	9.366	11.72	11.72
ω error		−0.5		−0.5		0
Fourth bending						
ζ	0.0051	0.0051	0.0062	0.0070	0.0051	0.0050
ω	12.58	12.53	12.81	12.69	25.00	25.01
ω error		−0.4		−0.9		0

TABLE H-IV

HIGHER BENDING ZEROS OF η_3 NUMERATOR

ZERO	LIFT-OFF		MAX Q		BURNOUT	
	Exact	Approx.	Exact	Approx.	Exact	Approx.
Second bending						
ζ	0.0051	0.0050	0.011	0.0092	0.0050	0.0049
ω	5.109	5.101	5.562	5.533	6.624	6.626
ω error		−0.2		−0.5		0
Fourth bending						
ζ	0.0050	0.0050	0.0072	0.0069	0.0051	0.0050
ω	12.39	12.37	12.53	12.48	24.96	24.97
ω error		−0.2		−0.4		0

ω in rad/sec ; error = $\left[(\text{approximate}-\text{exact})/\text{exact}\right] \times 100$

TABLE H-V

HIGHER BENDING ZEROS OF η_4 NUMERATOR

ZERO	LIFT-OFF		MAX Q		BURNOUT	
	Exact	Approx.	Exact	Approx.	Exact	Approx.
Second bending						
ζ	0.0053	0.0051	0.00008	0.0090	0.0057	0.0052
ω	5.203	5.161	5.955	5.802	7.245	6.820
ω error		−0.8		−2.6		−5.9
Third bending						
ζ	0.0050	0.0050	0.013	0.0072	0.0051	0.0050
ω	8.831	8.847	8.631	8.877	11.79	11.77
ω error		0.2		2.9		−0.2

ω in rad/sec ; error = $\left[(\text{approximate}-\text{exact})/\text{exact}\right] \times 100$

APPENDIX I

MODEL VEHICLE NO. 2 CHARACTERISTICS

This appendix summarizes the dynamic characteristics of the MSFC Model Vehicle No. 2. Various dynamic parameters are listed in Table I-I. Aerodynamic characteristics are given in Table I-II. Bending mode shapes and slopes are plotted in Figs. I-1 and I-2.

TABLE I-I

DYNAMIC PARAMETERS

PARAMETER	UNITS	FLIGHT CONDITION		
		Lift-Off	Max Q	Burnout
Time	sec	0	80	157
T	kg	5,193,233	5,819,805	4,786,200
X_a	kg	0	227,178	1,735
M	kg-sec^2/m	423,565	266,051	116,412
$\bar{g}$	m/sec^2	12.261	21.021	41.100
V_N	m/sec	0	519.3	2,520.5
q	kg/m^2	0	3,841	93
x_{cg}	m	37.8	41.2	67.2
I	kg-m-sec^2	282,200,000	251,100,000	90,400,000
l_β	m	−35.26	−38.66	−64.66
ζ_1		0.0050	0.0050	0.0050
ω_1	rad/sec	2.1564	2.3185	2.915
M_1	kg-sec^2/m	193,190	170,750	17,867
ζ_2		0.0050	0.0050	0.0050
ω_2	rad/sec	5.0617	5.6448	6.592
M_2	kg-sec^2/m	165,520	115,670	29,068

Table I-I (Continued)

PARAMETER	UNITS	FLIGHT CONDITION		
		Lift-Off	Max Q	Burnout
ζ_3		0.0050	0.0050	0.0050
ω_3	rad/sec	8.7826	9.1835	11.711
M_3	kg-sec^2/m	162,150	98,115	169,960
ζ_4		0.0050	0.0050	0.0050
ω_4	rad/sec	12.356	12.504	24.862
M_4	kg-sec^2/m	350,110	565,740	203,340
x_{s_1}	m	16.09	10.16	6.24
l_{s_1}	m	−21.71	−31.04	−60.96
ζ_{s_1}		0.0050	0.0050	0.0050
ω_{s_1}	rad/sec	2.1363	2.7646	3.5814
M_{s_1}	kg-sec^2/m	11,158	11,612	338
x_{s_2}	m	43.15	31.08	24.84
l_{s_2}	m	5.35	−10.12	−42.36
ζ_{s_2}		0.0050	0.0050	0.0050
ω_{s_2}	rad/sec	2.1363	2.7646	3.7699
M_{s_2}	kg-sec^2/m	17,048	18,399	772
x_{s_3}	m	61.35	61.35	61.35
l_{s_3}	m	23.55	20.15	−5.85
ζ_{s_3}		0.0050	0.0050	0.0050
ω_{s_3}	rad/sec	2.1363	2.8274	4.7124
M_{s_3}	kg-sec^2/m	11,173	11,173	11,173
C		4 →		
F		8 →		
M_E	kg-sec^2/m	925.07 →		
l_E	m	1.2014 →		

Table I-I (Concluded)

PARAMETER	UNITS	FLIGHT CONDITION		
		Lift-Off	Max Q	Burnout
I_E	kg-m-sec^2	3456.4	→	→
ζ_E		0.018421	→	→
ω_E	rad/sec	51.138	→	→
x_β	m	2.54	→	→
A	m^2	56.995	→	→
K_0	kg/m	1,249,300	→	→
K_1	m^2/sec	800	→	→
K_3	m^5/kg-sec	0.17	→	→
K_L	kg/m	223,780	→	→

TABLE I-II

AERODYNAMIC CHARACTERISTICS

(a) Max Q

PARAMETER	UNITS	VALUE
N_α	kg	1,468,100
$M_\alpha = N_{\dot{\phi}}$	kg-m	17,483,000
$M_{\dot{\phi}}$	kg-m^2	3.9679×10^9
N_{η_1}	kg/m	21,197
N_{η_2}	kg/m	−53,447
N_{η_3}	kg/m	15,556
N_{η_4}	kg/m	−291,640
$N_{\dot{\eta}_1}$	kg	1,084,200
$N_{\dot{\eta}_2}$	kg	239,790
$N_{\dot{\eta}_3}$	kg	1,152,000
$N_{\dot{\eta}_4}$	kg	−746,670
M_{η_1}	kg	4,549,400
M_{η_2}	kg	−2,938,300
M_{η_3}	kg	6,370,500
M_{η_4}	kg	−17,410,000
$M_{\dot{\eta}_1}$	kg-m	55,269,000
$M_{\dot{\eta}_2}$	kg-m	−64,429,000
$M_{\dot{\eta}_3}$	kg-m	21,005,000
$N_{\dot{\eta}_4}$	kg-m	−125,770,000
$N_{\eta_{11}}$	kg/m	114,520
$N_{\eta_{21}}$	kg/m	−90,160
$N_{\eta_{31}}$	kg/m	30,950
$N_{\eta_{41}}$	kg/m	−147,690
$N_{\eta_{12}}$	kg/m	−260,610
$N_{\eta_{22}}$	kg/m	117,170
$N_{\eta_{32}}$	kg/m	−94,150
$N_{\eta_{42}}$	kg/m	146,030
$N_{\eta_{13}}$	kg/m	199,240
$N_{\eta_{23}}$	kg/m	−192,820
$N_{\eta_{33}}$	kg/m	75,910
$N_{\eta_{43}}$	kg/m	−272,470
$N_{\eta_{14}}$	kg/m	−703,440
$N_{\eta_{24}}$	kg/m	447,530
$N_{\eta_{34}}$	kg/m	−483,210
$N_{\eta_{44}}$	kg/m	1,133,320
$N_{\dot{\eta}_{11}}$	kg	4,736,800
$N_{\dot{\eta}_{12}} = N_{\dot{\eta}_{21}}$	kg	−2,175,500
$N_{\dot{\eta}_{13}} = N_{\dot{\eta}_{31}}$	kg	1,997,800
$N_{\dot{\eta}_{14}} = N_{\dot{\eta}_{41}}$	kg	−3,633,900
$N_{\dot{\eta}_{22}}$	kg	2,673,400
$N_{\dot{\eta}_{23}} = N_{\dot{\eta}_{32}}$	kg	−1,015,400
$N_{\dot{\eta}_{24}} = N_{\dot{\eta}_{42}}$	kg	4,065,400
$N_{\dot{\eta}_{33}}$	kg	1,974,400
$N_{\dot{\eta}_{34}} = N_{\dot{\eta}_{43}}$	kg	−3,626,700
$N_{\dot{\eta}_{44}}$	kg	13,144,800

Table I-II (Concluded)

(b) Burnout

PARAMETER	UNITS	VALUE
N_α	kg	24,165
M_α	kg-m	-117,000
All other aerodynamic derivatives are assumed zero		

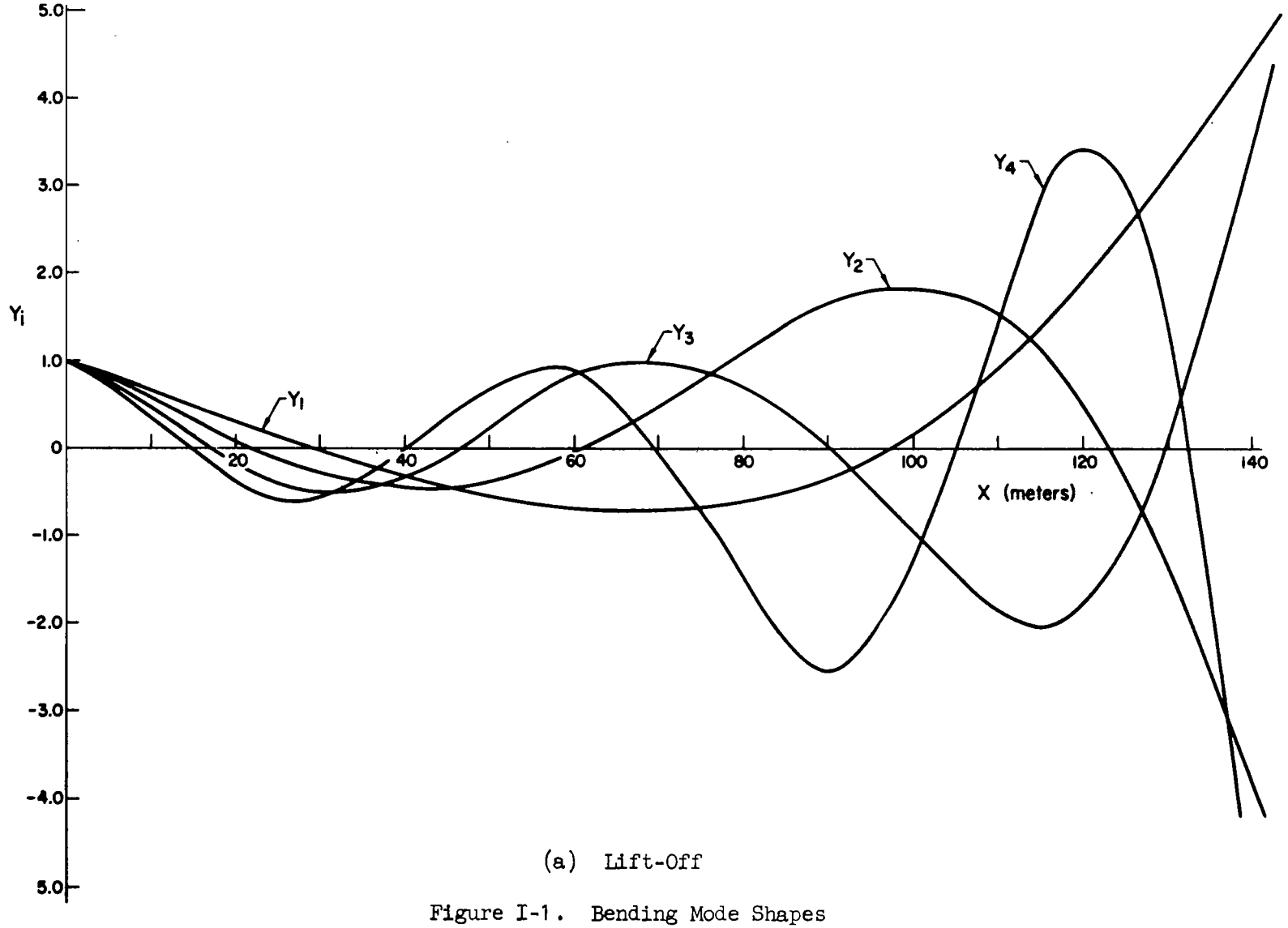

(a) Lift-Off

Figure I-1. Bending Mode Shapes

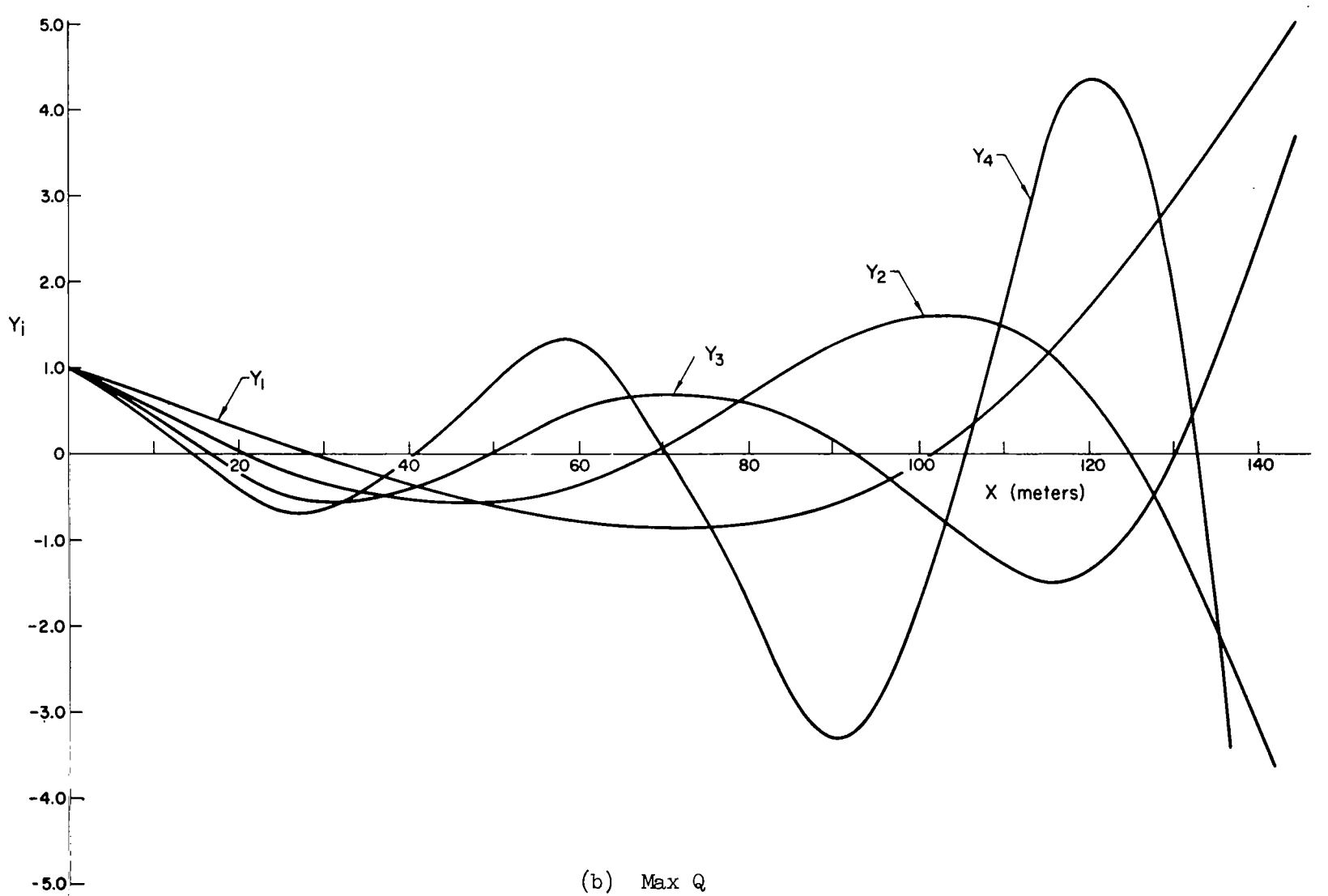

(b) Max Q

Figure I-1 (Continued)

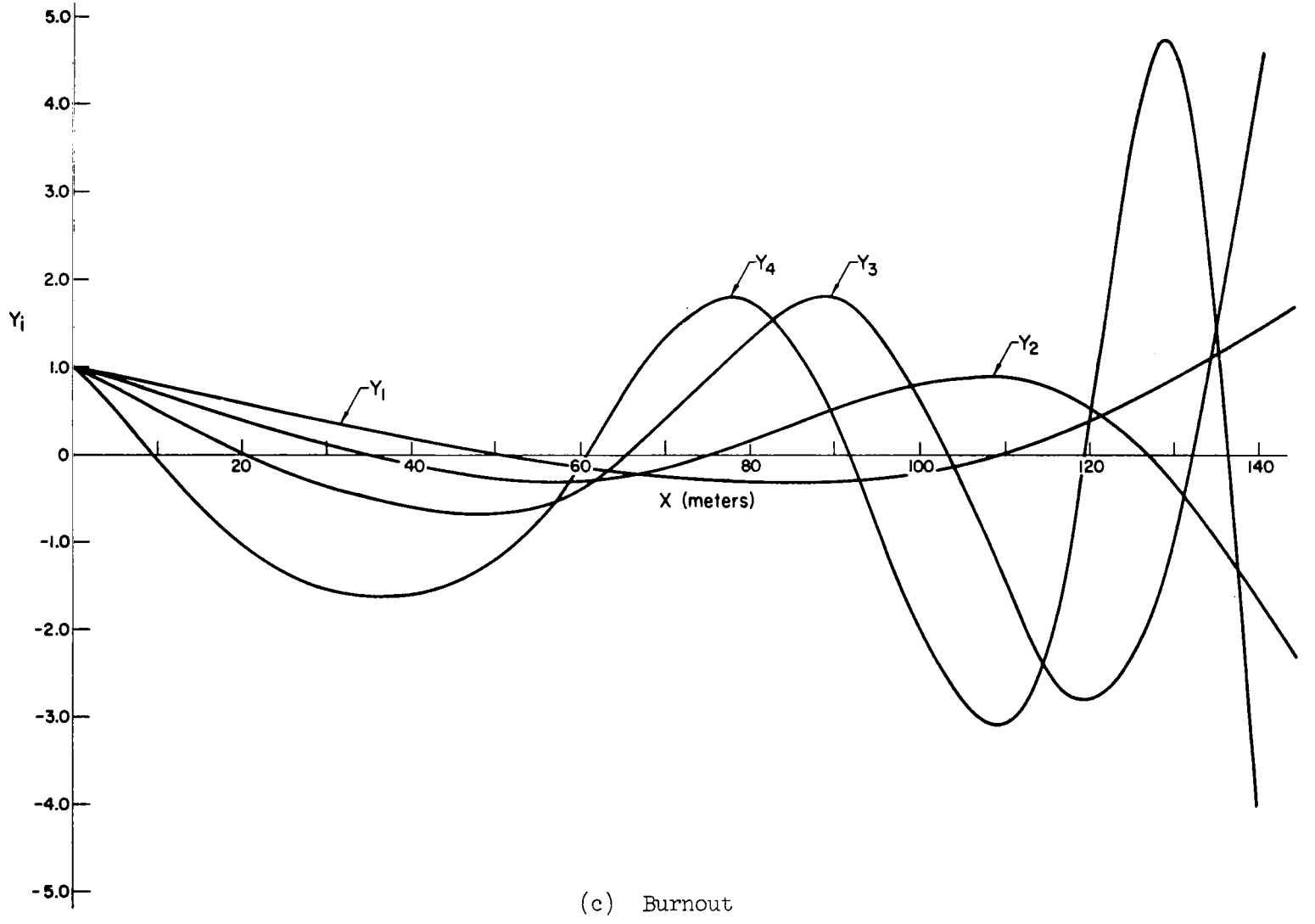

(c) Burnout

Figure I-1 (Concluded)

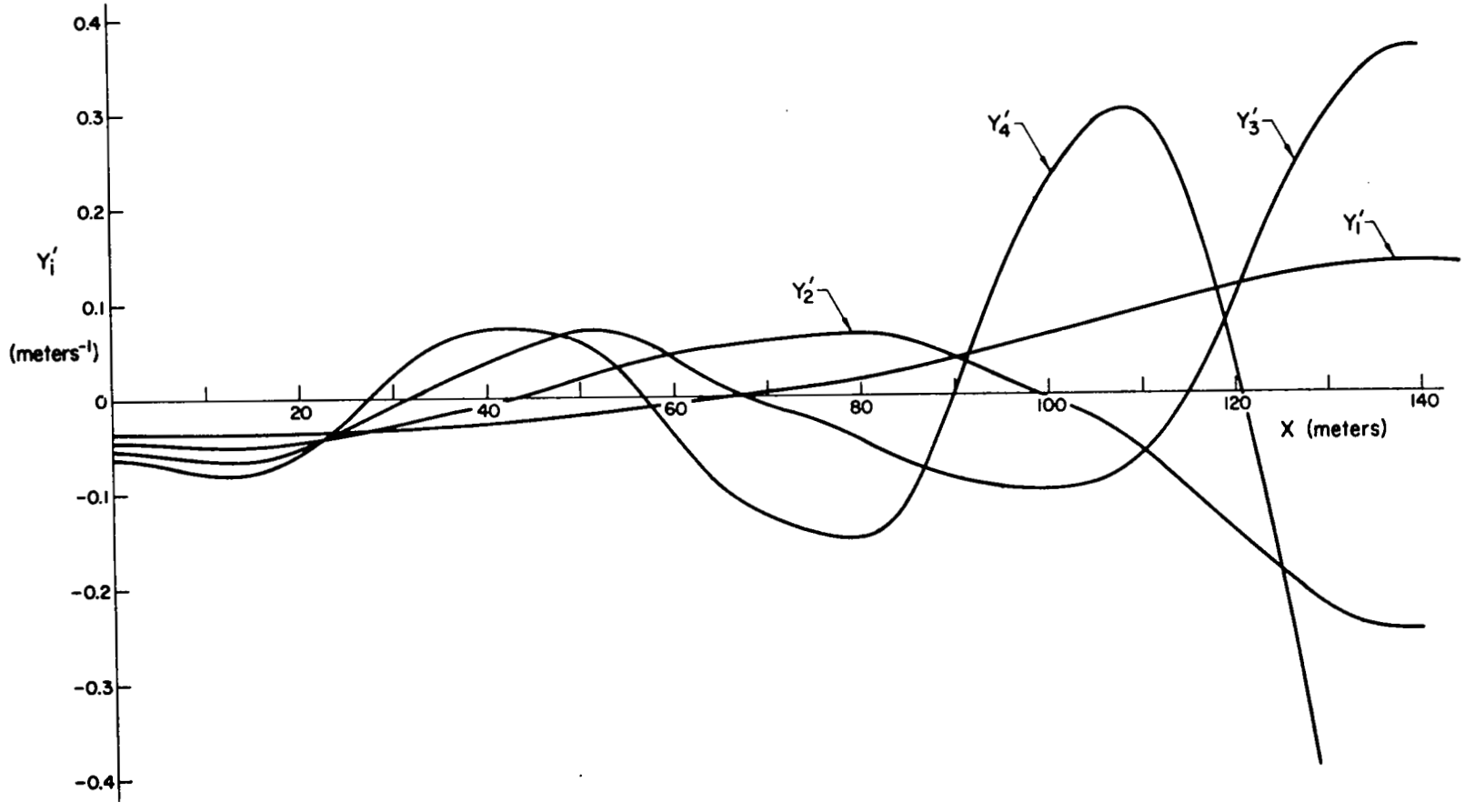

(a) Lift-Off

Figure I-2. Bending Mode Slopes

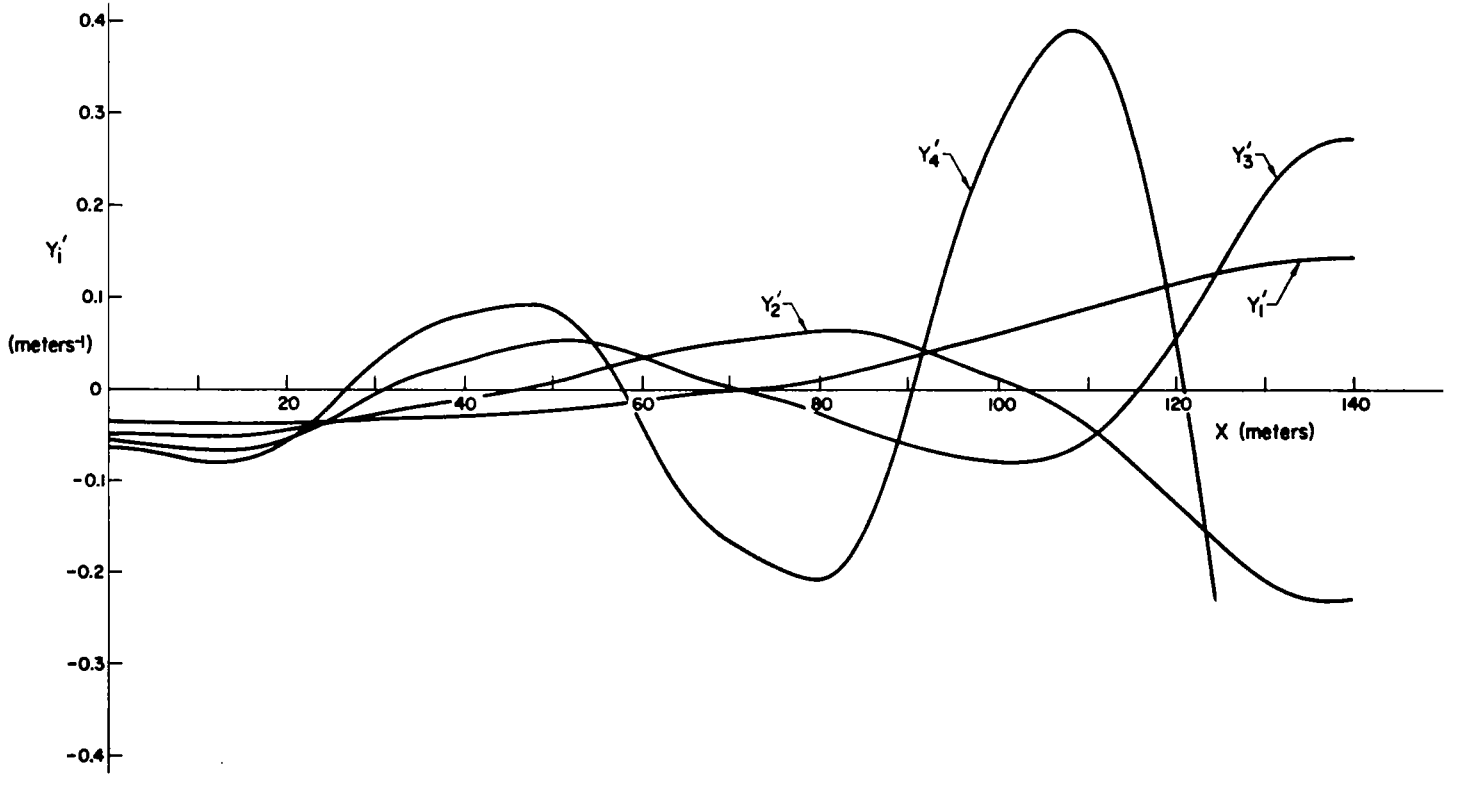

(b) Max Q

Figure I-2 (Continued)

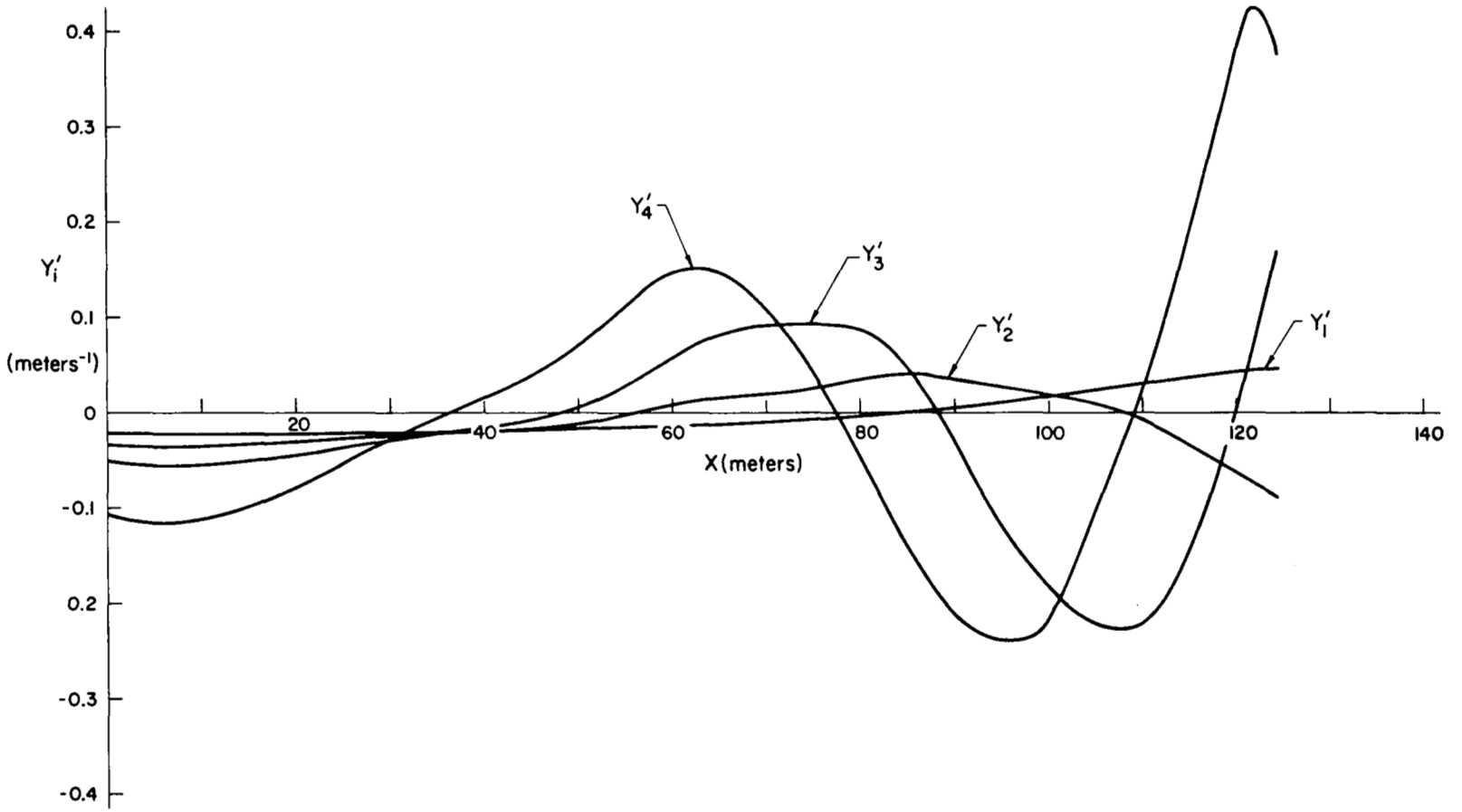

(c) Burnout

Figure I-2 (Concluded)

APPENDIX J

MODEL VEHICLE NO. 2 TRANSFER FUNCTIONS

The following pages list the transfer function poles and zeros for Model Vehicle No. 2 at "Lift-Off," "Max Q," and "Burnout." These "exact" values were obtained from the complete 11-by-11 matrix of Fig. 3. The matrix elements are also listed; column 13 represents the right side (β_c column) of the matrix.

MATRIX ELEMENTS

LIFT ØFF

RØW	CØL	CØEFFICIENTS s^2	s^1	s^0
1	1	0.	1.00000000E 00	0.
1	2	0.	0.	-1.22609998E 01
1	3	2.63429996E-02	-0.	-0.
1	4	4.02479994E-02	-0.	-0.
1	5	2.63779998E-02	-0.	-0.
1	6	0.	0.	4.26299995E-01
1	7	0.	0.	5.42999995E-01
1	8	0.	0.	6.75499994E-01
1	9	0.	0.	7.85599995E-01
1	10	-1.04959999E-02	-0.	-6.13049996E 00
1	11	0.	0.	0.
1	13	0.	0.	0.
2	1	0.	0.	0.
2	2	1.00000000E 00	-0.	-0.
2	3	-8.58389997E-04	-0.	-4.84789997E-03
2	4	3.23199996E-04	-0.	-7.40699989E-04
2	5	9.32389987E-04	-0.	-4.85439998E-04
2	6	0.	0.	-5.43799996E-03
2	7	0.	0.	-1.19599998E-02
2	8	0.	0.	-1.93599997E-02
2	9	0.	0.	-2.54999998E-02
2	10	6.04459989E-04	-0.	3.24639997E-01
2	11	0.	0.	0.
2	13	0.	0.	0.
3	1	0.	1.00000000E 00	0.
3	2	-2.17099994E 01	-0.	-1.22609998E 01
3	3	1.00000000E 00	2.13629997E-02	4.56379998E 00
3	4	0.	0.	0.
3	5	0.	0.	0.
3	6	4.53159994E-01	-0.	4.35999995E-01
3	7	2.81969997E-01	-0.	5.84399998E-01
3	8	7.13499993E-02	-0.	7.57399994E-01
3	9	-1.12279998E-01	-0.	8.74699986E-01
3	10	0.	0.	0.
3	11	0.	0.	0.
3	13	0.	0.	0.
4	1	0.	1.00000000E 00	0.
4	2	5.34999996E 00	-0.	-1.22609998E 01
4	3	0.	0.	0.
4	4	1.00000000E 00	2.13629997E-02	4.56379998E 00
4	5	0.	0.	0.
4	6	-3.98739997E-01	-0.	3.08099994E-01
4	7	-4.56719995E-01	-0.	-1.18999998E-02
4	8	-1.93569998E-01	-0.	-5.70499992E-01
4	9	2.15039998E-01	-0.	-8.62899995E-01
4	10	0.	0.	0.
4	11	0.	0.	0.
4	13	0.	0.	0.
5	1	0.	1.00000000E 00	0.
5	2	2.35499996E 01	-0.	-1.22609998E 01
5	3	0.	0.	0.
5	4	0.	0.	0.
5	5	1.00000000E 00	2.13629997E-02	4.56379998E 00
5	6	-6.99479997E-01	-0.	6.97999996E-02

Matrix Elements (Continued)

LIFT ØFF

RØW	CØL	COEFFICIENTS s^2	s^1	s^0
5	7	2.95599997E-02	-0.	-5.80899996E-01
5	8	9.00609994E-01	-0.	-3.60799998E-01
5	9	8.00199986E-01	-0.	7.88999993E-01
5	10	0.	0.	C.
5	11	0.	0.	C.
5	13	0.	0.	C.
6	1	0.	0.	C.
6	2	0.	0.	0.
6	3	2.61729997E-02	-0.	2.51799998E-02
6	4	-3.51869997E-02	-0.	2.71899998E-02
6	5	-4.04539996E-02	-0.	4.02999991E-03
6	6	1.00000000E 00	2.15639997E-02	5.52049994E C0
6	7	0.	0.	1.10869999E 00
6	8	0.	0.	1.37909999E C0
6	9	0.	0.	1.60389999E 00
6	10	-2.39009997E-02	-0.	-1.25159998E 01
6	11	0.	0.	C.
6	13	0.	0.	C.
7	1	0.	0.	C.
7	2	0.	0.	C.
7	3	1.90079999E-02	-0.	3.94799995E-02
7	4	-4.70419991E-02	-0.	-1.21999998E-03
7	5	1.99499999E-03	-0.	-3.92099994E-02
7	6	0.	0.	9.95649993E-01
7	7	1.00000000E 00	5.06169993E-02	2.68889996E 01
7	8	0.	0.	1.57749999E 00
7	9	0.	0.	1.83459999E 00
7	10	-2.81869999E-02	-0.	-1.43169998E 01
7	11	0.	0.	C.
7	13	0.	0.	C.
8	1	0.	0.	C.
8	2	0.	0.	C.
8	3	4.90999991E-03	-0.	5.21199995E-02
8	4	-2.03519997E-02	-0.	-5.99799997E-02
8	5	6.20569992E-02	-0.	-2.48599997E-02
8	6	0.	0.	9.93149996E-01
8	7	0.	0.	1.26509999E 00
8	8	1.00000000E 00	8.78259993E-02	7.87079984E 01
8	9	0.	0.	1.83010000E 00
8	10	-2.91179997E-02	-0.	-1.42819998E 01
8	11	0.	0.	C.
8	13	0.	0.	C.
9	1	0.	0.	0.
9	2	0.	0.	0.
9	3	-3.57839996E-03	-0.	2.78799999E-02
9	4	1.04709999E-02	-0.	-4.20199990E-02
9	5	2.55369997E-02	-0.	2.51799998E-02
9	6	0.	0.	4.51289994E-01
9	7	0.	0.	5.74849993E-01
9	8	0.	0.	7.14999992E-01
9	9	1.00000000E 00	1.23559998E-01	1.53500000E 02
9	10	-1.36239998E-02	-0.	-6.48949999E 00
9	11	0.	0.	C.
9	13	0.	0.	0.

Matrix Elements (Concluded)

LIFT ØFF

RØW	CØL	COEFFICIENTS s^2	s^1	s^0
10	1	0.	-3.21539998E-01	0.
10	2	1.23379998E 01	-0.	3.94239998E 00
10	3	0.	0.	0.
10	4	0.	0.	0.
10	5	0.	0.	0.
10	6	-3.33969998E-01	-0.	-1.37099999E-01
10	7	-3.37449998E-01	-0.	-1.74599999E-01
10	8	-3.41499999E-01	-0.	-2.17199999E-01
10	9	-3.44989994E-01	-0.	-2.52599999E-01
10	10	1.00000000E 00	1.88399999E 00	2.61899999E 03
10	11	0.	0.	-2.61509997E 03
10	13	0.	0.	0.
11	1	0.	0.	0.
11	2	0.	0.	0.
11	3	0.	0.	0.
11	4	0.	0.	0.
11	5	0.	0.	0.
11	6	0.	0.	0.
11	7	0.	0.	0.
11	8	0.	0.	0.
11	9	0.	0.	0.
11	10	0.	-1.02089998E 01	-6.67469990E 02
11	11	0.	6.72039992E 01	1.46750000E 03
11	13	0.	0.	8.00000000E 02

FLIGHT CONDITION: LIFT-OFF

DENOMINATOR

Coefficient of s^{20} = 46.510

Coefficient of s^{3} = 3.5209×10^{14}

Number of roots = 20

REAL ROOTS (sec^{-1}) POSITIVE IN LHP*	COMPLEX ROOTS	
	ζ	ω (rad/sec)
0	0.0044526	2.0299
0	0.0049657	2.1316
0	0.0051888	2.2211
14.563	0.0054400	2.6066
	0.0047900	5.2894
	0.0049015	9.1876
	0.0049500	12.589
	0.098434	47.040

*Left-half-plane

FLIGHT CONDITION: LIFT-OFF

$\dot{Z}/\beta_c$ NUMERATOR

Coefficient of s^{18} = 1.7354×10^{4}

Coefficient of s^{0} = -1.3209×10^{15}

$\dot{Z}/\beta_c$ High frequency asymptote = $373.12/s^2$

$\dot{Z}/\beta_c$ Low frequency asymptote = $-3.7516/s^3$

Number of roots = 18

REAL ROOTS (sec^{-1}) POSITIVE IN LHP	COMPLEX ROOTS	
	ζ	ω (rad/sec)
−0.86891	0.0043063	1.9135
0.86927	0.0060275	2.1345
	0.0039449	2.1345
	0.0060881	2.6364
	0.0053279	5.2445
	0.0050645	8.8709
	0.0050122	12.346
	-0.58985×10^{-4}	24.045

FLIGHT CONDITION: LIFT-OFF

φ/β_c NUMERATOR

Coefficient of s^{17} = -958.57

Coefficient of s^1 = -1.0773×10^{14}

φ/β_c High frequency asymptote = $-20.610/s^3$

φ/β_c Low frequency asymptote = $-0.30597/s^2$

Number of roots = 17

REAL ROOTS (sec^{-1}) POSITIVE IN LHP	COMPLEX ROOTS	
	ζ	ω (rad/sec)
0	0.027610	2.1395
	−0.017962	2.1403
	0.0050135	2.1410
	0.0052765	2.4173
	0.0049786	5.1687
	0.0052999	9.2745
	0.0051853	12.705
	0.25776×10^{-4}	23.224

FLIGHT CONDITION: LIFT-OFF

η_1/β_c NUMERATOR

Coefficient of s^{17} = 3.7896×10^{4}

Coefficient of s^{3} = 7.5694×10^{14}

η_1/β_c High frequency asymptote = $814.79/s^3$

η_1/β_c Low frequency asymptote = 2.1498

Number of roots = 17

REAL ROOTS (sec^{-1}) POSITIVE IN LHP	COMPLEX ROOTS	
	ζ	ω (rad/sec)
0	0.0076531	2.1355
0	0.0023185	2.1356
0	0.0052639	2.2673
	0.0050070	5.0715
	0.0053264	9.2413
	0.0052096	12.722
	0.23340×10^{-4}	22.924

FLIGHT CONDITION: LIFT-OFF

η_2/β_c NUMERATOR

Coefficient of s^{17} = 4.5444×10^{4}

Coefficient of s^{3} = 1.5753×10^{14}

η_2/β_c High frequency asymptote = $977.08/s^{3}$

η_2/β_c Low frequency asymptote = 0.44741

Number of roots = 17

REAL ROOTS (sec^{-1}) POSITIVE IN LHP	COMPLEX ROOTS	
	ζ	ω (rad/sec)
0	0.0046294	1.9928
0	0.0050077	2.1381
0	0.0052341	2.2202
	0.0055408	2.4274
	0.0052046	9.0433
	0.0051296	12.581
	0.63426×10^{-6}	22.535

FLIGHT CONDITION: LIFT-OFF

η_3/β_c NUMERATOR

Coefficient of s^{17} = 4.6838×10^{4}

Coefficient of s^{3} = 5.2103×10^{13}

η_3/β_c High frequency asymptote = $1007.1/s^3$

η_3/β_c Low frequency asymptote = 0.14798

Number of roots = 17

REAL ROOTS (sec^{-1}) POSITIVE IN LHP	COMPLEX ROOTS	
	ζ	ω (rad/sec)
0	0.0044529	1.9204
0	0.0049945	2.1357
0	0.0051954	2.2104
	0.0060444	2.6263
	0.0050948	5.1088
	0.0050254	12.391
	-0.60884×10^{-5}	22.129

FLIGHT CONDITION: LIFT-OFF

η_4/β_c NUMERATOR

Coefficient of s^{17} = 2.0845×10^{4}

Coefficient of s^{3} = 1.1915×10^{13}

η_4/β_c High frequency asymptote = $448.18/s^3$

η_4/β_c Low frequency asymptote = 0.033841

Number of roots = 17

REAL ROOTS (sec^{-1}) POSITIVE IN LHP	COMPLEX ROOTS	
	ζ	ω (rad/sec)
0	0.0043996	1.9055
0	0.0049715	2.1315
0	0.0051823	2.2100
	0.006173⅓	2.6583
	0.0052640	5.2029
	0.0050192	8.8305
	0.46563×10^{-6}	21.807

MAXIMUM DYNAMIC PRESSURE

MATRIX ELEMENTS

ROW	COL	s^2	COEFFICIENTS s^1	s^0
1	1	0.	1.00000000E 00	1.06259999E-02
1	2	0.	1.26539999E-01	-2.65389997E 01
1	3	4.36459994E-02	-0.	-0.
1	4	6.91559994E-02	-0.	-0.
1	5	4.19959998E-02	-0.	-0.
1	6	0.	7.84719986E-03	6.70569992E-01
1	7	0.	1.73559998E-03	1.20230000E 00
1	8	0.	8.33829987E-03	1.15189999E 00
1	9	0.	-5.40429997E-03	2.47180000E 00
1	10	-1.67099997E-02	-0.	-1.09369998E 01
1	11	0.	0.	0.
1	13	0.	0.	0.
2	1	0.	0.	1.34069997E-04
2	2	1.00000000E 00	3.04289997E-02	-6.96259993E-02
2	3	-1.43539998E-03	-0.	-9.72109997E-04
2	4	-7.41529995E-04	-0.	-1.54030000E-03
2	5	8.96589994E-04	-0.	-9.35349989E-04
2	6	0.	4.23849994E-04	-2.81649998E-02
2	7	0.	-4.94099993E-04	-9.16009986E-03
2	8	0.	1.61079998E-04	-5.52199996E-02
2	9	0.	-9.64559984E-04	3.23899996E-02
2	10	7.39519989E-04	-0.	4.48389995E-01
2	11	0.	0.	0.
2	13	0.	0.	0.
3	1	0.	1.00000000E 00	-0.
3	2	-3.10399997E 01	-0.	-2.10209996E 01
3	3	1.00000000E 00	2.76459998E-02	7.64299995E 00
3	4	0.	0.	0.
3	5	0.	0.	0.
3	6	6.54759991E-01	-0.	7.64699996E-01
3	7	5.31549996E-01	-0.	1.07699999E 00
3	8	4.22069997E-01	-0.	1.38399999E 00
3	9	3.29539999E-01	-0.	1.66000000E 00
3	10	0.	0.	0.
3	11	0.	0.	0.
3	13	0.	0.	0.
4	1	0.	1.00000000E 00	-0.
4	2	-1.01199998E 01	-0.	-2.10209996E 01
4	3	0.	0.	0.
4	4	1.00000000E 00	2.76459998E-02	7.64299995E 00
4	5	0.	0.	0.
4	6	-7.88699991E-02	-0.	6.71999997E-01
4	7	-3.82819998E-01	-0.	5.39199990E-01
4	8	-5.54559994E-01	-0.	1.31999999E-02
4	9	-6.03949994E-01	-0.	-7.77399993E-01
4	10	0.	0.	0.
4	11	0.	0.	0.
4	13	0.	0.	0.
5	1	0.	1.00000000E 00	-0.
5	2	2.01499996E 01	-0.	-2.10209996E 01
5	3	0.	0.	0.
5	4	0.	0.	0.
5	5	1.00000000E 00	2.82739997E-02	7.99419999E 00
5	6	-8.11119986E-01	-0.	2.13599998E-01

MAXIMUM DYNAMIC PRESSURE		MATRIX ELEMENTS COEFFICIENTS		
ROW	COL	s^2	s^1	s^0
5	7	-3.02619997E-01	-0.	-7.93499994E-01
5	8	5.65139991E-01	-0.	-5.93399990E-01
5	9	1.20420000E 00	-0.	1.58800000E 00
5	10	0.	0.	0.
5	11	0.	0.	0.
5	13	0.	0.	0.
6	1	0.	0.	1.22269998E-02
6	2	0.	6.23310000E-01	-6.34959996E 00
6	3	4.45279992E-02	-0.	5.20099998E-02
6	4	-8.49819994E-03	-0.	7.24099994E-02
6	5	-3.30759996E-02	-0.	1.39799999E-02
6	6	1.00000000E 00	7.66039991E-02	5.79169995E 00
6	7	0.	-2.45349997E-02	2.97719997E 00
6	8	0.	2.25299999E-02	5.86819994E-01
6	9	0.	-4.09809995E-02	6.11279994E 00
6	10	-2.70689997E-02	-0.	-1.58459999E 01
6	11	0.	0.	0.
6	13	0.	0.	0.
7	1	0.	0.	3.99209994E-03
7	2	0.	-1.07259999E 00	-2.07309997E 00
7	3	5.33619994E-02	-0.	1.08089998E-01
7	4	-6.08909994E-02	-0.	8.57599986E-02
7	5	-2.92309999E-02	-0.	-7.66499990E-02
7	6	0.	-3.62179995E-02	2.34399998E 00
7	7	1.00000000E 00	1.00950000E-01	3.29389992E 01
7	8	0.	-1.69039999E-02	4.19109994E 00
7	9	0.	6.76799989E-02	-1.00029999E 00
7	10	-4.04809994E-02	-0.	-2.28079996E 01
7	11	0.	0.	0.
7	13	0.	0.	0.
8	1	0.	0.	2.26089996E-02
8	2	0.	4.12249994E-01	-1.17409998E 01
8	3	4.99519998E-02	-0.	1.63749997E-01
8	4	-1.03989999E-01	-0.	2.47999999E-03
8	5	6.43579996E-02	-0.	-6.75799996E-02
8	6	0.	3.92099994E-02	1.49059999E 00
8	7	0.	-1.99279998E-02	3.37029999E 00
8	8	1.00000000E 00	1.30589999E-01	8.64769983E 01
8	9	0.	-7.11789995E-02	8.23639989E 00
8	10	-4.82489997E-02	-0.	-2.63259998E 01
8	11	0.	0.	0.
8	13	0.	0.	0.
9	1	0.	0.	-2.54149997E-03
9	2	0.	-4.28109998E-01	1.31979999E 00
9	3	6.76379997E-03	-0.	3.40799996E-02
9	4	-1.96419998E-02	-0.	-2.52799997E-02
9	5	2.37819999E-02	-0.	3.13599998E-02
9	6	0.	-1.23689999E-02	5.69109994E-01
9	7	0.	1.38379999E-02	1.53069998E-01
9	8	0.	-1.23449999E-02	9.78609991E-01
9	9	1.00000000E 00	1.69779998E-01	1.54910000E 02
9	10	-8.44349980E-03	-0.	-4.49059999E 00
9	11	0.	0.	0.
9	13	0.	0.	0.

MAXIMUM DYNAMIC PRESSURE		MATRIX ELEMENTS COEFFICIENTS		
ROW	COL	s^2	s^1	s^0
10	1	0.	-3.21539998E-01	-0.
10	2	1.34309998E 01	-0.	6.75909996E 00
10	3	0.	0.	0.
10	4	0.	0.	0.
10	5	0.	0.	0.
10	6	-3.34299996E-01	-0.	-2.41199997E-01
10	7	-3.38659996E-01	-0.	-3.21999997E-01
10	8	-3.42409998E-01	-0.	-3.89199996E-01
10	9	-3.45489997E-01	-0.	-4.42299998E-01
10	10	1.00000000E 00	1.88399999E 00	2.62179998E 03
10	11	0.	0.	-2.61509997E 03
10	13	0.	0.	0.
11	1	0.	0.	0.
11	2	0.	0.	0.
11	3	0.	0.	0.
11	4	0.	0.	0.
11	5	0.	0.	0.
11	6	0.	0.	0.
11	7	0.	0.	0.
11	8	0.	0.	0.
11	9	0.	0.	0.
11	10	0.	-1.02089998E 01	-6.67469990E 02
11	11	0.	6.72039992E 01	1.46750000E 03
11	13	0.	0.	8.00000000E 02

FLIGHT CONDITION: MAX Q

DENOMINATOR

Coefficient of s^{20} = 35.506

Coefficient of s^{0} = 1.0175×10^{13}

Number of roots = 20

REAL ROOTS (sec^{-1}) POSITIVE IN LHP	COMPLEX ROOTS	
	ζ	ω (rad/sec)
−0.042015	0.014084	2.2338
−0.27859	0.0049756	2.7504
0.36441	0.0057068	3.0471
14.516	0.0087034	3.1313
	0.0083847	6.0224
	0.0071205	9.9440
	0.0063856	12.894
	0.098643	47.526

FLIGHT CONDITION: MAX Q

$\dot{Z}/\beta_c$ NUMERATOR

Coefficient of s^{18} = 2.4024×10^4

Coefficient of s^0 = -2.4500×10^{16}

$\dot{Z}/\beta_c$ High frequency asymptote = $676.62/s^2$

$\dot{Z}/\beta_c$ Low frequency asymptote = -2407.9

Number of roots = 18

REAL ROOTS (sec^{-1}) POSITIVE IN LHP	COMPLEX ROOTS	
	ζ	ω (rad/sec)
−1.0885	0.014463	2.0718
1.1226	0.0052282	2.7227
	0.0049970	2.7670
	0.0080914	3.1154
	0.0087558	5.9292
	0.0066186	9.7527
	0.0067059	12.726
	−0.00014872	25.528

FLIGHT CONDITION: MAX Q

φ/β_c NUMERATOR

Coefficient of s^{17} = −1054.1

Coefficient of s^0 = -1.1924×10^{13}

φ/β_c High frequency asymptote = $-29.688/s^3$

φ/β_c Low frequency asymptote = −1.1719

Number of roots = 17

REAL ROOTS (sec^{-1}) POSITIVE IN LHP	COMPLEX ROOTS	
	ζ	ω (rad/sec)
0.013693	0.021978	2.1424
	0.0040212	2.7504
	0.0052771	2.7636
	0.0064583	3.0809
	0.0069610	5.7827
	0.0082900	9.7948
	0.0062388	12.983
	-0.48013×10^{-4}	24.635

FLIGHT CONDITION: MAX Q

η_1/β_c NUMERATOR

Coefficient of s^{17} = 3.8546×10^4

Coefficient of s^0 = 6.5067×10^{13}

η_1/β_c High frequency asymptote = $1085.6/s^3$

η_1/β_c Low frequency asymptote = 6.3948

Number of roots = 17

REAL ROOTS (sec^{-1}) POSITIVE IN LHP	COMPLEX ROOTS	
	ζ	ω (rad/sec)
−0.041119	0.0087036	2.7740
−0.47142	0.0014088	2.7740
0.56825	0.0056331	3.0652
	0.011804	5.3933
	0.0063531	9.8491
	0.0070377	12.911
	0.37070×10^{-5}	24.200

FLIGHT CONDITION: MAX Q

η_2/β_c NUMERATOR

Coefficient of s^{17} = 5.7803×10^4

Coefficient of s^0 = 3.9497×10^{12}

η_2/β_c High frequency asymptote = $1628.0/s^3$

η_2/β_c Low frequency asymptote = 0.38818

Number of roots = 17

REAL ROOTS (sec^{-1}) POSITIVE IN LHP	COMPLEX ROOTS	
	ζ	ω (rad/sec)
−0.041556	0.025814	1.9941
−0.25845	0.0050075	2.7678
0.31176	0.0075405	2.9611
	0.0049662	3.0554
	0.0086865	9.4150
	0.0061540	12.807
	0.73635×10^{-5}	23.725

FLIGHT CONDITION: MAX Q

η_3/β_c NUMERATOR

Coefficient of s^{17} = 6.8743×10^4

Coefficient of s^0 = 6.6955×10^{12}

η_3/β_c High frequency asymptote = $1936.1/s^3$

η_3/β_c Low frequency asymptote = 0.65803

Number of roots = 17

REAL ROOTS (sec^{-1}) POSITIVE IN LHP	COMPLEX ROOTS	
	ζ	ω (rad/sec)
−0.040980	0.011872	2.0962
−0.48967	0.0050189	2.7659
0.57284	0.0051527	3.0531
	0.0069228	3.1960
	0.010667	5.5624
	0.0072286	12.526
	0.55631×10^{-4}	23.352

FLIGHT CONDITION: MAX Q

η_4/β_c NUMERATOR

Coefficient of s^{17} = 1.1884×10^{4}

Coefficient of s^{0} = -2.8081×10^{11}

η_4/β_c High frequency asymptote = $334.70/s^3$

η_4/β_c Low frequency asymptote = -0.027598

Number of roots = 17

REAL ROOTS (sec^{-1}) POSITIVE IN LHP	COMPLEX ROOTS	
	ζ	ω (rad/sec)
-0.040217	0.029712	0.40607
	0.032842	1.8615
	0.0050104	2.7636
	0.0053053	3.0471
	0.011209	3.2097
	0.78300×10^{-4}	5.9553
	0.012640	8.6312
	0.73576×10^{-4}	23.081

MATRIX ELEMENTS

BURN OUT

ROW	COL	COEFFICIENTS s^2	s^1	s^0
1	1	0.	1.00000000E 00	8.23599982E-05
1	2	0.	-3.98799998E-04	-4.13099992E 01
1	3	2.90399998E-03	-0.	-0.
1	4	6.63199997E-03	-0.	-0.
1	5	9.59799993E-02	-0.	-0.
1	6	0.	0.	8.63099992E-01
1	7	0.	0.	1.29200000E 00
1	8	0.	0.	2.09299999E 00
1	9	0.	0.	4.52599996E 00
1	10	-3.81889999E-02	-0.	-2.05579996E 01
1	11	0.	0.	0.
1	13	0.	0.	0.
2	1	0.	0.	-5.13399994E-07
2	2	1.00000000E 00	-0.	1.29399998E-03
2	3	-2.27899995E-04	-0.	-1.53699999E-04
2	4	-3.61799997E-04	-0.	-3.50999996E-04
2	5	-7.23099995E-04	-0.	-5.07999992E-03
2	6	0.	0.	-2.11599997E-02
2	7	0.	0.	-5.79299992E-02
2	8	0.	0.	-1.26699999E-01
2	9	0.	0.	-3.35199997E-01
2	10	3.33269998E-03	-0.	1.71370000E 00
2	11	0.	0.	0.
2	13	0.	0.	0.
3	1	0.	1.00000000E 00	-0.
3	2	-6.09599990E 01	-0.	-4.10999995E 01
3	3	1.00000000E 00	3.58139998E-02	1.28259999E 01
3	4	0.	0.	0.
3	5	0.	0.	0.
3	6	8.80179989E-01	-0.	8.66399992E-01
3	7	8.20299995E-01	-0.	1.30800000E 00
3	8	7.08199990E-01	-0.	2.13799998E 00
3	9	3.68299997E-01	-0.	4.66399997E 00
3	10	0.	0.	0.
3	11	0.	0.	0.
3	13	0.	0.	0.
4	1	0.	1.00000000E 00	-0.
4	2	-4.23599994E 01	-0.	-4.10999995E 01
4	3	0.	0.	0.
4	4	1.00000000E 00	3.76989999E-02	1.42119998E 01
4	5	0.	0.	0.
4	6	4.91729993E-01	-0.	8.35199988E-01
4	7	2.48040000E-01	-0.	1.14500000E 00
4	8	-1.91019998E-01	-0.	1.61199999E 00
4	9	-1.36250000E 00	-0.	2.16399997E 00
4	10	0.	0.	0.
4	11	0.	0.	0.
4	13	0.	0.	0.
5	1	0.	1.00000000E 00	-0.
5	2	-5.84999996E 00	-0.	-4.10999995E 01
5	3	0.	0.	0.
5	4	0.	0.	0.
5	5	1.00000000E 00	4.71239996E-02	2.22069997E 01
5	6	-1.52579997E-01	-0.	5.22799999E-01

BURN OUT

MATRIX ELEMENTS

ROW	COL	COEFFICIENTS s^2	s^1	s^0
5	7	-2.95999995E-01	-0.	-4.31999993E-01
5	8	-3.04589996E-01	-0.	-2.82499999E 00
5	9	1.27239998E-01	-0.	-6.82709998E 00
5	10	0.	0.	0.
5	11	0.	0.	0.
5	13	0.	0.	0.
6	1	0.	0.	0.
6	2	0.	0.	0.
6	3	1.66499998E-02	-0.	1.63899997E-02
6	4	2.12499997E-02	-0.	3.60899994E-02
6	5	-9.54139996E-02	-0.	3.26899996E-01
6	6	1.00000000E 00	2.91499996E-02	1.38939998E 01
6	7	0.	0.	8.07719994E 00
6	8	0.	0.	1.30889998E 01
6	9	0.	0.	2.82999998E 01
6	10	-2.54639998E-01	-0.	-1.28539999E 02
6	11	0.	0.	0.
6	13	0.	0.	0.
7	1	0.	0.	0.
7	2	0.	0.	0.
7	3	9.53999996E-03	-0.	1.52100000E-02
7	4	6.58699995E-03	-0.	3.04200000E-02
7	5	-1.13769999E-01	-0.	-1.65999998E-01
7	6	0.	0.	3.24929997E 00
7	7	1.00000000E 00	6.59199995E-02	4.83129990E 01
7	8	0.	0.	7.88039994E 00
7	9	0.	0.	1.70389996E 01
7	10	-1.58359998E-01	-0.	-7.73939985E 01
7	11	0.	0.	0.
7	13	0.	0.	0.
8	1	0.	0.	0.
8	2	0.	0.	0.
8	3	1.40799999E-03	-0.	4.25299996E-03
8	4	-8.67699993E-04	-0.	7.31999993E-03
8	5	-2.00229999E-02	-0.	-1.85699999E-01
8	6	0.	0.	5.34219992E-01
8	7	0.	0.	7.99549997E-01
8	8	1.00000000E 00	1.17109999E-01	1.38449998E 02
8	9	0.	0.	2.80129999E 00
8	10	-2.76779997E-02	-0.	-1.27239999E 01
8	11	0.	0.	0.
6	13	0.	0.	0.
9	1	0.	0.	0.
9	2	0.	0.	0.
9	3	6.12199992E-04	-0.	7.75299990E-03
9	4	-5.17299998E-03	-0.	8.21399987E-03
9	5	6.99149996E-03	-0.	-3.75129998E-01
9	6	0.	0.	3.92909996E-01
9	7	0.	0.	5.88059998E-01
9	8	0.	0.	9.52899992E-01
9	9	1.00000000E 00	2.48619998E-01	6.20179993E 02
9	10	-2.46879998E-02	-0.	-9.35819995E 00
9	11	0.	0.	0.
9	13	0.	0.	0.

MATRIX ELEMENTS

BURN OUT

ROW	COL	COEFFICIENTS s^2	s^1	s^0
10	1	0.	-3.21539998E-01	-0.
10	2	2.17909998E 01	-0.	1.32149997E 01
10	3	0.	0.	0.
10	4	0.	0.	0.
10	5	0.	0.	0.
10	6	-3.29069996E-01	-0.	-2.77499998E-01
10	7	-3.32929999E-01	-0.	-4.15299994E-01
10	8	-3.40239996E-01	-0.	-6.72999990E-01
10	9	-3.63089997E-01	-0.	-1.45519999E 00
10	10	1.00000000E 00	1.88399999E 00	2.62829998E 03
10	11	0.	0.	-2.61509997E 03
10	13	0.	0.	0.
11	1	0.	0.	0.
11	2	0.	0.	0.
11	3	0.	0.	0.
11	4	0.	0.	0.
11	5	0.	0.	0.
11	6	0.	0.	0.
11	7	0.	0.	0.
11	8	0.	0.	0.
11	9	0.	0.	0.
11	10	0.	-1.02089998E 01	-6.67469990E 02
11	11	0.	6.72039992E 01	1.46750000E 03
11	13	0.	0.	8.00000000E 02

FLIGHT CONDITION: BURNOUT

DENOMINATOR

Coefficient of s^{20} = 38.752

Coefficient of s^{0} = -1.0817×10^{13}

Number of roots = 20

REAL ROOTS (sec^{-1}) POSITIVE IN LHP	COMPLEX ROOTS	
	ζ	ω (rad/sec)
−0.014276	0.17621	0.040733
14.142	0.0038963	3.4091
	0.0047959	3.6800
	0.0043226	4.0265
	0.0050804	4.9510
	0.0027954	7.4185
	0.0045739	11.858
	0.0052562	24.991
	0.097951	52.504

FLIGHT CONDITION: BURNOUT

$\dot{Z}/\beta_c$ NUMERATOR

Coefficient of s^{18} = 6.2570×10^{4}

Coefficient of s^{0} = -2.8261×10^{19}

$\dot{Z}/\beta_c$ High frequency asymptote = $1614.6/s^2$

$\dot{Z}/\beta_c$ Low frequency asymptote = 2.6126×10^{6}

Number of roots = 18

REAL ROOTS (sec^{-1}) POSITIVE IN LHP	COMPLEX ROOTS	
	ζ	ω (rad/sec)
-2.1262	0.0041410	2.9855
2.1282	0.0049869	3.5730
	0.0049300	3.7389
	0.0048511	4.7765
	0.0061474	7.5465
	0.0051887	11.926
	-0.0017662	23.704
	0.0068535	24.582

FLIGHT CONDITION: BURNOUT

φ/β_c NUMERATOR

Coefficient of s^{17} = -5805.3

Coefficient of s^0 = -5.3401×10^{13}

φ/β_c High frequency asymptote = $-149.81/s^3$

φ/β_c Low frequency asymptote = 4.9368

Number of roots = 17

REAL ROOTS (sec^{-1}) POSITIVE IN LHP	COMPLEX ROOTS	
	ζ	ω (rad/sec)
0.78038×10^{-4}	0.0040671	3.4742
	0.0051065	3.5672
	0.0050046	3.7503
	0.0050636	4.9179
	0.0053231	7.1027
	0.0050488	11.796
	-0.86895×10^{-4}	22.709
	0.0051197	24.964

FLIGHT CONDITION: BURNOUT

η_1/β_c NUMERATOR

Coefficient of s^{17} = 4.4892×10^{5}

Coefficient of s^{0} = -8.4765×10^{13}

η_1/β_c High frequency asymptote = $11584/s^3$

η_1/β_c Low frequency asymptote = 7.8363

Number of roots = 17

REAL ROOTS (sec^{-1}) POSITIVE IN LHP	COMPLEX ROOTS	
	ζ	ω (rad/sec)
-0.014118	0.18375	0.038639
	0.0050012	3.5833
	0.0050138	3.7814
	0.0051851	4.9916
	0.0052222	6.7156
	0.0050273	11.741
	-0.54560×10^{-4}	22.456
	0.0050836	24.992

FLIGHT CONDITION: BURNOUT

η_2/β_c NUMERATOR

Coefficient of s^{17} = 2.7821×10^5

Coefficient of s^0 = -1.0743×10^{13}

η_2/β_c High frequency asymptote = $7179.2/s^3$

η_2/β_c Low frequency asymptote = 0.99316

Number of roots = 17

REAL ROOTS (sec^{-1}) POSITIVE IN LHP	COMPLEX ROOTS	
	ζ	ω (rad/sec)
-0.014227	0.17857	0.040066
	0.0050047	2.9126
	0.0050076	3.5887
	0.0050946	3.8145
	0.0053173	5.0364
	0.0050088	11.718
	-0.37078×10^{-4}	22.106
	0.0050696	24.996

FLIGHT CONDITION: BURNOUT

η_3/β_c NUMERATOR

Coefficient of s^{17} = 4.7266×10^{4}

Coefficient of s^{0} = -6.6713×10^{11}

η_3/β_c High frequency asymptote = $1219.7/s^3$

η_3/β_c Low frequency asymptote = 0.061674

Number of roots = 17

REAL ROOTS (sec^{-1}) POSITIVE IN LHP	COMPLEX ROOTS	
	ζ	ω (rad/sec)
-0.014477	0.16616	0.043810
	0.0049589	2.8661
	0.0050092	3.5957
	0.0052536	3.8816
	0.0053616	5.0142
	0.0049513	6.6243
	-0.25339×10^{-4}	21.489
	0.0050674	24.961

FLIGHT CONDITION: BURNOUT

η_4/β_c NUMERATOR

Coefficient of s^{17} = 3.7504×10^{4}

Coefficient of s^{0} = -1.4447×10^{11}

η_4/β_c High frequency asymptote = $967.80/s^3$

η_4/β_c Low frequency asymptote = 0.013356

Number of roots = 17

REAL ROOTS (sec^{-1}) POSITIVE IN LHP	COMPLEX ROOTS	
	ζ	ω (rad/sec)
−0.014835	0.14669	0.050856
	0.0047408	2.7244
	0.0049988	3.6062
	0.0057537	4.0972
	0.0049564	4.7805
	0.0057028	7.2448
	0.0050610	11.785
	-0.53415×10^{-4}	19.285

REFERENCES

1. Lukens, D. R., A. F. Schmitt, and G. T. Broucek, Approximate Transfer Functions for Flexible-Booster-and-Autopilot Analysis, WADD-TR-61-93, Apr. 1961.

2. Rheinfurth, M. H., Control-Feedback Stability Analysis, Army Ballistic Missile Agency Rept. DA-TR-2-60, Jan. 1960.

3. Patha, J. T., R. L. Schultz, and S. J. Wallace, New Dynamic Analysis Techniques for Rapid Preliminary Design of Automatically Controlled Flexible Missiles, The Boeing Company Doc. D2-22034, Dec. 1963.

4. Clingan, B. E., Dynamic Loads Due to Wind Shear, AIAA Paper 63-207, June 1963.

5. Decker, D. W., M. A. Sloan, Jr., and A. W. Meagher, Summary Report for Dual Gyro Blender System (M-AERO-DS), Northrop Space Labs., Apr. 1964.

6. Hofmann, L. G., and A. Kezer, Simplified Analysis of Flexible Booster Flight Control Systems, MIT, Instrumentation Lab., Rept. E-1210, June 1962.

7. Seide, P., Effect of Constant Longitudinal Acceleration on the Transverse Vibration of Uniform Beams, Aerospace Corp. Rept. TDR-169(3560-30)T, Oct. 1963.

8. Glaser, R. F., Vibration and Stability Analysis of Compressed Rocket Vehicles, NASA TN D-2533, Jan. 1965.

9. Pearce, B. F., W. A. Johnson, and R. K. Siskind, Analytical Study of Approximate Longitudinal Transfer Functions for a Flexible Airframe, ASD-TDR-62-279, June 1962.

10. Schwendler, R. G., and R. H. MacNeal, Optimum Structural Representation in Aeroelastic Analyses, ASD-TR-61-680, Mar. 1962.

11. Model Vehicle No. 2 for Advanced Control Studies, NASA, Marshall Space Flight Center, unpublished Working Paper, 1964.